UNIVERSITÀ DEGLI STUDI DI TORINO

SCUOLA DI DOTTORATO

DOTTORATO IN
SCIENZE AGRARIE, FORESTALI E ALIMENTARI

CICLO: XXXVI

UNRAVEL THE COMPLEXITIES OF URBAN SOIL CONTAMINATION: REGULATED AND EMERGING METALS CONTAMINANTS IN A POST-INDUSTRIAL CITY

Annapaola Giordano

Docente guida:
Dott. Elio Padoan

Coordinatore del Ciclo:
Prof. Domenico Bosco

Settore scientifico disciplinare: AGR/13 CHIMICA AGRARIA

ANNI
2021; 2022; 2023

Sommario

CHAPTER 1

Introduction

1.1. Urban soils: a general framework

The urban environment is a complex system, where various anthropogenic activities contribute to the dispersion of metal(loids) into environmental compartments with different responses to contamination. With urbanization, the original soils undergo significant alterations, including burial, truncation, removal, and compaction, leading to a complex urban soil substrate distinct from rural soils (Burghardt, 1994; Yang and Zhang, 2015). Human activities exert a profound influence on urban soil formation and characteristics, as redevelopment and space reuse involve the incorporation of materials from diverse sources with varying physical and chemical properties (Pouyat et al., 2020). Consequently, urban soil horizons often exhibit irregularities, with anthropogenic layers and high heterogeneity. Construction rubble, comprising materials such as cement, concrete, brick, structural metal components, wood, and various wastes, frequently contributes to the composition of urban soils. Furthermore, soil structure degradation occurs due to the presence of artifacts, technogenic substrata, mechanical compaction, and human trampling (Scalenghe and Ajmone-Marsan, 2009). These physical alterations often diminish urban soil's water infiltration capacity and storage, exacerbating pressure on sewerage systems and increasing flood risk significantly (De La Paix et al., 2013). Soil is a very critical environmental component, as it is the final recipient of many types of pollutant inputs and represents the focal point from which various contamination pathways (soil-root-plant-food chain, percolation into groundwater, runoff leading to discharge into surface water, and transport to the air-soil interface) are possible. On the other hand, there are numerous and diverse human activities that can involve material inputs into soils. In fact, various sources of point and diffuse pollution coexist, such as traffic exhaust and non-exhaust emissions, residential heating, waste disposal, industrial activities, and all can involve material inputs into soils. Indeed, it can be asserted that all major anthropogenic processes are in some way responsible for soil contamination, and consequently, there are numerous potentially hazardous elements or chemical compounds that can be found in them (Ajmone-Marsan and Biasioli, 2010; Khodadadi et al., 2022; Liang et al., 2019). The soil buffer capacity can effectively prevent the immediate

contamination of other environmental compartments, but it can also, through accumulation, led to a release of pollutants with negative effects on the ecosystem and human health through exposure pathways (Antoniadis et al., 2017; Wei et al., 2020; Yadav et al., 2019; Zahran et al., 2013).

1.2. Regulated Potentially Toxic Elements: sources, pathways, and health risks.

Among the pollutants of particular concern are the Potentially Toxic Elements (PTE), consisting of a group of metals and metalloids, including cadmium (Cd), chromium (Cr), copper (Cu), lead (Pb), nickel (Ni), zinc (Zn), vanadium (V) and antimony (Sb), which, being simple elements, are not subject to any metabolism and remain in the soil until they are transported by some chemical-physical mechanism, and are known to have adverse effects on human health (Li et al., 2021; Verma et al., 2020). These elements can enter the body through various pathways, such as inhalation, ingestion, and skin contact, causing a range of health problems depending on the duration of exposure and the concentration levels. Potential sources of PTE in the environment, including the pedosphere, can be categorized into two main types: natural and anthropogenic. The primary natural source originates from the rock substrate. Through physical weathering and chemical alteration processes during pedogenesis, the rock substrate releases trace elements contained within the crystal lattice of its constituents into the soil (Wilson, 2004). The presence of specific PTE in these minerals depends on isomorphic substitution within the crystal structure by ions with similar radius and charge. In ferromagnesian minerals of basic and ultrabasic rocks, and their metamorphic derivatives, elements such as cobalt (Co), nickel (Ni), zinc (Zn), and chromium (Cr) are relatively abundant due to their substitution of iron (Fe) and magnesium (Mg) (Graf, 1980). In sedimentary rocks, the concentration of PTE depends not only on the mineralogy of the clastic material but also on the adsorptive capacity of the fine and colloidal fraction and the original concentrations in the waters in which the sediments were deposited or subsequently encountered (Miranda et al., 2022). The geochemical inheritance of trace elements typically reflects the elements most strongly bound to the soil's substrate. Consequently, high concentration values and apparent contaminations are sometimes attributed to the presence of geochemical anomalies in the parent rock; typical examples include chromium (Cr) and nickel (Ni) in soils derived from ultrabasic rock substrates (Kelepertzis et al., 2013).

The second source of PTE arises from anthropogenic activities, such as industrial processes, mining operations, agricultural practices, and improper waste disposal. These sources emit particulates containing PTE which are directly deposited on soil surfaces, roads, and tree leaves through wet and dry atmospheric deposition (Luo et al., 2019; Shi et al., 2008). The deposition of these PTE-enriched particulates contributes to soil pollution. It has been indicated that soil fine fractions, particularly the particles <10 μm or finer, exhibits higher PTE accumulation than the coarser fractions due to their higher surface area and higher content of reactive clay minerals and organic matter (Ajmone-Marsan et al., 2008; Padoan et al., 2017). More recently, Kelepertzis et al., (2020) reported the appropriateness of using the soil dust to trace the anthropogenic impact in the industrial area of Volos, Greece, and confirmed the sensitivity of soil fine fraction to anthropogenic contamination in industrial and high-density traffic cities. Soils, however, behave not only as a sink, but also as a source of pollutants under certain conditions, as fine particles have a higher resuspension potential compared to the bulk soil (BS).

The dust generated from soil resuspension or from the resuspension of dust particles deposited along road edges and park walkways can influence the elemental concentrations in other urban compartments, contributing to the complexity of the contamination conditions, and enhancing human health risks from PTE exposure (Li et al., 2021; Padoan and Amato, 2018; Zahran et al., 2013). Road dust (RD) is composed, apart from soil dust, by different particles transported and suspended by vehicles or wind, including brake, tire, road wear particles and other particles from various origins (salt, sand, exhaust emissions, secondary compounds, other mineral dust, etc.) (Padoan and Amato, 2018). In the last years, it has been shown that resuspension, redistribution, and transport of PTE-containing particles from soils and RD contribute significantly to urban particulate matter <10 μm (PM_{10}) in all urbanized areas (Padoan and Amato, 2018). For example, in the city of Milan, located in the Po Valley, one of the most contaminated sites in Europe, the so-called local dust (sourced from soil and RD), has been calculated to contribute to PM_{10} more than vehicle exhaust (8% of local dust vs 7% of vehicle exhaust) (Amato et al., 2016). Similarly to soil dust, RD fine particles (i.e., <10 μm) contain PTE concentrations higher than the bulk material in urban areas, as noticed in previous studies (Padoan et al., 2017; Vlasov et al., 2021). Likewise, Khademi et al., (2019) observed that the fraction <10 μm showed the largest accumulation of PTE in RD in both natural and industrial areas in Murcia city, south-eastern Spain. In urban areas, the average concentration of

fine PM is more than twice higher than in rural areas, often exceeding allowable levels with a higher percentage of the population exposed. PM_{10} is classified as a carcinogen to humans by the International Agency for Research on Cancer (IARC) (IARC Scientific Publication No. 161). Particulate pollution has a significant impact on public health and the environment: short-term exposure to particulate air pollution can trigger acute health events, leading to higher rate of emergency department accesses, especially when associated with high air temperatures; long-term exposure increases the risk of cardiovascular and respiratory diseases and reduces life expectancy (Contiero et al., 2019). In 2015, diseases attributable to air pollution caused 18 million deaths worldwide (Roth et al., 2017), with Italy recording 239,514 deaths in the same year (World Health Organization Mortality Database).

In response to growing concerns about the negative effects of PTE on human health and the environment, regulatory measures have been implemented to control their emissions and limit their concentrations in various environmental compartments. In Italy, the Legislative Decree No 152 of 3 April 2006 sets legal thresholds for PTE concentrations in soil, water and air. These regulatory thresholds are established based on scientific evidence and risk assessment studies, considering factors such as known toxicity, exposure pathways and current knowledge of environmental fate.

Among PTE, Pb is one of the most widespread contaminants in urban settings, primarily due to its historical use as a gasoline additive and its presence in various industrial emissions (Facchetti, 1989; Wu et al., 2017). Although no longer used in gasoline, Pb remains a significant concern in urban areas due to its persistence and neurotoxicity (Becker et al., 2022; Gelly et al., 2019; Morton-Bermea et al., 2011). Recent studies suggest that the remobilization of historically deposited Pb is a key source of pollution, resulting from soil resuspension caused by wind and vehicular movement (Becker et al., 2022; Laidlaw and Filippelli, 2008).

1.3. Emerging contaminants: Rare Earth Elements

Emerging contaminants are a diverse group of pollutants receiving growing attention for their potential environmental and health impacts. Despite their widespread presence, regulations and monitoring protocols are often lacking. The Rare Earth Elements (REE) are an example. REE are considered as a homogenous group of elements with similar physical-chemical characteristics, encompassing 15 lanthanide series

elements (La-Lu), and yttrium (Y) (Cheisson and Schelter, 2019; Liang et al., 2008). A series of unique physical and chemical properties, such as malleability, ductility, and good electrical conductivity, made them invaluable to a variety of critical technologies (Lima and Ottosen, 2021). Frequently, according to their mass and atomic numbers, they are divided into Light Rare Earth Elements (LREE) from La to Eu, and Heavy Rare Earth Elements (HREE), from Gd to Lu and Y (Laveuf and Cornu, 2009; Li et al., 2020). A further classification based on their behavior is recurrent: LREE (La-Pm), Medium Rare Earth Elements (MREE) from Sm to Dy, and HREE (Ho-Lu, Y) (Grawunder et al., 2014; Migaszewski et al., 2016). Particularly the HREE, are widely used in green energy, electronic industry and medical applications, while LREE are mainly used for industry and manufacturing (Gwenzi et al., 2018; Orani et al., 2020).

In the last decades, REE have been extensively exploited and used in industrial production and the global demand is increasing by 4-9% per year (Tan et al., 2015). Because of this fast increase in use, a substantial amount of REE can enter and accumulate in the environment through a variety of pathways, including mineral mining, waste disposal, fertilization, coal and fuel combustion, car parts and asphalt as well as industry processes (Gwenzi et al., 2018; Mihajlovic et al., 2019).

REE have been documented to induce several eco-toxicological adverse effects (e.g., pulmonary toxicity, kidney failure, anaphylactic shock, and eventually death from exposure to Gd). It has been shown that the LREE are primarily deposited in the liver, whereas the HREE, with an ionic radius similar to calcium, are mainly distributed to the bones (Gwenzi et al., 2018). Thus, they pose significant environmental and health risks due to their widespread use and potential adverse effects.

The behavior of REE in the environment depends on their speciation, which is influenced by both environmental and chemical factors. REE are primarily present as trivalent ions (REE^{3+}), except for cerium (Ce) and europium (Eu), which can exist in different oxidation states (Ce^{4+} and Eu^{2+}) under specific redox conditions (Tyler, 2004). The interaction of trivalent lanthanides with geological media occurs through the formation of surface complexes that determine their speciation. Organic matter, clay content, and soil minerals such as iron and manganese oxides are some of the factors that define the available sorption sites, which can influence the mobility of REE. Additionally, pH and redox conditions are crucial factors in determining whether REE are present as free cations or complexes (Fendorf, 1996; Pourret et al., 2007; Bao and Zhao, 2008; Ramos et al., 2016; Lozano et al., 2020).

Substantial research reported the concentration and distribution of REE in water bodies, plants, soil and dust to understand the geochemistry and the anthropogenic impact of REE and suggesting that there has

been a considerable increase in REE concentrations (Censi et al., 2017; Hatje et al., 2016; Ramírez-Guinart et al., 2018; Shajib et al., 2020; Tepe et al., 2014).

Thus, REE must be considered as emerging contaminants and, compared to other compartments, fewer studies investigated soils, being most of the existing ones limited to Chinese mining areas (Li et al., 2013; Sun et al., 2017), where high concentrations of REE in human hair and blood have been found to be associated with soil levels. Being emerging contaminants means that there is no unified analytical protocol for the determination of REE to assess soil contamination. Considering the studies in the literature, a comparison becomes difficult as the acid dissolution method applied is not unique. The urgent implementation of regulations and monitoring protocols is crucial to mitigate their impact on ecosystems and human health. Proactive measures are needed to address the challenges posed by the accumulation of REE and ensure environmental quality and human well-being.

1.4. Effects of climate change on contaminants mobility

The concentration of PTE in soil is only one aspect of a soil quality assessment, offering a limited perspective on the actual risks they pose to human health and ecosystems (Hirabayashi and Kanae, 2009). In recent years, the importance of comprehending the mobility of these elements has been increasingly recognised, providing a more conscious understanding of their potential hazards. Numerous studies (Madrid et al., 2008; Poggio et al., 2009; Sialelli et al., 2011; Padoan et al., 2017; Li et al., 2023), have emphasised the importance of considering the available and bioaccessible fractions of contaminants when assessing their impact on human health in urban environments. A crucial factor influencing the transfer of contaminants from soil to adjacent environmental compartments, e.g., water bodies, is the dynamic nature of the soil matrix itself.

Climate models increasingly show that extreme weather events are likely to become more frequent (hotter, drier summers and increased intensity of rainfalls), contributing to pluvial and riverine flooding and causing occasional inundation of lands that have rarely been flooded in the past (Ponting et al., 2021).

Prolonged floodplain inundation, associated with reducing conditions alternating with oxygen-driven processes of dry periods and frequent water-table fluctuations, lead to alterations in soil balance and the release of previously bound components. Although most trace metals do not participate directly in redox reactions, the solubilization of iron and manganese oxides during submergence can release PTE previously

adsorbed or occluded in their mineral structures. This phenomenon has been documented in several studies, including those by Ajmone-Marsan et al., (2019); Du Laing et al., (2009); Grybos et al., (2007); Rinklebe et al., (2016); Shaheen et al., (2018); Vodyanitskii and Plekhanova, (2014). The increased mobilization of PTE resulting from such processes may increase the potential for adverse toxicological effects associated with soil contamination, as demonstrated by Alderman et al. (2012).

It is important to recognize that conditions conducive to anaerobiosis, fostered from soil sealing and compaction in urban environments, are becoming increasingly common (Kudas et al., 2024; Skougaard Kaspersen et al., 2017). Elevated levels of contaminants in riverine soils are of severe environmental concern: the input of particulates from bank erosion and leaching of the floodplain sediments play a crucial role in their dispersion. Alternating oxidizing and reducing conditions strongly influence the mobility of elements. Soil redox potential (E_H), pH, and binding agents such as iron (Fe), manganese (Mn), dissolved organic and inorganic carbon (DOC and DIC), and sulfate (SO_4^{2-}) may be important factors controlling the release dynamics of contaminants in soils. The fate of contaminants can lead to several scenarios, impacting water quality, ecosystem health and potential contamination of surface and groundwater, with consequent risks to drinking water sources and potential effects on aquatic organisms. In addition, contaminants can be absorbed by plants, resulting in phytotoxicity and reduced plant growth and productivity. The release of contaminants from submerged soils underlines the importance of monitoring and managing submerged environments to mitigate negative impacts.

1.5. Aim and structure of the work

Soil pollution is a significant global concern due to its harmful effects on both the environment and human health. Contaminated soils act as reservoirs for pollutants - accumulate over time, reflecting the history of contamination and anthropogenic activities - and potential sources of further environmental contamination.

Given the complexity and variety of possible sources of pollution, especially in the most industrialized countries, monitoring and assessing risk situations become of primary importance for improving quality of life and environmental protection. Understanding the behavior and fate of contaminants in soils is key to developing effective management strategies and remediation techniques to mitigate their impact.

The dust generated from soil resuspension or from the resuspension of dust particles deposited along road edges and park walkways can influence the elemental concentrations in other urban compartments, contributing to the complexity of the contamination conditions, and enhancing human health risks from PTE exposure (Zahran et al., 2013; Padoan and Amato, 2018; Li et al., 2021a).

In the last decades, REE has been used in various fields due to their magnetic, optical, and catalytic properties. The increasing use in industrial applications and their high content in waste, suggests that REE released into the environment are likely to increase with potential impacts on public health and ecological risk. Thus, REE are now recognized as emerging contaminants with increasing environmental concentrations. While substantial research has been conducted on REE concentrations in various environmental compartments, limited studies have focused on soils, especially in urban areas. Compared with the data that we have for many trace elements, the knowledge about REE in soils is still poor. Studies show the correlation between their behavior in the soil and different factors. The speciation and geochemical conditions play a critical role in the behavior of this element (e.g., sorption site available, pH and redox potential). The REE behavior into the natural soil is a complex process that deserves to be explored to better understand their effects on the ecosystem.

Climate change poses new challenges, including altered patterns of contaminant mobility that could increase risks to ecosystems and human health. Vulnerable cities, particularly those located in floodplains, face increased risks of contamination due to anthropogenic activities and alterations of natural river courses. Schulz-Zunkel et al. (2013) and Popescu et al. (2013) emphasized the significant impact of changes in redox potential on sediment contamination, highlighting the transformation of sediments from sinks to pollutant sources under specific conditions. Similarly, Shaheen et al. (2014) demonstrated how the periodic inundation of contaminated alluvial soils alters the dynamics of various metals due to changes in environmental factors such as pH, dissolved organic carbon and the chemistry of elements such as iron, manganese and sulphur. This increased mobility of metals in flooded urban soils, as observed by Florido et al. (2011), is attributed to the dissolution of iron and manganese oxides. Studies suggest that wetland soil components, particularly organic matter, can sequester REE, the fate of which is influenced by soil components and organic matter dynamics dictated by prevailing redox conditions. Research by Šmuc et al. (2012) on contaminated paddy field soils in Macedonia, an

anthropogenic wetland, revealed high concentrations of REE mainly related to organic matter and soil minerals. Investigations by Chen et al. (2014) on paddy soil profiles with different cultivation histories revealed REE accumulation due to paddy cultivation. Sequential extractions in studies under oxidising conditions showed that REE are predominantly associated with organic and residual fractions (Pédrot et al., 2008; Davranche et al., 2011; Mihajlovic et al., 2014). However, under reducing conditions, the solubilisation of organic phases releases REE into wetland solutions, raising questions about their bioavailability compared to organic ligands.

Understanding the behavior and fate of contaminants in soil is crucial for developing effective management strategies and remediation techniques to mitigate their impact.

In light of these considerations, the thesis aims to address key gaps and research objectives in three chapters. Chapter 2 elucidate the spatial influence of contamination sources in urban environments, assessing the variability of PTE in different urban receptors, and trace the origin of Pb, the most common urban soil contaminant. Chapter 3 optimize the mineralization procedures of REE, evaluate their presence in urban soils, and identify potential sources of contamination and enrichment, providing a preliminary analysis of the factors contributing to their distribution and concentration. Additionally, this study lays the groundwork for identifying potentially vulnerable sites to establish an environmental monitoring network for REE. Chapter 4 assess the effects of changes in redox conditions caused by climate change-induced floods on the release of PTE and REE from urban soils, elucidating the redox-driven processes influencing their release. Through these interdisciplinary investigations, the thesis aims to contribute to a deeper understanding of the complexities of urban soil contamination and provide insights for the development of effective management and remediation strategies to safeguard human health and the environment.

CHAPTER 2

Potentially toxic elements and lead isotopic signatures in the 10 µm fraction of urban dust: Environmental risk enhanced by resuspension of contaminated soils

Annapaola Giordano[a], Mery Malandrino[b]* Ajmone-Marsan Franco[a], Padoan Elio[a]

[a] University of Turin, Department of Agricultural, Forest and Food Sciences, 10095, Grugliasco, Italy

[b] University of Turin, Department of Chemistry, 10125, Turin, Italy

Adapted from the published paper:

Potentially toxic elements and lead isotopic signatures in the 10 µm fraction of urban dust: Environmental risk enhanced by resuspension of contaminated soils. Environmental Research 242 (2024), 117664964. https://doi.org/10.1016/j.envres.2023.117664

2.1. Introduction

Several studies have been conducted on the PTE accumulation in the fine fraction of sources contributing to PM_{10} in the urban environment. However, most of them consider a single environmental compartment without observing the interdependence among them. In addition, most of the research is limited to the observation of the instantaneous potential emission (Pachon et al., 2021), neglecting the physical process of particle fragmentation and breakdown that occur in urban exposure scenario. Such mechanical processes may cause larger particle size reduction that could further contribute to PM_{10} by affecting the mechanisms of PTE accumulation, transport, and exposure in urban context. Pb isotope ratios (IRs) remain unchanged throughout physicochemical and atmospheric processes (Li et al., 2018). Accordingly, in surface soils or RD, Pb signature of anthropogenic and natural sources is preserved in the IRs and could be used as a fingerprint to identify and trace Pb pollution sources. Starting from these

considerations, this paper inspects PTE concentrations and Pb isotopic ratio in the bulk soils and in the resuspended fractions of soils and road dusts with the following aims: i) to clarify the spatial influence of the contamination sources in the urban environment; ii) to evaluate the variability of PTE contents in different urban receptors; iii) to distinguish the natural from anthropogenic origin of Pb and trace its source routes via isotopic ratio study twenty years after the phasing out of leaded gasoline; iv) to investigate the interconnection of urban receptors by focusing on <10 μm resuspended fraction for a better insight of the drivers that contribute to the PTE accumulation and subsequent exposure.

2.2. Materials and methods

2.2.1. Study area

Turin is located at the western end of the Po Valley (45 04′24″ N; 7 40′32″ E), one of the most industrialized areas in Europe. It is a densely populated city with a high volume of vehicular traffic. For more than a century, the economy of Turin province has been strongly linked to industry, particularly to mechanical manufacturing with a strong focus on automotive production and all the ancillary industries related to it. The marked presence of the automotive sector has resulted in one of the highest engine rates in Italy, with 664 cars per 1000 inhabitants. In fact, the transport fleet is dominated by cars (44%), using a prevalence of gasoline (48%) and diesel (40%) fuel. Public transport is used for the 10% of the urban movements and is characterized by a large and widespread tram network (Berrone et al., 2019). According to Köppen classification, Turin has a warm temperate climate (Cfa); in the last decades, the rainy days are decreasing, consequently increasing the maximum length of dry periods (Arpa Piemonte, 2016). The average annual temperature is about 10 °C, with an average temperature anomaly of about +1.3 ◦C compared with 1971–2000 data. The Po Valley is characterized by a morphological conformation negatively influencing the pollutants dispersion, worsening its air quality (Padoan et al., 2016). In fact, frequent periods of high pollution occur, during which PM_{10} concentrations exceed the daily average limit of 50 $\mu g/m^3$ set by the *Directive 2008/*50/EC (Implementation of the Directive 2008/50/EC of the European Parliament and of the Council of 21 May 2008 on ambient air quality and cleaner air for Europe, adopted in Italy 2010, 2008). On average, in last years, the daily average has been exceeded 100 days per year, against a limit of 35 times per year.

2.2.2. Sampling and resuspension

The sampling sites were chosen to encompass the variability of the pollution sources in an urban context. BS and RD samples were collected in areas with different traffic densities and in parks within the urban and suburban area of Torino (Figure 2.1) as in Padoan et al. (2017). Previous studies (Biasioli et al., 2006; Li et al., 2021b) have shown that these locations are the most representative of soil pollution in Turin for both traffic areas and parks, for their long exposure to airborne diffuse contamination. In addition, two roadside soils sampled (samples ID: 15; 16) in the early 2000s were selected from a previous work (Biasioli et al., 2006) with the aim to observe the isotopic signature of gasoline in soils samples before the leaded gasoline phasing out. These are referred to as *historical samples*. BS and RD were sampled in the same area when possible, following the methodology described in Padoan et al. (2017). In total, 20 soil sites and 17 road dust sites were selected for this work. To examine steady-state conditions of deposition, sampling was done after one week without precipitations (Amato et al., 2012). For BS samples, three subsamples were collected at 1 m from each other along the road edge at the same distance from the curb and mixed into a single composite sample. Surface soils (0–5 cm) were considered for the current study because they are more easily resuspended. For RD, three subsamples were collected from sites of 1 m^2 using a polyethylene brush, carefully avoiding re-suspension. For sites belonging to the traffic category, RD samples were sampled at the center of the rightmost active lane. For those in parks at the center of the paved way. All samples were dried at room temperature and sieved to 2 mm.

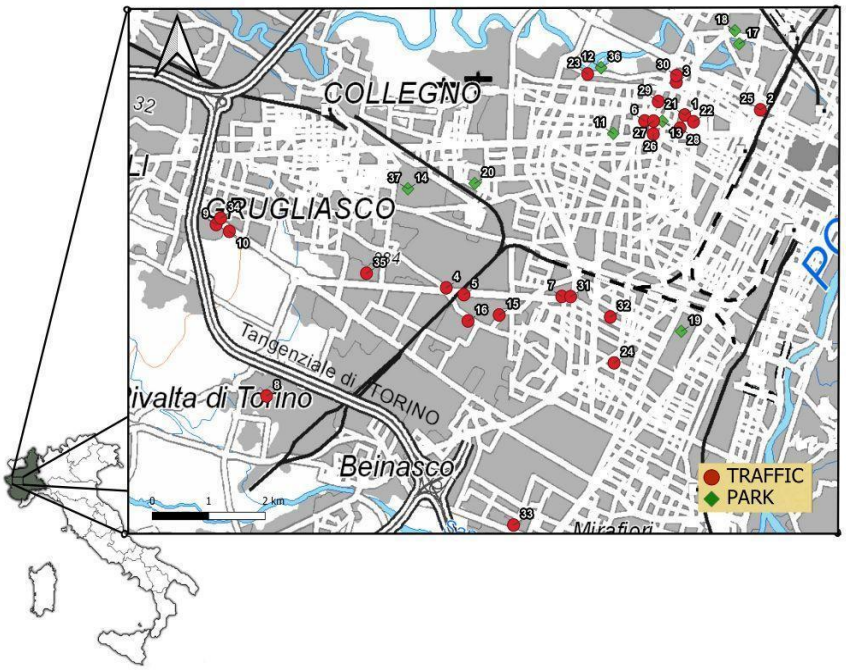

Figure 2.1. Map of the sampling sites within Turin urban area, Italy. Traffic sites are represented by red circles, parks by green rhombuses. The numbers represent the samples ID referred to in the text and reported in Table 2.1.

The fraction <10 of all samples was separated using the equipment illustrated in Figure 2.2. The samples analyzed were: 20 bulk soils (BS), 20 samples obtained by resuspension of BS (Res-BS), and 17 samples obtained by resuspension of RD (Res-RD). In the Supplementary Material (Table 2.1) the sample list is reported, with coordinates, categorization, and relevant traffic flow.

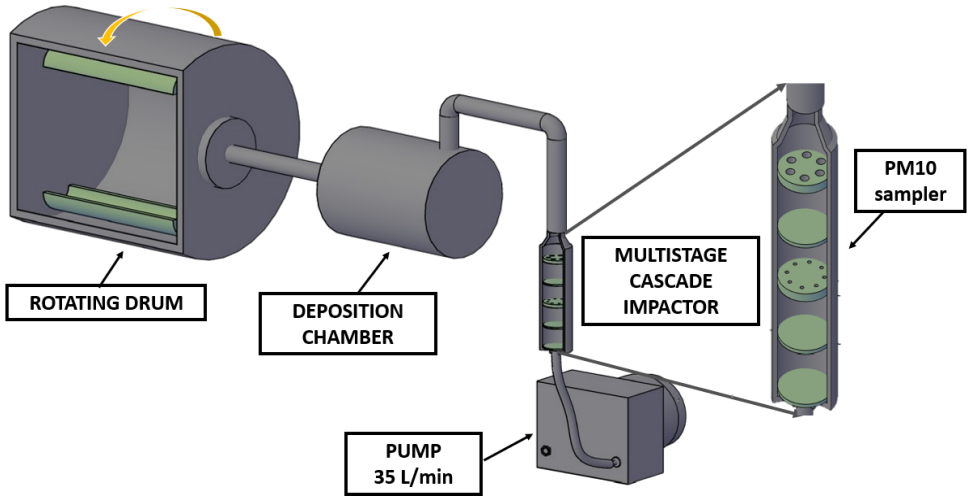

Figure 2.2. Scheme of the resuspension system. On the right, an enlargement of multistage cascade impactor to show the PM_{10} collector.

Starting from the small rotating drum in Padoan et al. (2021), we built a closed metal-free setup to directly sample the PM10 fraction produced by resuspension of the sample without dimensional pretreatment. The experiment was conducted using 15 g of dry BS or RD placed in the rotating drum and revolved at 26 rpm for 1 h. The fall of the sample generates separation of finer particles and additional fine particles are produced from the collision between the particles and the impact with the chamber wall (Mendez et al., 2013). Dust particles are transported to the deposition chamber by the vacuum pump located downstream of the system. The deposition chamber allows the deposition of the larger and heavier particles that would damage the PM impactor, avoiding any size pre-treatment. Particles <10 µm are collected on a micro-quartz fiber filter (47 mm, Ahlstrom-Munksjo) using a multistage impactor (MSI, TCR TECORA) according to the ISO 23210-2009 method. Each filter was weighed on an analytical balance (Sartorius CP225D-0CE) before and after the resuspension to calculate the dust load.

Table 2.1. Description of sample types (BS: bulk soil; Res-BS: resuspended bulk soil; Res-RD: resuspended road dust), coordinates, urban area categories, and traffic flow expressed in vehicles/day. T= Traffic; P= Park. [a]Fraction referring to BS. [b]Fraction referring to Res-BS

ID	Name	Location	Coordinates		Category	Traffic flow (vehicles/day)	Size fraction
			LONG	LAT			
1	BS1|Res-BS1	P.zza Risorgimento	7.654	45.079	T	1000-2500	<2 mm[a]|<10 µm[b]
2	BS2|Res-BS2	C.so Principe Oddone	7.671	45.080	T	0-1000	<2 mm[a]|<10 µm[b]
3	BS3|Res-BS3	C.so Svizzera	7.652	45.084	T	2500-5000	<2 mm[a]|<10 µm[b]
4	BS4|Res-BS4	C.so Allamano 3	7.601	45.052	T	5000-10000	<2 mm[a]|<10 µm[b]
5	BS5|Res-BS5	C.so Allamano 4	7.605	45.051	T	5000-10000	<2 mm[a]|<10 µm[b]
6	BS6|Res-BS6	C.so Lecce	7.645	45.078	T	10000-100000	<2 mm[a]|<10 µm[b]
7	BS7|Res-BS7	C.so Sebastopoli	7.627	45.051	T	5000-10000	<2 mm[a]|<10 µm[b]
8	BS8|Res-BS8	SITO	7.561	45.035	T	0-1000	<2 mm[a]|<10 µm[b]
9	BS9|Res-BS9	C.so Allamano 1	7.549	45.061	T	5000-10000	<2 mm[a]|<10 µm[b]
10	BS10|Res-BS10	C.so Allamano 2	7.552	45.060	T	5000-10000	<2 mm[a]|<10 µm[b]
11	BS11|Res-BS11	Tesoriera	7.638	45.076	P	5000-10000	<2 mm[a]|<10 µm[b]
12	BS12|Res-BS12	Pellerina	7.635	45.086	P	0-1000	<2 mm[a]|<10 µm[b]
13	BS13|Res-BS13	Pilo	7.649	45.078	P	0-2500	<2 mm[a]|<10 µm[b]
14	BS14|Res-BS14	Campus Agraria	7.592	45.067	P	0-1000	<2 mm[a]|<10 µm[b]
15	BS15|Res-BS15 (Historical sample)	218 URBSOIL	7.613	45.048	T	-	<2 mm[a]|<10 µm[b]
16	BS16|Res-BS16 (Historical sample)	132 URBSOIL	7.606	45.047	T	-	<2 mm[a]|<10 µm[b]
17	BS17|Res-BS17	Dora Michelin	7.666	45.090	P	0-1000	<2 mm[a]|<10 µm[b]
18	BS18|Res-BS18	Dora Vitali	7.665	45.092	P	0-1000	<2 mm[a]|<10 µm[b]
19	BS19|Res-BS19	P.za D'armi	7.654	45.046	P	0-1000	<2 mm[a]|<10 µm[b]
20	BS20|Res-BS20	Grugliasco-Paradiso	7.607	45.068	P	0-1000	<2 mm[a]|<10 µm[b]
21	Res-RD21	P.zza Risorgimento	7.654	45.079	T	1000-2500	<10 µm
22	Res-RD22	Via Bianzè	7.656	45.078	T	2500-5000	<10 µm
23	Res-RD23	C.so Appio 192a	7.632	45.085	T	-	<10 µm
24	Res-RD24	Via Boston	7.639	45.041	T	5000-10000	<10 µm
25	Res-RD25	Via Medici	7.671	45.080	T	10000-100000	<10 µm
26	Res-RD26	C.so Francia	7.647	45.076	T	10000-100000	<10 µm
27	Res-RD27	C.so Lecce	7.647	45.078	T	0-1000	<10 µm
28	Res-RD28	C.so Principe Oddone	7.653	45.077	T	0-1000	<10 µm
29	Res-RD29	C.so Lecce 68	7.648	45.081	T	10000-100000	<10 µm
30	Res-RD30	C.so Svizzera 101	7.652	45.085	T	2500-5000	<10 µm
31	Res-RD31	C.so Allamano	7.629	45.051	T	10000-100000	<10 µm
32	Res-RD32	C.so Sebastopoli	7.638	45.048	T	10000-100000	<10 µm
33	Res-RD33	Via Faccioli	7.617	45.016	T	2500-5000	<10 µm
34	Res-RD34	C.so Allamano (Roundabout)	7.55	45.062	T	5000-10000	<10 µm
35	Res-RD35	Via San Martino	7.583	45.054	T	0-1000	<10 µm
36	Res-RD36	C.so Pellerina	7.635	45.086	P	0-1000	<10 µm
37	Res-RD37	Agraria	7.592	45.067	P	0-1000	<10 µm

2.2.3. Analytical procedures

BS, Res-BS and Res-RD samples were characterized for pseudo-total elemental concentrations using aqua regia extraction and microwave digestion (Milestone Ethos D, ISO 54321:2020). Duplicate extractions were performed using 0.2 g of soil sample, ground to 0.15 mm, and 10 mL of aqua regia. For the resuspended samples, the entire filter was mineralized. The following heating steps were applied: 10 min ramp until 200 °C, 10 min dwell at 200 °C, and 20 min of ventilation. The resulting solutions were filtered on cellulose filters (Whatman N°41) and diluted to 50 mL with deionized water. Accuracy was verified using a certified reference material for aqua regia soluble contents using CRM 141 R certified soil (Community Bureau of Reference, Geel, Belgium); average recovery was 97.9 % (94–103 %). All reagents were of ultrapure or analytical grade. The concentrations of Al, Cd, Cr, Cu, Fe, Ni, Pb, Sb, V and Zn were determined using an Inductively Coupled Plasma Optical Emission Spectroscopy (ICP-OES), Agilent 5800, and an Inductively Coupled Plasma Mass Spectrometer (ICP-MS), Agilent 7500ce. The Pb relative isotopic composition was determined for the ^{204}Pb, ^{206}Pb, ^{207}Pb, and ^{208}Pb isotopes, using a Sector Field Inductively Coupled Plasma Mass Spectrometer (SF-ICP-MS, Thermo Finnigan Element 2). To obtain a precise and accurate assessment the dependence of analytical precision and accuracy was studied by going to investigate integration window, sapling points per peak and integration times, with the use of face-centered composite experimental design. More details are given in Ziegler et al. (2021). The determination was performed using the low-resolution mode, using two standard solutions of the certified reference material (CRM) SRM 981 (Common Lead NIST, USA) at concentrations of 2.4 and 24 µg/L. The correction for mass bias was performed analyzing the SRM 981 every six samples. The CRM consists of four isotopes and reflect the Pb natural isotopic abundance: 204 (1.4255 ± 0.0012%), 206 (24.1442 ± 0.0057%), 207 (22.0833 ± 0.0027%), 208 (52.347 ± 0.0086%). The counts of each isotope were obtained by subtracting the blank signal. On the ^{204}Pb isotope, the interference of ^{204}Hg was subtracted. Considering the natural abundance of the different Hg isotopes, the mathematical correction of the interference of ^{204}Hg was calculated by determining the isotope ^{200}Hg, free from interferences.

2.2.4. Statistical analysis and data processing

Statistical analyses were conducted using RStudio software (R version 4.0.3) and XlStat 2023. Normality and homoscedasticity of the data were checked using Shapiro-Wilk's and Levene's tests. Non-normal data were log-scaled. One-way ANOVA was used to detect differences in mean

values between groups. Tukey-HSD test was applied for post hoc pairwise comparisons. Correlation matrices were computed using the non-parametric Spearman method. To identify the main PTE sources and their contribution to the composition of the different media, principal component analysis (PCA) was applied. Factors were distinguished by the magnitude of factor loadings. Matrices adopted for PCA were scaled and centered before performing the analysis and generating biplots. Enrichment Factors (EFs) were calculated using the following formula:

$$EF = \left({}^{C_i}/_{C_r}\right)_{sample} / \left({}^{C_i}/_{C_r}\right)_{background}$$

where (C_i/C_r) sample and (C_i/C_r) background are the ratios between the concentration of the i-element and the concentration of the reference element in the sample, and in the background soil, or in the Earth's upper crust. We computed the EFs according to the background values in Turin soils for Cr, Cu, Ni, Pb, Sb, V, and Zn using Fe as reference element because only for these elements regional background levels were available. These values were calculated from the Regional Agency for Environmental Protection according to ISO 19258/2005 norms (ARPA Piemonte, 2015). For Cd, values from the Upper Crust (Wedepohl, 1995) were used instead. Iron was used as a reference element because the use of local background concentration might be the best strategy to reduce the distortion induced in EFs calculation from the typical use of average values of rocks or Upper Crust (Bern et al., 2019). There are no generally accepted grades for the EFs. In this study, we used EFs levels according to Vlasov et al. (2021): <2 depletion to minimal enrichment, 2–5 moderate enrichment; 5–20 significant enrichment and pollution; 20–40 very high enrichment and pollution, and >40 extreme enrichment and pollution.

2.3. Results and discussion

2.3.1. PTE distribution in BS, Res-BS, and Res-RD

Descriptive statistics regarding PTE in samples are reported in Table 2.2. Data for Al, Cd, Cr, Cu, Fe, Ni, Pb, Sb, V and Zn is reported in Table 2.3. In line with the findings of previous studies on Turin soils, high concentrations of all the elements were found through the city area (Ajmone-Marsan et al., 2008; Li et al., 2021; Padoan et al., 2017). However, no significant differences (at p = 0.05) were found in BS samples between park and roadside soils (Figure 2.3). Iron and Al are abundant metals found as minerals in the soil; apart from their lithogenic origin, they may also be released into the environment in much lower concentrations by anthropogenic activities. However, given their

abundant presence in the soil, both were considered as typical geogenic markers in this study. Traffic soils had averages exceeding the tabulated values for Cr, Ni, Pb and Zn, with some samples also having Sb and Cu concentrations higher than the legislative limits for residential areas.

Table 2.2. Descriptive statistics of the elemental concentrations of selected elements in BS (n=20), Res-BS (n=20) and Res-RD (n=17). The mean, median, minimum, and maximum value of pseudo total concentrations in mg/kg are shown in the table. The relative standard deviation (RSD%) was calculated by multiplying the standard deviation by 100 and dividing this product by the mean.

			Cd	**Cr**	**Cu**	**Ni**	**Pb**	**Sb**	**V**	**Zn**
			mg/kg	mg/kg	mg/kg	mg/kg	mg/kg	mg/kg	mg/kg	mg/kg
BS (n=20)	Park (n=8)	**Mean**	**0.53**	**138**	**57**	**129**	**47**	**1.7**	**54**	**125**
		RSD%	45	24	25	22	40	30	15	33
		Median	0.38	138	50	121	41	1.71	52	93
		Min	0.3	105	39	101	18	0.9	43	87
		Max	0.95	205	75	192	71	2.7	67	195
	Traffic (n=12)	**Mean**	**1**	**191**	**92**	**155**	**173**	**4.1**	**51**	**178**
		RSD%	68	36	56	28	107	91	22	61
		Median	0.98	203	75	164	124	2.78	52	164
		Min	0.12	92	32	82	12	0.6	31	63
		Max	2.1	292	199	214	557	12	71	426
Res-BS (n=20)	Park (n=8)	**Mean**	**1.7**	**643**	**196**	**360**	**147**	**10**	**342**	**460**
		RSD%	44	27	24	26	35	74	28	33
		Median	1.34	634	185	324	144	6.89	350	456
		Min	1	367	134	263	65	4.1	183	287
		Max	32	946	290	585	228	26	486	727
	Traffic (n=12)	**Mean**	**3.8**	**844**	**256**	**405**	**513**	**23**	**416**	**644**
		RSD%	56	46	36	34	117	91	38	66
		Median	3.01	842	218	406	250	16	389	458
		Min	1	357	123	211	51	4.4	241	255
		Max	8.7	1872	421	666	2012	82	840	1687
Res-RD (n=17)	Park (n=2)	**Mean**	**2.2**	**1200**	**266**	**585**	**70**	**13**	**544**	**683**
		RSD%	48	27	29	49	48	18	11	37
		Median	2	1200	266	585	70	13	544	683
		Min	1.3	881	189	300	37	11	485	431
		Max	3.6	1519	343	870	104	15	602	934
	Traffic (n=15)	**Mean**	**13**	**1788**	**1211**	**575**	**300**	**94**	**1054**	**2336**
		RSD%	54	57	64	40	109	56	65	41
		Median	12	1284	1109	507	209	80	726	2236
		Min	5.2	787	413	232	71	26	200	905
		Max	33	4094	3475	1168	1506	266	2672	4781

The high concentrations of Cr and Ni could be ascribed to the presence in the soil parent material of ultramafic rocks, such as serpentinitic peridotites and serpentinites, as reported in previous studies in the same area (Biasioli et al., 2006) and in the Regional Environmental Protection Agency study (ARPA Piemonte, 2020) that consistently supported the hypothesis that the high concentrations of these elements were related to the area-specific pedogenesis, lithological composition and prevailing physico-chemical conditions.

Table 2.3. Pseudo-total concentrations of the studied elements reported for BS samples as mg/kg or percentages (w/w) and for Res-BS and Res-RD samples as mg/kg or percentages (w/w).

Name	Al	Cd	Cr	Cu	Fe	Ni	Pb	Sb	V	Zn
	%	mg/kg	mg/kg	mg/kg	%	mg/kg	mg/kg	mg/kg	mg/kg	mg/kg
BS1	3.11	0.12	214	32	3.77	172	12	1	66	63
BS2	3.30	1.20	92	37	3.31	82	17	1	50	66
BS3	2.43	0.42	291	54	3.75	206	58	1	54	100
BS4	2.21	1.02	203	90	3.40	149	362	5	41	190
BS5	1.93	0.74	165	75	3.55	164	137	5	37	164
BS6	1.06	1.90	266	199	3.13	178	169	11	31	243
BS7	2.56	0.98	258	83	3.49	208	125	3	48	187
BS8	4.76	0.23	116	49	4.36	106	29	1	71	113
BS9	4.04	1.72	157	117	3.98	135	124	8	61	183
BS10	1.68	1.87	292	144	3.60	214	557	12	41	426
BS11	3.98	0.63	149	75	3.76	121	60	2	61	195
BS12	2.79	0.95	138	68	3.73	135	71	3	44	157
BS13	4.31	0.77	157	74	3.90	130	68	2	57	161
BS14	3.77	0.38	108	43	4.16	111	30	2	52	90
BS15	4.51	0.39	113	71	4.62	117	80	1	52	114
BS16	2.23	2.08	211	182	3.68	192	551	4	52	374
BS17	4.39	0.30	205	39	4.20	192	18	1	67	87
BS18	2.89	0.37	107	50	4.08	115	37	1	45	93
BS19	4.47	0.26	105	59	4.09	99	28	1	57	89
BS20	3.41	0.31	105	47	3.67	101	41	1	50	93
Res-BS1	3.93	3.32	357	196	4.30	461	67	82	550	255
Res-BS2	5.11	8.73	1872	360	5.80	358	94	35	840	440
Res-BS3	3.35	2.90	1132	203	4.55	569	179	10	376	519
Res-BS4	3.36	3.79	936	300	3.21	247	743	16	454	863
Res-BS5	5.60	2.51	993	222	6.93	529	304	18	465	449
Res-BS6	1.73	2.80	965	244	2.12	245	233	24	477	639
Res-BS7	2.32	3.08	828	177	3.53	422	266	11	402	456
Res-BS8	3.79	1.00	476	123	3.75	211	51	4	264	264
Res-BS9	2.71	2.95	468	191	3.60	268	204	10	241	460
Res-BS10	5.66	5.93	856	421	6.30	666	2012	45	273	1687
Res-BS11	4.91	2.02	712	241	3.77	333	131	15	401	437
Res-BS12	5.41	2.60	636	209	4.46	305	157	9	352	649
Res-BS13	6.27	3.15	946	290	5.82	406	210	26	486	727
Res-BS14	3.28	1.15	784	167	4.58	263	65	9	446	287
Res-BS15	10.37	1.79	582	215	9.31	390	448	7	321	366
Res-BS16	5.37	6.46	660	417	6.26	494	1548	16	323	1332
Res-BS17	6.52	1.24	632	159	7.12	585	110	5	287	475
Res-BS18	5.44	1.07	367	134	6.85	316	107	4	183	312
Res-BS19	6.33	0.97	443	176	7.21	312	165	5	237	296
Res-BS20	6.52	1.44	627	195	7.48	363	228	5	348	495
Res-RD21	0.84	18.10	1900	1657	4.91	551	200	99	1102	2863
Res-RD22	1.57	25.06	997	2124	6.90	489	209	130	487	2526
Res-RD23	<LD	5.24	2645	1109	1.45	734	120	60	1717	1978
Res-RD24	5.26	12.77	2042	923	8.90	911	1506	80	1032	2419
Res-RD25	0.95	12.02	861	1145	3.96	476	205	77	461	2236
Res-RD26	0.80	12.49	1888	1236	4.00	467	188	116	1174	4781
Res-RD27	<LD	11.01	1130	462	0.91	350	71	26	710	1859
Res-RD28	6.46	9.13	787	774	6.66	617	237	57	200	1314
Res-RD29	<LD	32.52	3159	3475	7.70	1168	285	266	1945	3415

Res-RD30	<LD	15.41	3198	1622	4.35	553	246	99	1949	2596
Res-RD31	1.79	12.77	1284	924	5.39	507	257	122	726	1542
Res-RD32	1.52	7.49	1099	578	4.02	339	311	82	647	1260
Res-RD33	<LD	15.96	4094	1282	2.89	726	276	76	2672	3154
Res-RD34	1.79	5.43	822	435	4.77	232	206	71	514	2192
Res-RD35	2.75	5.29	918	413	4.21	504	184	55	482	905
Res-RD36	1.29	3.60	881	344	2.38	300	104	15	485	934
Res-RD37	<LD	1.28	1519	189	1.30	870	37	11	602	431

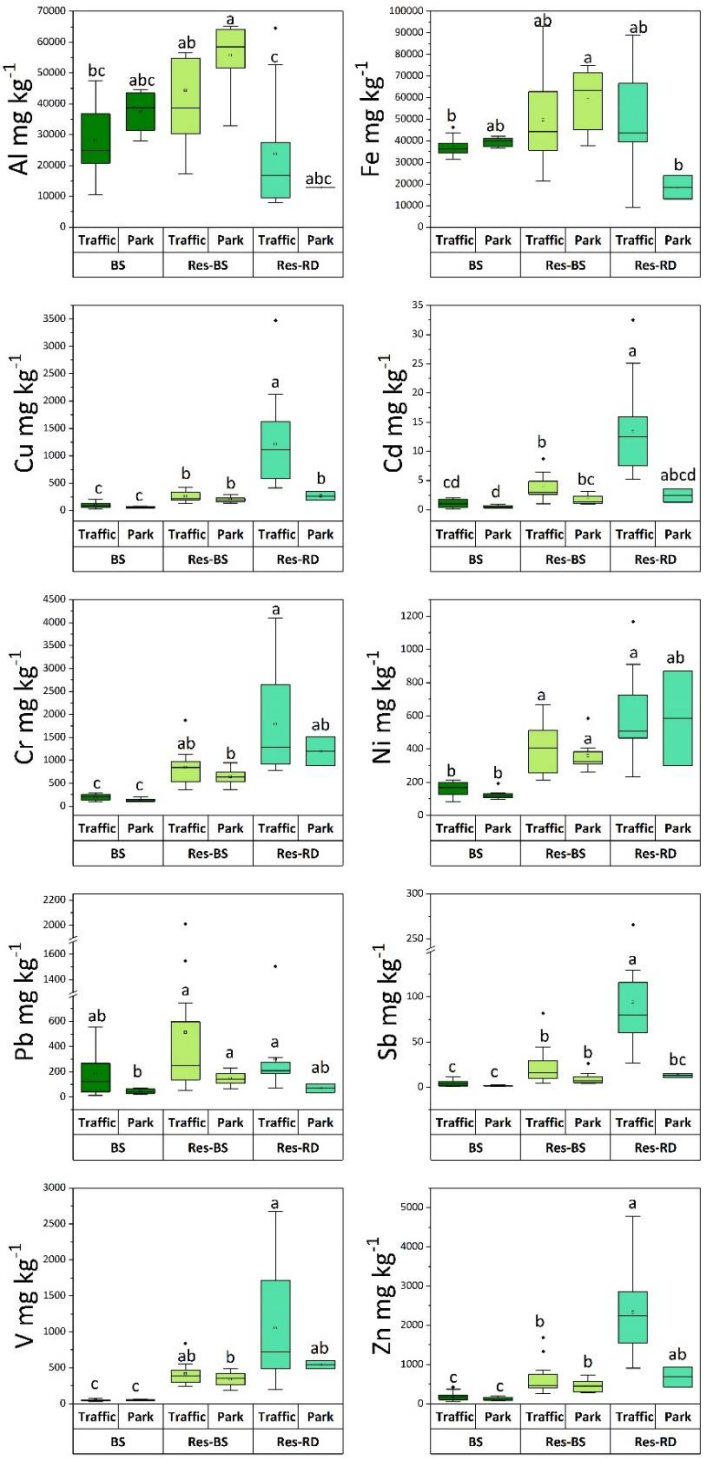

Figure 2.3. Elemental concentrations (mg/kg) in the individual matrices (BS, Res-BS and Res-RD) divided by the categories (traffic and park). Superscript

letters indicate the statistically significant groups obtained using Tukey-HSD test. The length of the box indicates the interquartile range whereas the horizontal line within each box represents the median. Whiskers indicate minimum and maximum values while outliers are represented as points.

Vanadium had the lowest variability among studied PTE, while Pb and Sb had the highest. Lead, Sb, Cu, and Zn, in urban areas, have their main sources related to anthropic activities, and it is noticeable that the relative standard deviation (RSD%), was considerably higher in soils located in traffic areas for Pb, Zn, and Sb. Park soils had, in general, lower PTE concentrations than traffic ones. On average, Ni was the only element slightly exceeding the Italian legislative limit for residential and park sites (D.Lgs. 152/2006), while, looking at the maximum values, Cr and Zn also exceeded the limits in some park samples. This variability within the city reflects the diverse, intermittent, and long-term effects of human activities on the urban environment, causing highly localized variations in metal concentrations and often preventing the possibility to discriminate soils according to the current land use. Compared to cities with a similar industrial history, Turin's soils had higher PTE concentrations (Table 2.3). Notable is the high concentration of Zn and Pb in all the cities, probably because of a convergence of geochemical substrata and pollution sources, as metallurgical industries, and traffic. Res-BS samples (descriptive statistics reported in Table 2.2) display two to eight times higher average concentrations and higher variability than BS samples in both parks and traffic areas, suggesting a homogeneity of sources affecting both areas. Antimony and V are the elements showing the highest enrichments in Res-BS. While Sb is emitted mainly from brake and tire wear (Grigoratos and Martini, 2015), V is emitted from metallurgical works, combustion of fuel oil, coal, and diesel vehicles (Zhang et al., 2023) pointing to a diffuse, long-term accumulation of V in the fine fraction of soils. In traffic sites, Cr, Zn and Pb had the highest concentrations, with Pb having the highest maximum values and RSD% between traffic and park sites, evidencing the long-term influence of Pb diffuse contamination on urban soils twenty years after the phasing out of leaded fuel. Furthermore, all other elements have higher coefficients of variation in traffic than in park sites due to the complexity of the sources at roadside sites. Generally, Res-BS samples displayed lower average concentrations in parks than in traffic sites, with Cr, Zn and Ni showing the highest concentrations, followed by V, Cu and Pb, while Sb had the highest RSD%, evidencing the possible presence of site-specific contaminations.

Table 2.4. Concentration in mg/kg of Cr, Cu, Ni, Pb and Zn in literature studies concerning soils in cities having an industrial history.

City	Cr	Cu	Ni	Pb	Zn	Reference
Turin, Italy	173	79	146	129	159	This study
Guanghzou, China	55	44	24	57	153	(Liang et al., 2019)
Shanghai, China	108	59	31	71	301	(Shi et al., 2008)
Koyang, Korea	47	59	47	88	238	(Ajmone-Marsan and Biasioli, 2010)
Athens, Greece	95	72	131	157	174	(Kelepertzis and Argyraki, 2015)
Berlin, Germany	35	80	11	119	243	(Ajmone-Marsan and Biasioli, 2010)
Madrid, Spain	75	72	14	161	210	(Ajmone-Marsan and Biasioli, 2010)
Denver, USA	37	35	20	107	171	(Johnson, 2011)
Melbourne, Australia	17	40	15	102	218	(Laidlaw et al., 2018)

The various sources present in an urban area contribute to the complexity of the spatial pattern but, in general, Res-BS samples collected in sites with the most trafficked roadways were more contaminated. Average results for the Res-RD samples are reported in Table 2.2, while the complete dataset is reported in Table 2.3. In traffic sites, Res- RD average concentrations of Cd, Cu, Pb, Sb and Zn were high, in line with previous works (Padoan et al., 2017) and with literature studies, if we consider only city centers and industrial areas (Khodadadi et al., 2022; Vlasov et al., 2021). Ni was the only element having similar average concentrations in park and traffic sites, while all other PTE exhibited lower values in parks than in traffic sites. This behavior could be due to the presence of different prevalent sources in the two land uses (e.g., soil in RD from parks and wear in RD from traffic sites). Res-RD samples have, generally, higher concentrations and variability than other matrices (as visible in Figure 2.4), especially compared to BS, and particularly high concentrations were observed for Cd, Cu, Sb and Zn. The large variability of Res-RD is due to its buildup, as it generates from different materials: soil coming from ridges or roadsides, exhaust emissions, wear of vehicular mechanical parts, asphalt, nearby industrial emissions (Padoan and Amato, 2018). All these sources contribute differently in the different sites, increasing the elemental variability. Less marked differences between Res-RD and Res-BS were observed for Ni, while for Pb no significant difference was observed in the concentrations of the examined matrices, suggesting shared sources (leaded gasoline and industry) and processes, leading to a similar Pb distribution in urban areas, although with some divergences.

2.3.2. Enrichment factors

The Enrichment factors (EF) calculated for all samples against local background values are depicted in Figure 2.4 as boxplots for each category.

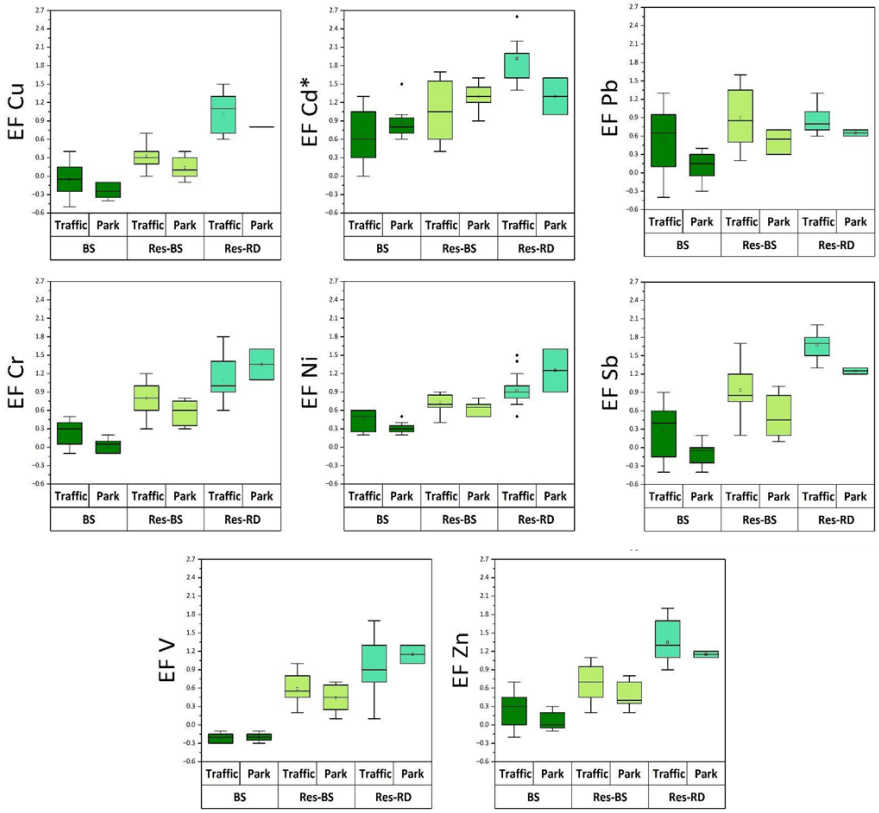

Figure 2.4. Enrichment factors calculated for BS, Res-BS, and Res-RD against local background values represented on a logarithmic scale; Fe was used as a reference element. The length of the box indicates the interquartile range whereas the horizontal line within each box represents the median. Whiskers indicate minimum and maximum values, while outliers are represented as points. *Enrichment factors calculated in relation to upper crust values from Wedepohl (1995).

In BS samples, most of the elements displayed a minimal or moderate enrichment. No marked differences are evident comparing EF in park and traffic sites, with Cd having, on average, the highest values. A higher average EF value and variability was observed for Pb and Sb in traffic soils than in parks. The highest EF value was observed for Pb at the sites with highest traffic flow, in large avenues, namely at sites BS4,

BS6, and BS10 (EF = 14, 7 and 20 respectively). For the same sites, except for BS4, high EF values were also present for Sb (EF > 8). Despite their concentrations, the low EF values calculated for Cr and Ni are justified considering their partial lithogenic origin in Turin soils, as previously discussed.

Results for the Res-BS samples are also shown in Figure 2.4. Generally, EF values for parks were lower than those for traffic sites, although the complexity of the spatial pattern of sources in urban areas partially overwhelms this simple partition. In soils located in traffic areas, all elements except Cu exhibited a significant enrichment, especially Cd, Pb and Sb. Significant enrichments of Cr and V were found in four avenues (sites Res-BS1, Res-BS2, Res-BS6 and Res-BS7). The same sites also had extreme and significant enrichments of Sb (EFs = 45, 14, 26, and 7, respectively), likely emitted in road environment during the brake pad wear process (Grigoratos and Martini, 2015). This increase in trafficked sites is related to traffic congestion or tram and bus stops, where vehicles break down more frequently, and it also reflects the vehicles flow intensity (Chang et al., 2021). Accordingly, EF decreased in sites with low vehicular traffic, reaching the lowest values in parks, where EF were always under 5, also observable in Figure 2.5(a–e), where the spatial distributions of the EF are shown in relation to traffic flows. Traffic data were obtained from the Piedmont regional geoportal (TGM, 2018). Local anomalies of Pb and Zn, and significant enrichment of Sb were observed also near industrial zones in sites Res-BS10 (Pb EF = 41; Zn EF = 11; Sb EF = 26) and Res-BS4 (Pb EF = 30; Zn EF = 11; Sb EF = 12). Zinc is emitted during the galvanization process in steel and iron industries to protect iron from rusting (Verma et al., 2020). High Pb values were probably due to the long-term influence of past use of Pb fuels, while Sb originated from vehicle component wear, due to the use of it in brake pads formulation (Grigoratos and Martini, 2015; Pant and Harrison, 2013; Zhu et al., 2020). The presence of anomalies once again confirms the high variability of the distribution of PTE in urban soils. The high enrichment factors observed in Res-BS may be attributed to its chemico-physical characteristics. Fine particles typically exhibit higher concentrations of metals than coarser ones due to a higher surface area, content of clay minerals and organic matter, and to the presence of Fe–Mn oxide phases acting as PTE sorbents (Ajmone-Marsan et al., 2008). These factors promote the accumulation of metals by co-precipitation, occlusion, adsorption, and complexation. Among the studied matrices, Res-RD samples were the most enriched in all the selected elements (Figure 2.4). Contrarily to Res-BS, for Res-RD land use was a driver. EFs in parks for Cd, Cu, Sb and Zn were markedly lower than in traffic

sites, whereas Cr, Ni and V were higher. In traffic sites Cu, Sb and Zn were the most enriched elements, with roadside values nearly twice as high as in parks. Analogously to Res-BS, the high accumulation of Sb and Zn were found in sites with high vehicles flow and frequent stop-start maneuvers and trajectory changes, were intensified tire and brake wear is expected (Alves et al., 2020; Ferreira et al., 2016; Nazzal et al., 2013; Pant and Harrison, 2013).

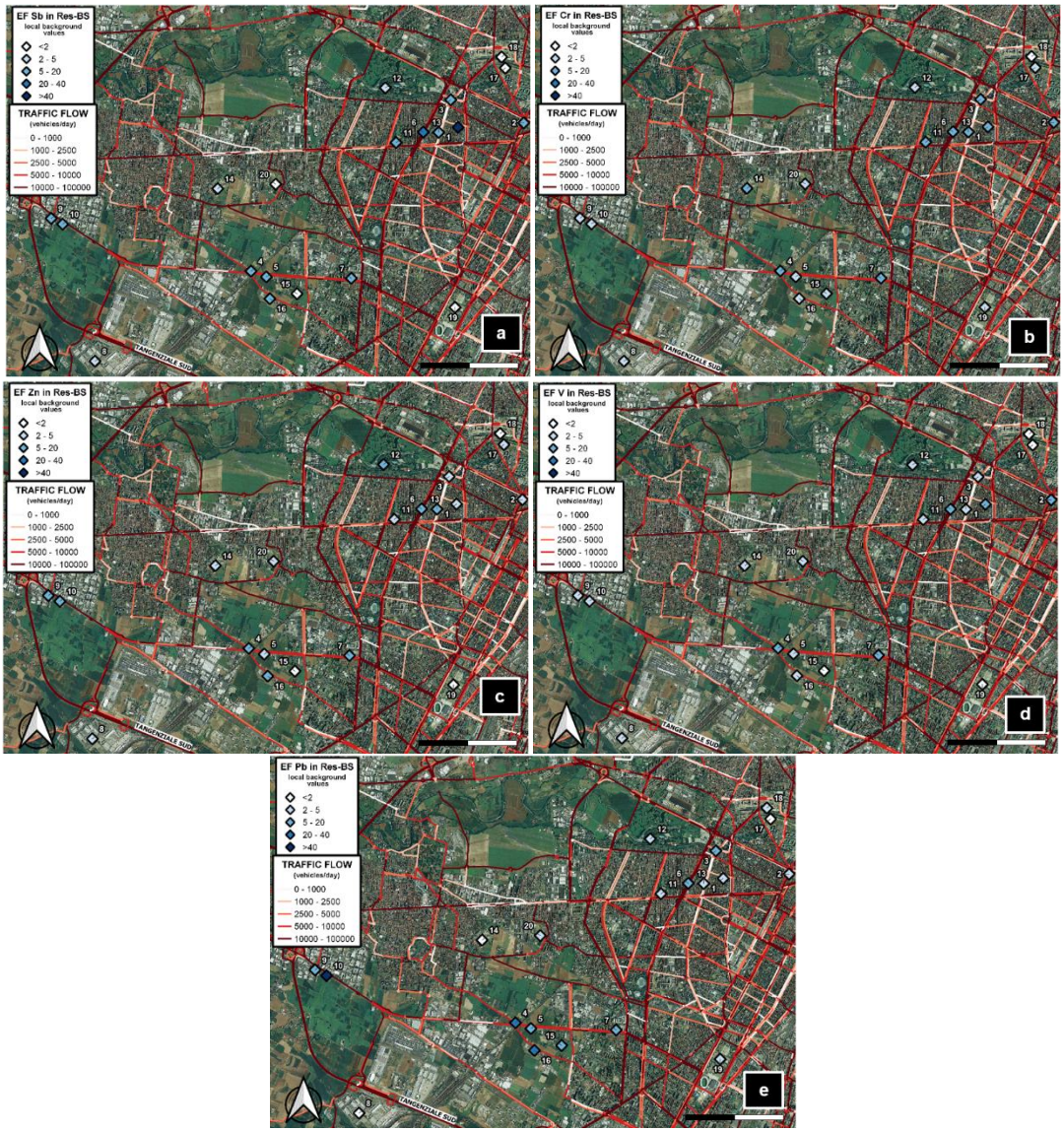

Figure 2.5. Spatial distribution of EFs values in Res-BS in relation to traffic flow for Sb(a), Cr(b), Zn(c), V(d), and Pb(e). Traffic data were obtained from the Piedmont regional geoportal. The numbers represent the samples ID reported in Table 2.1. EFs levels: <2 depletion to minimal enrichment, 2-5 moderate enrichment; 5-20 significant enrichment and pollution; 20-40 very high enrichment and pollution, and >40 extreme enrichment and pollution. The increasing intensity of traffic flow is indicated by the increasing intensity of red color.

Likewise, Cu is a typical tracer of brake wear emissions, but it also may be emitted by metallurgical plants and machinery companies and can be deposited on the ground from other sources than non-exhaust traffic emissions. In Res-RD samples, the non-exhaust emission is supported from Cu/Sb ratio, averaging 14 in traffic sites, while increasing to 23 in parks. Typical ratios found in Res-RD traffic samples from different cities ranged from 5 to 18 (Alves et al., 2015, 2020; Ramírez et al., 2019). These studies reported that a higher ratio was related to the decrease in Sb concentrations due to the lesser influence of brake wear, suggesting a greater importance of geogenic sources for Cu in parks. Such high enrichments make particles <10 μm an environmental hazard to citizens due to their susceptibility to resuspension, and their potential to be transported over considerable distances, contributing to urban dust and, atmospheric particulate matter. The Po Valley, of which Piedmont is part, is one of the most polluted areas in Europe, with an estimated 2500 deaths per year in the Piedmont region due to air pollution (VIIAS Project). Being surrounded by mountains to the north, west and south, air circulation is limited, causing long periods of stagnant air and, consequently, some of the highest levels of air pollution in Europe (Raaschou-Nielsen et al., 2013; Van Donkelaar et al., 2015). Moreover, the deleterious impact of air pollution also affects animal and plant health, and ecological systems at large (with further consequential impacts on the productivity of agricultural and forestry resources). Although Europe has made progress in regulating air quality air pollution remains a persistent problem (World Health Organization. Regional Office for Europe, 2015).

2.3.3. Multivariate analysis

To characterize the underlying contamination sources, we calculated the Spearman’s correlation for BS samples (Table 2.5). A considerable high correlation is appreciable for Cd, Cu, Pb, Zn and Sb, typical urban contaminants in soils. These elements, indeed, relate to traffic (e.g., Cu, Zn and Sb are currently emitted, in urban areas, mostly from brake and

tire wear), and to industrial emissions. Activities such as smelting, coal combustion, and construction have been regarded as the major sources of these elements in the environment (Yadav et al., 2019). Moreover, the high correlation between Zn and Cd ($r_{Zn-Cd} = 0.82$; $p < 0.05$) may be an indication of contamination in roadside soils by tire wear. Zinc can be traced, in part, to ZnO used during tire vulcanization process. Cadmium has been associated with impurities in vulcanized tires, as Cd is closely associated with zinc in its natural state (Alves et al., 2020; Pant and Harrison, 2013). Vanadium shows no correlation with the other elements of interest, indicating a prevalent natural origin.

Table 2.5 Spearman correlation matrix for BS (n=20) samples on the upper diagonal; p-value (<0.05 significant) on the lower diagonal.

	Fe	**Al**	**Cd**	**Cr**	**Cu**	**Pb**	**Zn**	**Ni**	**Sb**	**V**
Fe	1	**0.79**	-0.56	-0.47	-0.43	-0.36	-0.37	-0.33	-0.47	**0.62**
Al	*0.00*	1	-0.58	**-0.65**	-0.59	-0.58	-0.55	**-0.60**	**-0.63**	**0.81**
Cd	*0.01*	*0.01*	1	0.44	**0.88**	**0.75**	**0.82**	0.39	**0.81**	-0.48
Cr	*0.04*	*0.00*	*0.05*	1	0.52	0.52	0.56	**0.94**	0.55	-0.25
Cu	*0.06*	*0.01*	*0.00*	*0.02*	1	**0.75**	**0.85**	0.47	**0.84**	-0.49
Pb	*0.12*	*0.01*	*0.00*	*0.02*	*0.00*	1	**0.92**	0.53	**0.66**	-0.41
Zn	*0.11*	*0.01*	*0.00*	*0.01*	*0.00*	*0.00*	1	0.55	**0.77**	-0.40
Ni	*0.15*	*0.01*	*0.09*	*0.00*	*0.04*	*0.02*	*0.01*	1	0.45	-0.20
Sb	*0.04*	*0.00*	*0.00*	*0.01*	*0.00*	*0.00*	*0.00*	*0.04*	1	-0.57
V	*0.00*	*0.00*	*0.03*	*0.28*	*0.03*	*0.07*	*0.08*	*0.39*	*0.01*	1

Lastly, the high correlation between Cr and Ni confirms their common origin from the soil geological substrate. However, a contribution from metallurgical activities in Turin cannot be ruled out. Spearman's correlations were also calculated on Res-BS and Res-RD samples, together with principal component analysis (PCA). For Res-BS samples, results of the correlations and loadings of the first four components, accounting for the 91% of total variance, are reported in Table 2.6(a) and Table 2.7, respectively. Scores and loadings on the first two PCs are displayed via biplot in Figure 2.6. The first component (PC1) is strongly influenced by Cd, Cu, Pb and Zn, elements also showing a high intercorrelation between them, especially in the industrial area and in sites along heavily congested roads. The highly correlated elements Cr and V, conversely, contribute negatively to the second principal component (PC2), suggesting similar sources in the fine fraction, as an anthropic contribution from diffuse sources, i.e., deposition of particulate matter coming from fossil fuel burning or manufacturing activities due to

their use in metal alloys that make up engine components (Long et al., 2021). This anthropic addition was presumably hindered in the BS samples from the high natural background.

Table 2.6. Spearman's correlation for (a) Res-BS (n=20) and (b) Res-RD (n=17) samples. Coefficients are on the upper diagonal; p-value (<0.05) on the lower diagonal. Coefficients higher than 0.6 are in bold.

(a)	Fe	Al	Cd	Cr	Cu	Pb	Zn	Ni	Sb	V
Fe	**1**	**0.91**	-0.07	-0.11	0.06	0.17	0.03	0.42	-0.17	-0.22
Al	*0.00*	**1**	-0.10	-0.14	0.10	0.14	0.04	0.29	-0.15	-0.18
Cd	*0.79*	*0.69*	**1**	**0.70**	**0.87**	0.54	0.59	0.33	0.49	0.59
Cr	*0.63*	*0.55*	*0.00*	**1**	0.55	0.07	0.19	0.08	0.17	**0.81**
Cu	*0.81*	*0.68*	*0.00*	*0.01*	**1**	**0.79**	**0.84**	0.43	0.39	0.36
Pb	*0.48*	*0.56*	*0.02*	*0.78*	*0.00*	**1**	**0.94**	0.56	0.21	-0.20
Zn	*0.91*	*0.88*	*0.01*	*0.44*	*0.00*	*0.00*	**1**	0.52	0.21	-0.10
Ni	*0.06*	*0.22*	*0.17*	*0.75*	*0.07*	*0.01*	*0.02*	**1**	0.37	-0.02
Sb	*0.46*	*0.54*	*0.03*	*0.48*	*0.10*	*0.40*	*0.39*	*0.12*	**1**	0.52
V	*0.35*	*0.45*	*0.01*	*0.00*	*0.13*	*0.41*	*0.67*	*0.92*	*0.02*	**1**

(b)	Fe	Al	Cd	Cr	Cu	Pb	Zn	Ni	Sb	V
Fe	**1**	**0.69**	**0.63**	-0.06	0.49	**0.64**	0.29	0.29	0.59	-0.10
Al	*0.02*	**1**	-0.15	-0.03	-0.23	0.55	-0.31	**0.65**	-0.27	-0.29
Cd	*0.01*	*0.67*	**1**	0.44	**0.94**	0.14	0.63	0.44	**0.87**	0.43
Cr	*0.83*	*0.95*	*0.08*	**1**	0.53	0.15	0.53	0.61	0.40	**0.99**
Cu	*0.05*	*0.49*	*0.00*	*0.03*	**1**	0.06	**0.64**	0.55	**0.91**	0.53
Pb	*0.01*	*0.08*	*0.58*	*0.57*	*0.82*	**1**	0.15	0.37	0.13	0.09
Zn	*0.27*	*0.36*	*0.01*	*0.03*	*0.01*	*0.56*	**1**	0.19	0.61	0.56
Ni	*0.28*	*0.03*	*0.08*	*0.01*	*0.02*	*0.15*	*0.46*	**1**	0.48	0.51
Sb	*0.02*	*0.41*	*0.00*	*0.11*	*0.00*	*0.63*	*0.01*	*0.05*	**1**	0.40
V	*0.71*	*0.39*	*0.08*	*0.00*	*0.03*	*0.75*	*0.02*	*0.04*	*0.11*	**1**

The elements of most likely geogenic origin, Fe and Al, contribute positively to PC2. Park sites are most influenced by the natural component. In fact, these are placed at diffuse values along PC2 and additionally are negatively influenced by the component expressing anthropic elements, confirming for park sites greater influence by elements of natural origin. Spearman's correlation and PCA analysis were performed also on Res-RD.

Table 2.7. Loading of Principal Component Analysis (PCA) for resuspended soil samples <10 µm fraction (Res-BS, n=20). The PCA was performed on the correlation matrix.

	PC1	PC2	PC3	PC4
Proportion of Variance	0.40	0.26	0.16	0.09
Al	0.03	0.74	0.59	-0.05
Cd	0.90	-0.27	0.11	-0.13
Cr	0.59	-0.49	0.42	-0.37
Cu	0.96	0.06	-0.06	-0.16
Fe	0.04	0.78	0.59	-0.03
Ni	0.54	0.46	0.15	0.38
Pb	0.75	0.47	-0.42	-0.06
Sb	0.52	-0.29	0.06	0.76
V	0.44	-0.70	0.52	0.06
Zn	0.80	0.34	-0.44	-0.12

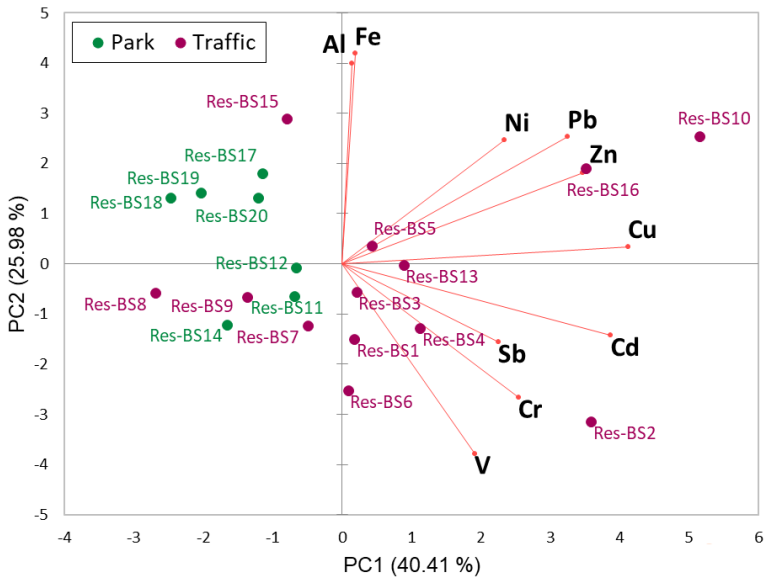

Figure 2.6. Biplot graph of PC1vsPC2, representing both loadings and scores for PCA obtained for resuspended <10 µm fraction of soil samples (Res-BS). Matrices adopted for PCA were scaled and centered prior to performing the analysis and generating biplots.

Correlation results are reported in Table 2.6(b) while PCA loadings for the first four components, accounting for the 94% of total variance, are reported in Table 2.8. Scores and loadings on the first and second

principal components are displayed via biplot in Figure 2.7. In Res-RD samples, elements of likely anthropogenic origin appear distributed over different components.

Table 2.8. Loading of Principal Component Analysis for the Res-RD samples (n=17). The PCA was performed on the correlation matrix.

	PC1	PC2	PC3	PC4
Proportion of Variance	0.46	0.28	0.16	0.04
Al	0.08	0.92	-0.17	0.28
Cd	0.78	-0.27	-0.53	-0.17
Cr	0.83	-0.01	0.53	-0.08
Cu	0.74	-0.40	-0.48	-0.07
Fe	0.67	0.62	-0.33	0.08
Ni	0.69	0.65	-0.01	-0.08
Pb	0.55	0.70	0.28	-0.16
Sb	0.74	-0.42	-0.28	0.08
V	0.72	-0.24	0.63	-0.09
Zn	0.70	-0.46	0.25	0.45

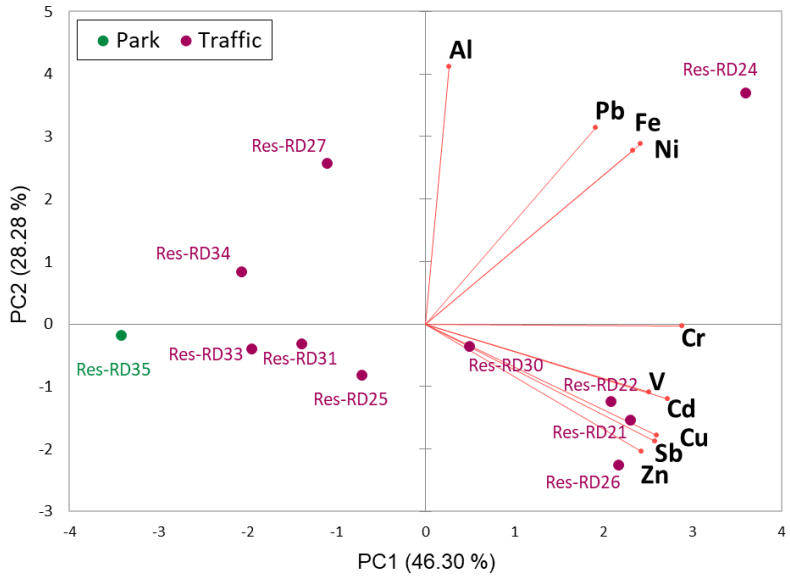

Figure 2.7. Biplot graph, representing both loadings and scores for PCA obtained for the resuspended <10 µm fraction of road dust samples (Res-RD). Matrices adopted for PCA were scaled and centered prior to performing the analysis and generating biplots.

This behavior is due to the multiple anthropogenic activities influencing Res-RD production, reflecting the higher variability of Res-RD compared to Res-BS. Along the first calculated PC, anthropic-derived elements, such as Sb, Cu, Cd, Cr, V and Zn, influenced traffic samples (e.g., Res-RD21, Res- RD22, and Res-RD26) while samples from city parks resulted as not affected. In particular, the Zn and Cu positive correlation was previously found in tramway emissions and railway transport (Vlasov et al., 2021). The emission of all these elements due to vehicle wear is also suggested from the high correlation between Cu, Cd, and Sb ($r_{Cu-Cd} = 0.94$; $r_{Cu-Sb} = 0.91$; $r_{Cd-Sb} = 0.87$). Vanadium and Cr are characterized by positive loadings on PC3, exhibiting a strong correlation between them ($r_{V-Cr} = 0.99$), higher than in Res-BS, probably because of their common sources in soils, in the traffic-derived wear of metallic parts and asphalts, and in the manufacturing activities of metal products. Aluminum, Fe, Ni and Pb contributed positively to the PC2. The presence of Pb together with crustal elements suggests also for Pb a soil-derived origin in Res-RD, pointing to contaminated soil dust resuspension as a major origin for Pb in road dust also in Turin, as suggested in previous studies outside Europe (Laidlaw and Filippelli, 2008) but never suggested in Italian sites, to our best knowledge. Multivariate PCA was performed considering the three matrices grouped (Figure 2.8 and Table 2.9), to observe the distribution of the different matrices in relation to the considered elements. The total cumulative variance of the first two components is 80%. Examining the biplot graph obtained from the multivariate analysis, the characteristic variability of the different matrices is confirmed, as soil have the lowest variance while Res-RD the highest. The inter-variability between matrices is mainly related to PC2 (related mainly to Fe and Al), with BS samples grouped, indicating common elemental sources. Instead, BS and Res-RD samples are discriminated from PC1 (related to Cd, Cr, Cu, Sb, Zn, V and, to a lower extent, Ni), arising from anthropogenic activities. It is noteworthy to observe that the Res-BS samples appear as a transition between the BS and the Res-RD samples as if to indicate the Res-BS matrix as a precursor in the formation of the fine fraction of RD. This suggests a priority relevance of the composition of Res-BS for proper assessment of citizen health risks. Lead, instead, has the highest loading on PC3. Using PC3, the different matrices were not distinguished, confirming the ubiquity of this element in urban settings and, probably, a common origin in contaminated soils, widespread in historically industrialized towns as Turin.

Table 2.9. Loading of Principal Component Analysis for BS, Res-BS and Res-RD (n=57). The PCA was performed on the correlation matrix.

	PC1	PC2	PC3	PC4
Proportion of Variance	0.59	0.21	0.08	0.06
Al	-0.15	0.92	0.25	-0.01
Cd	0.92	-0.17	0.06	-0.27
Cr	0.89	0.04	0.05	0.41
Cu	0.90	-0.22	0.10	-0.31
Fe	0.43	0.81	0.26	-0.21
Ni	0.81	0.43	-0.08	0.11
Pb	0.40	0.48	-0.77	-0.06
Sb	0.90	-0.25	0.09	-0.15
V	0.88	-0.04	0.13	0.42
Zn	0.90	-0.18	-0.09	-0.05

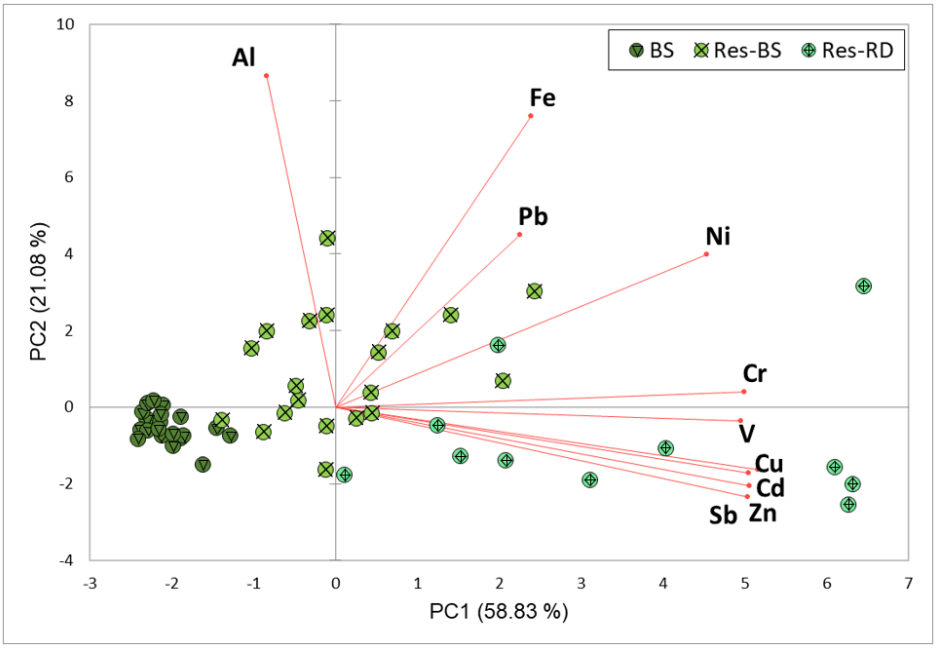

Figure 2.8. Biplot graph representing both loadings and scores for PCA obtained considering all the matrices. Data were scaled and centered prior to performing the analysis and generating biplots.

2.3.4. Lead isotopic composition

To better identify pollution sources, Pb isotope ratios (IRs) were used. Lead has four stable isotopes: 208, 207, 206, and 204; the first three deriving from Th and U radioactive decay, while ^{204}Pb being the only stable isotope with a constant abundance on Earth. Natural materials

have, thus, characteristic IRs because of the geological evolution of the area (Doe, 1970). This technique has been used in environmental studies to identify Pb sources in soils, sediments, and particulate matter, helping to distinguish the contribution from geological and anthropogenic sources (Gioia et al., 2017; Hansson et al., 2019; Kelepertzis et al., 2020). It can be expressed using different ratios, with the $^{206}Pb/^{207}Pb$ ratio being the most preferred because of the relative high abundances of these isotopes. The idea of historically contaminated soils as main source of Pb in urban settings appeared after the phasing out of leaded gasoline (Laidlaw and Filippelli, 2008) because, in many urban areas, Pb levels in heavily contaminated areas affected blood Pb levels and human health. Twenty years after this event, Pb is still present in soils and RD and, although atmospheric Pb has decreased substantially in European countries, it still has some industrial sources. In our sites, Pb had strikingly similar concentrations in the different media with no significant difference between BS, Res-BS and Res-RD (Figure 2.3). This result suggests a common source in all media and a redistribution pathway from soil to RD through resuspension of fine fraction. In this study, the $^{206}Pb/^{207}Pb$ ratios ranged from 1.117 to 1.121 for traffic BS, while from 1.143 to 1.178 for park BS; from 1.131 to 1.187 for traffic Res-BS, and from 1.127 to 1.174 for park Res-BS. The $^{206}Pb/^{207}Pb$ ratios for Res-RD samples ranged from 1.134 to 1.194 for traffic sites, and from 1.147 to 1.157 for park sites (Table 2.10). Although the observed differences in IRs are indicative of different relative contributions of common sources to the Pb content of soils and dusts (Bi et al., 2018; Hu et al., 2014), no significant differences were found in the Pb isotopic composition between BS, Res-BS and Res-RD.

Table 2.10. Descriptive statistic of lead isotope ratios, for the different environmental media investigated (BS, Res-BS and Res-RD). The mean, standard deviation (SD), median, and range of minimum and maximum values are given in table.

			206/204	207/204	208/204	208/206	206/207
BS (n=20)	Park (n=8)	Mean ± SD	18.776± 0.237	16.139± 0.176	38.887± 1.088	2.071± 0.053	1.163± 0.011
		Median	18.812	16.111	38.815	2.050	1.162
		Range	18.316-19.003	15.896-16.431	37.562-41.225	1.997-2.173	1.143-1.178
	Traffic (n=12)	Mean ± SD	18.471± 0.468	16.031± 0.285	39.312± 0.793	2.129± 0.046	1.152± 0.024
		Median	18.350	15.910	38.991	2.137	1.154
		Range	17.837-19.443	15.693-16.554	38.513-41.092	2.018-2.178	1.117-1.207
Res-BS (n=20)	Park (n=8)	Mean ± SD	18.650± 0.166	16.171± 0.272	39.124± 0.978	2.098± 0.055	1.154± 0.017
		Median	18.617	16.197	39.161	2.093	1.156
		Range	18.454-18.965	15.769-16.564	37.535-41.105	2.028-2.214	1.127-1.174
	Traffic (n=12)	Mean ± SD	18.287± 0.385	15.763± 0.380	38.687± 0.932	2.116± 0.017	1.160± 0.017
		Median	18.277	15.743	38.559	2.122	1.158
		Range	17.703-18.783	14.955-16.366	36.978-40.085	2.079-2.135	1.131-1.187

Res-RD (n=17)	Park (n=2)	Mean ± SD	18.231± 0.227	15.827± 0.129	39.324± 0.373	2.158± 0.047	1.152± 0.005
		Median	18.231	15.827	39.324	2.158	1.152
		Range	18.005-18.458	15.698-15.956	38.950-39.697	2.110-2.205	1.147-1.157
	Traffic (n=15)	Mean ± SD	18.437± 0.388	15.871± 0.470	39.049± 0.964	2.118± 0.041	1.162± 0.018
		Median	18.324	15.732	38.744	2.119	1.159
		Range	17.981-19.272	15.260-16.992	37.761-41.214	2.053-2.191	1.134-1.194

The results on all the samples are plotted using the $^{206}Pb/^{207}Pb$ and $^{208}Pb/^{206}Pb$ ratios in Figure 2.9. Such plot highlights Pb sources (Gonzalez et al., 2016; Khondoker et al., 2018). To this aim, different IRs of possible Pb sources (e.g., vehicle exhaust, gasoline and natural sources) from other studies were compared with our results (Gioia et al., 2010, 2017; Lahd Geagea et al., 2008; Facchetti, 1989). In addition, IRs determined in PM10 samples collected in Turin (Ziegler et al., 2021) are also plotted. The first indication arising from Figure 2.9 is the overlapping of the ratios of the different media, giving a hint on the mixing processes involving the urban environments. Most of the samples lye in the typical area of traffic sources, suggesting vehicular traffic, historical or present, as main Pb source in all the media. In the same area of the graph are present also Turin PM10 samples, in agreement with signatures found in other cities, suggesting that Pb is well mixed within the urban environment. In soils, the geogenic contribution is characterized by a lower $^{208}Pb/^{206}Pb$ ratio (Morton-Bermea et al., 2011), and the natural end member of parent material shows also higher $^{206}Pb/^{207}Pb$ ratios compared with the anthropogenic-related sources, as found in previous studies (Kelepertzis et al., 2016, 2020). Traffic sources are, in soil, mixed to Pb coming from the parent material, and to atmospheric particulate matter deposition from anthropogenic activities. Conversely, in Res-RD Pb should derive only from current sources, thus non-exhaust traffic emissions, resuspension of soil dust, and possibly, industrial Pb emissions. Accordingly, samples in the lowest part of the plot have a greater natural Pb input. In our case, samples in that area are mostly BS from urban parks, while the respective Res-BS samples are positioned in the upper part of the graph. Only one BS from a traffic site (BS9) lies in this area. At this site, Pb concentration was lower than in neighboring traffic sites, likely because the surface had been renovated only some years before the sampling. However, the corresponding Res-BS sample showed a lead isotopic signature comparable with the sites in the same area confirming that, in case of low anthropic contribution, the enrichment is mainly in the soil fine fractions. In this work, Res-BS and Res-RD sampled in the same area showed comparable Pb isotopic ratios, suggesting that contaminated soil is, indeed, a driving factor of the Pb presence in road dust. Also, the, PM_{10} samples of the city of Turin obtained in the work of Ziegler et al. (2021), lie in the range of values found in this work for Res-BS and Res-RD, confirming the interconnection between the different environmental compartments. As leaded gasoline is thought to be the most important Pb source in urban soils, it is crucial to gather data concerning the origin of gasoline used in studied regions, as Pb isotopic composition was dependent on economic

factors, such as the availability and price of Pb ores, and has evolved over time. In the city of Turin, a ten-year study (Facchetti, 1989) was conducted to track Pb used in petrol in the atmosphere by studying Pb isotopic composition. Considering the IR in Turin leaded gasoline ($^{206}Pb/^{207}Pb$ = 1.19) (Figure 2.9), it is evident that all recent samples are far from that level. On the other hand, the isotopic signature of leaded gasoline, can be clearly observed only in the fine fraction of the historical samples, while BS are far from the point.

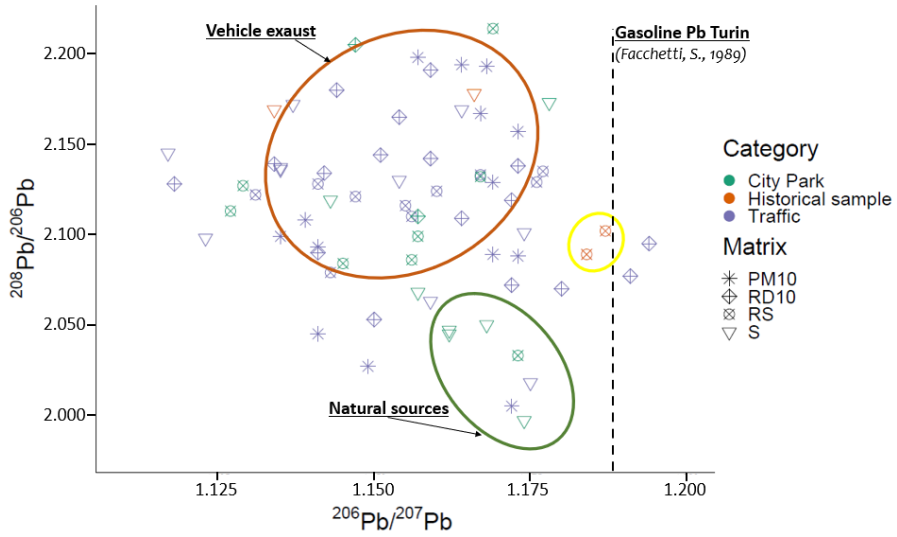

Figure 2.9. Isotopic ratios of all the analyzed samples. Circles display ratios of potential anthropogenic sources found in literature: vehicle exhaust (orange circle), gasoline (yellow circle) and natural sources (green circle) (Gioia et al. 2010, 2017; Facchetti, 1989). Ratios of PM_{10} samples collected in Turin are depicted using the asterisk symbol (Ziegler et al. 2021).

The fact that only the Res-BS fraction had the characteristic isotopic ratio demonstrates the importance of this fraction for tracing the contribution of lead from anthropogenic activities within the environment. A second ratio useful for this discrimination is $^{206}Pb/^{204}Pb$. Lead of unpolluted soils derives from weathered bedrocks in which the Pb isotopic composition evolved over time reflecting the U/Pb and Th/Pb of the parent material. Lead isotopic signatures of natural soils are thus generally more radiogenic ($^{206}Pb/^{204}Pb$: 18.5–19.5) than those of industrial Pb that comes from mining and has a ratio, in Europe, in the range 17.9–18.4 (Doe, 1970). BS and Res-BS Park samples showed higher $^{206}Pb/^{204}Pb$ ratios compared to traffic sites (Table 2.11), and this

trend is confirmed plotting this ratio against the total Pb concentrations (Figure 2.10), showing the relation between the highest Pb concentrations and the lowest $^{206}Pb/^{204}Pb$ ratios.

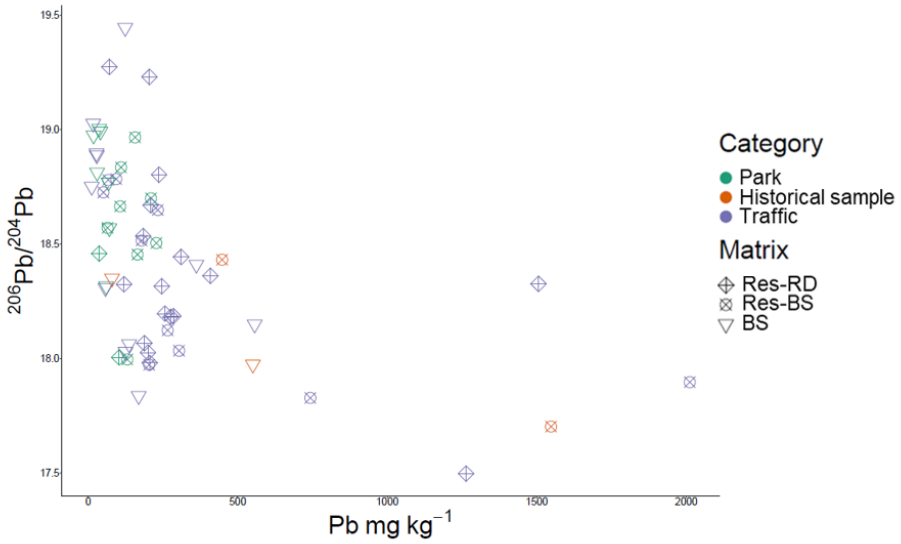

Figure 2.10. Plot of $^{206}Pb/^{204}Pb$ vs Pb in mg/kg.

It is noteworthy that these samples are all Res-BS coming from trafficked areas. Figure 2.11 compares Res-BS and BS averages in park and traffic sites using average normalized element concentrations of Cu, Pb, Zn, Ni and Sb (using Al as normalizing element), and average $^{206}Pb/^{207}Pb$ ratios. As discussed in section 3.1, concentrations of these elements were higher in the Res-BS than in BS, whereas the $^{206}Pb/^{207}Pb$ isotopic ratio was lower for Res-BS samples. As evidenced from Figure 2.11, sites with a higher anthropogenic Pb input (i.e., traffic sites), had lower $^{206}Pb/^{207}Pb$ ratios, while park samples were characterized by higher ratios, attributed to a likely natural origin. Since trace metals tend to accumulate in fine fractions, the decrease of the ratio indicated the corresponding enrichment of anthropogenic Pb in fine particle fractions of urban soils. Ultimately, these results highlight the potential risks related to human health via inhalation of Res-BS and Res-RD. Therefore, information on the distribution of PTE in fine fractions should be considered to produce a realistic assessment of the human health risks associated with metals in urban soils.

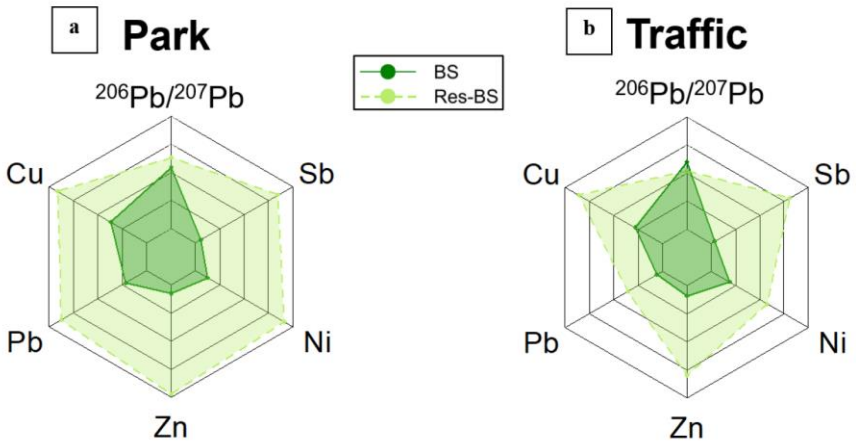

Figure 2.11. Comparison between bulk soils (BS) and resuspended fractions <10 μm (Res-BS) of soils within park (a) and traffic sites (b) using selected variables. In each diagram, average elemental concentrations for each area are normalized using Al to facilitate comparison between BS and Res-BS. The solid line represents average BS data while dashed line average Res-BS data.

CHAPTER 3

Assessment of Rare Earth Elements (REE) contamination in soils affected by urban and industrial activities.

3.1. Introduction

Among ecosystems, urban areas are one potentially more impacted from REE contamination, though limited information is present on REE contents in urban soils, especially in areas located next to industrial centers or storage hotspot as electronics-waste landfills, even though these areas relate to the highest risk (Borowiak et al., 2018; Wang et al., 2022). The concentration and distribution of REE may vary over space because of the complicated land use history and heterogeneous nature of urban soils. Studies conducted in soils near busy roads also observed REE concentration decreases with distance from the road (Mleczek et al., 2018). This information is thus significant to identify contamination hotspot areas and assess the potential polluting sources for urban management (Yuan et al., 2018). Such knowledge is essential to assess potential risks related to urban soil REE. Turin has the second-largest metropolitan area in northern Italy and a long history of industrialization and urbanization. Long-term industrial processes may lead to REE discharges directly in soils or emissions into the atmosphere and eventually deposit into soils (Sun et al., 2017; Suzuki et al., 2011).

REE are poorly soluble elements with a high affinity for oxygen. They easily precipitate or form complexes with carbonates, fluorides, phosphates or humic and fulvic acids.
In soils, REE are mainly found in mineral like fluorocarbonates, phosphates, silicates, and oxides. Adsorption/desorption phenomena may occur when these elements are present in the liquid phase of the soil, affecting their distribution within the soil (; Hu et al., 2006; Bispo et al., 2021; Sager and Wiche, 2024). These characteristics play a key role in determining the effectiveness of the chemical dissolution process.

The selection of the dissolution method is crucial to accurately determine the pseudo-total content in soil, essential to provide relevant information for environmental management and protection decisions. Therefore, it is decisive to compare and verify the applicability of the most widely used methods with certified reference materials (CRM). Unfortunately, because of limited availability of CRM for these elements, no large comparisons had been made, albeit some studies evaluated methods using some CRM reporting indicative REE values (Ferreira et al., 2021).

For a better assessment, it was deemed necessary to undertake comparison to ensure the selection of the most appropriate method to apply.

The objectives of this articles are: a) the optimization of a mineralization procedure; b) the assessment of possible contamination due to REE in urban and electronics-waste landfill soils, to determine how such activities may have contributed to the spread of REE; c) the investigation of the association of REE with well-established anthropogenic contaminants as PTE (Potentially Toxic Elements, e.g., Cr, Ni, Cu, Zn, Pb) in urban areas.

3.2. Materials and methods

3.2.1. Sampling area and method

Soil samples were taken in the urban and suburban area of Turin, the fourth largest Italian city by population, as well as the capital city of Piedmont region. Turin is in the northwest of Italy and resides on an alluvial plain formed by four rivers (Po, Sangone, Stura di Lanzo and Dora Baltea), whose sediments contributed to the parent material of the urban alluvial soils.

Turin is one of the most important economic-productive centers nationwide. In the past, it hosted several industrial activities in the metallurgical and automotive sectors. These activities may affected soil properties, often contributing to contamination, due to industrial emissions, vehicular traffic, and waste production and storage.

Urbanization strongly influences soil formation and characteristics, as original soils are often buried, truncated, removed, and compacted. Soil horizons are often irregular with anthropogenic layers and a high degree of heterogeneity (Bullock and Gregory, 1991). Moreover, redevelopment and reuse of urban spaces often involve the addition of materials from various sources, with different physical and chemical properties. Typically, organic wastes or materials such as construction debris, concrete, and bricks are found, leading a higher presence of carbon and carbonates in urban soils (Biasioli et al., 2007).

Due to this heterogeneity, urban soils are normally sampled in relation to the land uses, according to the surrounding different anthropogenic activities, at one or different depths from the surface. As in urban areas the highest risk to citizens due to contaminated soils comes from the topsoil, due to their exposure to wind erosion and resuspension of fine particles, the most indicated sampling depth is from the surface to 10 cm depth (Ajmone-Marsan et al., 2010).

To assess the potential risk due to REE within the Turin urban area, 50 sites were selected encompassing five different land uses were REE may have had different sources: roadside, industrial, park, e-waste landfill, and agricultural sites. All the agricultural sites were in the peri-urban area.

Sampling sites within the area are illustrated in Figure 3.1, while sampling coordinates in Table 3.1

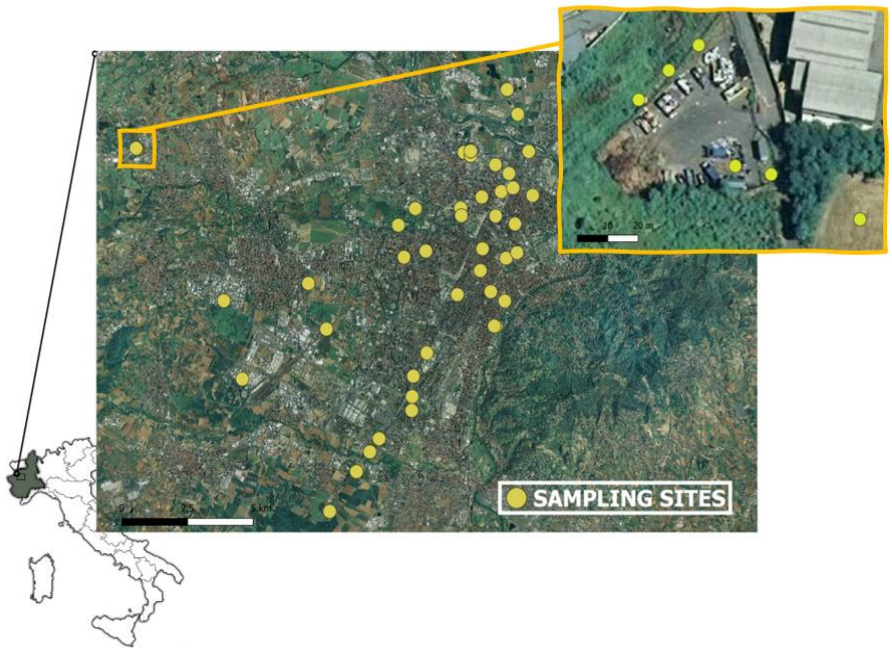

Figure 3.1. Distribution of sampling sites in urban area; the electronic-waste landfill samples are depicted in the small square.

Among samples, twenty belonged to a previous sampling campaign where only trace elements were considered (Li et al., 2021), while the other thirty have been sampled to consider all land uses within the urban area. All the samples (0-10 cm) were a composite of three sub-samples taken at 1 m away from each other, mixed and quartered on the field.

3.2.2. Analytical characterization

Samples were air-dried at room temperature and sieved through a 2-mm plastic sieve before laboratory analysis. The following chemical and

physical analyses were carried out on all samples according to the official Italian methods for soils (Colombo and Miano, 2015): pH (1:2.5, soil:water), carbonates (volumetric method, ISO 10693:1995), total carbon and nitrogen via elemental analysis (UNICUBE, Elementar Analyses System GmbH, Langensbold, Germany), texture was measured via the pipette method. The determination of amorphous and crystalline iron oxide forms was done by extraction in oxalate and sodium dithionite-citrate-bicarbonate (Colombo and Miano, 2015).
The physical-chemical characterization and the sampling coordinates of each soil sample is reported in Table 3.1.
To determine REE and other trace elements of interest, a pretreatment step involving the mineralization of the sample by microwave acid digestion is needed. To ensure the homogeneity of the samples, they were ground to 0.15 mm with an agate mortar prior to the analysis. Extraction method optimization will be discussed in detail in section 3.2.3 but, in general, the concentration of the analytes in the obtained solutions was determined by atomic emission spectroscopy with inductively coupled plasma source (ICP-OES) for the determination of Al, Cr, Mn, Fe, Ni, Cu, Zn and Pb and by inductively coupled plasma source mass spectrometry (ICP-MS) for the determination of REE. Calibration was performed by external calibration method, and standards were prepared by matrix matching method. The instrumental parameters used for the analysis are given in Table 3.2.

Table 3.1. Physical-chemical characterization of the samples and respective sampling coordinates. A=Agricultural; P= Park; R=Roadside; I=Industrial; E=E-waste landfill

ID	Land use	Coordinates		pH	Clay	Silt	Sand	Inorganic C	Organic C	Fe in amorphous oxides	Crystalline Grade
		LAT	LONG	in H_2O	%	%	%	%	%	g/kg	
REEURB1	A	44.991	7.604	7.0	5	35	60	0.1	3.7	3.9	32
REEURB2	A	45.005	7.617	5.7	6	26	68	0.1	0.7	2.6	32
REEURB3	P	45.011	7.623	6.3	3	29	68	0.1	5.3	4.9	34
REEURB4	R	45.016	7.628	7.4	5	23	72	0.1	2.1	3.2	28
REEURB5	R	45.025	7.643	6.5	4	28	68	0.1	6.3	3.6	29
REEURB6	R	45.030	7.643	7.8	5	20	75	0.2	4.6	3.3	31
REEURB7	R	45.044	7.650	7.3	4	25	71	0.1	2.4	4.2	39
REEURB8	R	45.064	7.664	7.4	3	21	76	0.1	2.7	4.7	54
REEURB9	R	45.495	7.634	7.6	3	23	74	0.1	4.4	5.9	45
REEURB10	R	45.072	7.675	7.7	7	42	51	0.1	5.8	4.5	36
REEURB11	R	45.079	7.676	7.5	6	40	54	0.3	2.7	4.9	38
REEURB12	R	45.090	7.682	7.3	1	17	82	0.1	6.3	9.8	51
REEURB13	P	45.096	7.676	7.5	6	38	56	0.1	3.4	2.8	15
REEURB14	P	45.098	7.685	6.9	5	28	67	0.0	2.1	3.4	32
REEURB15	R	45.099	7.691	7.6	5	35	61	0.2	5.3	3.9	19
REEURB16	P	45.097	7.700	7.4	7	41	52	0.1	4.9	2.6	42
REEURB17	R	45.104	7.688	7.2	6	41	53	0.0	3.3	4.9	32
REEURB18	R	45.112	7.698	7.6	0	15	85	0.1	4.7	3.2	59
REEURB19	A	45.124	7.692	6.0	2	38	60	0.0	3.2	3.6	49
REEURB20	A	45.132	7.687	6.1	1	27	72	0.0	3.4	3.3	40
REEURB21	P	45.076	7.638	7.9	4	33	63	0.3	3.1	4.2	27
REEURB22	P	45.086	7.635	8	16	47	37	0.5	*	4.7	26
REEURB23	P	45.067	7.592	7.9	12	15	73	0.8	0.0	5.9	25
REEURB24	P	45.078	7.649	7.2	6	31	62	0.4	3.5	4.5	25
REEURB25	P	45.090	7.666	8	8	28	64	0.5	1.7	4.9	23
REEURB26	P	45.092	7.665	7.8	10	34	56	0.3	1.7	9.8	22
REEURB27	R	45.060	7.552	8	11	14	75	0.2	0.1	2.8	38
REEURB28	R	45.052	7.601	7.4	13	23	65	0.1	0.3	3.4	26
REEURB29	I	45.035	7.561	6.2	8	42	51	0.3	2.4	3.7	23
REEURB30	P	45.076	7.688	7.3	4	28	69	0.8	2.0	6.5	56
REEURB31	R	45.037	7.644	6.5	5	7	88	0.2	4.9	3.6	55
REEURB32	P	45.076	7.688	5.3	15	42	43	*	1.9	10.2	45
REEURB33	I	45.092	7.643	7.1	6	14	80	0.6	3.0	4.1	55
REEURB34	R	45.087	7.692	5.4	11	15	74	*	1.9	4.3	15
REEURB35	P	45.062	7.687	7.3	3	13	84	0.6	1.6	3.6	58
REEURB36	P	45.065	7.681	7.1	9	17	74	0.7	2.7	3.3	43
REEURB37	I	45.078	7.693	6.6	5	3	92	*	4.8	4.0	53
REEURB38	I	45.090	7.666	7.9	7	11	82	2.0	1.8	3.2	36
REEURB39	P	45.054	7.683	6.9	8	8	84	0.3	0.4	3.2	25
REEURB40	P	45.054	7.682	7.1	7	28	65	0.2	1.7	3.6	46
REEURB41	P	45.111	7.667	7.5	5	33	62	0.3	2.3	5.7	31
REEURB42	I	45.110	7.670	7.3	2	18	80	0.2	8.3	3.6	35
REEURB43	I	45.111	7.670	6.9	5	29	66	0.2	5.4	3.8	26
REEURB44	I	45.107	7.682	7.5	7	41	52	0.6	4.7	7.3	35
REEURB45	E	45.110	7.509	8	4	33	63	0.7	1.9	10.6	22
REEURB46	E	45.110	7.508	7.2	3	29	69	0.1	2.8	8.9	24
REEURB47	E	45.110	7.509	7.7	3	35	62	0.2	3.3	10.7	24
REEURB48	E	45.110	7.508	7.7	3	30	66	1.1	2.6	2.3	24
REEURB49	E	45.110	7.508	7.6	3	28	69	0.3	3.1	6.9	24
REEURB50	E	45.110	7.508	7.6	4	32	64	0.3	6.4	5.4	24

Table 3.2. Instrumentation operating parameters for analytes determination

Equipment	**ICP-OES**	**ICP-MS**
Peristaltic pump speed	1.5 mL/min	0.2 rps
Argon flow (L min^{-1})	15	0.68
Auxiliary flow (L min^{-1})	0.2	0.11
Plasma Power (W)	1300	1500

3.2.3. Extraction method optimization

Due to the recent interest in REE determination, no acid dissolution method raised as standard in literature studies. To usefully evaluate results, a comparison of the most used digestion methods with certified reference materials (CRM) had been considered as necessary.
Two certified reference materials were selected for comparison: the ERM-CC690, collected from a calcareous soil in Italy, and the NIST SRM 2709 San Joaquin Soil, collected from the topsoil of a plowed field. The procedure aimed to develop a microwave acid digestion method for soil samples with different chemical properties by examining the efficiency of varying solvent combinations, proportions, and sample/solvent ratios. The tested mixtures (Table 3.3) were selected among the most used in literature for soils (Ardini et al., 2010; Cao et al., 2000; Ferrat et al., 2012; Trommetter et al., 2020).

Table 3.3. Methods tested for the extraction of certified reference samples

Method	**Acid mixture attack**	**Sample weight [g]**
A	9 ml HNO_3+ 1 ml HCl	0.1
B	5 ml *aqua regia* (3 HCl: 1 HNO_3)	0.1
C	12 ml inverted *aqua regia* (1 HCl: 3 HNO_3)	0.5
D	8 ml *aqua regia* + 2 ml H_2O_2	1

All mixtures did not involve the use of hydrofluoric acid, as the purpose was to evaluate possible anthropogenic contributions of REE through an easily applicable microwave-assisted acid digestion. The parameters used during the microwave digestion are shown in Table 3.4.

Table 3.4. Microwave extraction programme (Milestone Ethos Start D). T_1= Initial temperature [°C], T_2=final temperature [°C]

Step	Minuts	W	T_1	T_2
1	10	1200	0	200
2	15	1200	200	200
3	90	0	200	25

The selected isotopes, based on abundance and lack of mass interferences, were as follows: ^{39}Y, ^{139}La, ^{140}Ce, ^{141}Pr, ^{143},^{144},^{146}Nd, ^{147},^{149}Sm, ^{151},^{153}Eu, ^{157},^{158}Gd, ^{159}Tb, ^{163}Dy, ^{165}Ho, ^{167}Er, ^{169}Tm, ^{172},^{174}Yb, ^{175}Lu. Pm was not considered, as it is radioactive and has no stable isotopes. Tests were conducted in triplicate by different operators in two laboratories to test the reproducibility of the method.

3.2.4. Quality assurance

All laboratory ware was soaked in 5% nitric acid solution overnight and rinsed three times with ultrapure water before use. For microwave-assisted digestions, H_2O_2 was of ultrapure grade and acid addition was carried out under clean laboratory conditions. Microwave vessels were pre-cleaned with 5 mL HNO_3, 2 mL H_2O_2 and 2 mL ultrapure H_2O for 20 min at 180°C in the microwave. Acid concentrations for the digestions were as follows: 65%(v/v) HNO_3, 37% (v/v) HCl, and 30% (v/v) H_2O_2. External calibration solutions for ICP-MS (0.05-50 µg/L) and ICP-OES (0.05-3 mg/L) were prepared using the matrix matching method by diluting multi-elemental standard solutions: TraceCERT® (Sigma-Aldrich) containing 50 mg/L REE and Certipur® containing 1000 mg/l of Al, Cr, Mn, Fe, Ni, Cu, Zn and Pb, respectively. Limits of detection (LOD) values were calculated as three times the standard deviation of the reagent blank. The blank samples were prepared similarly to the samples. The results for LOD were (µg L^{-1}): Y (0.02), La (0.02), Ce (0.18), Pr (0.01), Nd (0.02), Sm (0.01), Eu (0.02), Gd (0.01), Tb (0.02), Dy (0.01), Ho (0.02), Er (0.02), Tm (0.02), Yb (0.01), Lu (0.02), Al (28), Cr (7), Mn (1.4), Fe (6.2), Ni (10), Cu (5.4), Zn (1.8), Pb (42). Concentrations of the reagent blanks were subtracted from sample concentrations to eliminate the contribution of the digestion process and storage.

3.2.5. REE-normalized patterns, fraction, anomalies and emission factors

To investigate the potential soil contamination with REE, REE-normalized patterns, REE fractionation indices and enrichment factors (EFs) were calculated. To compare the REE concentrations related to different parent materials and to identify possible contaminations, REE distribution is typically observed using normalized patterns against geological reservoirs (Bispo et al., 2021). In this study, the normalization with the Upper Continental Crust (UCC) will be used.

REE indices were calculated using UCC-normalized values to interpret the geochemical pattern (Fernández-Caliani and Grantcharova, 2021).

To display possible anthropogenic REE inputs, the EF enrichment factor was calculated using Eq. 3.1:

$$\mathrm{EF} = \frac{\frac{X_{\mathrm{sample}}}{RE_{\mathrm{sample}}}}{\frac{X_{bck}}{Re_{bck}}} \quad \text{(Eq. 3.1)}$$

where X_{sample} and RE_{sample} indicate the content of the investigated element, expressed in mg/kg, and of the reference element in the soil sample. Al was used as the reference element and the UCC values were chosen as background level. The contamination level was divided into six classes: EF<1 unenriched, 1 ≤ EF < 2 slightly enriched, 2 ≤ EF < 5 moderately enriched, 5 ≤ EF < 20, significantly enriched, 20 ≤ EF < 40 strongly enriched, and EF ≥ 40 extremely enriched.

3.2.6. Statistical analysis and PMF model

Normality and homoscedasticity of the data were checked using Shapiro-Wilk's and Levene's tests. One-way ANOVA was used to identify differences in mean values among different land use categories. Tukey-HSD test was applied for post hoc pairwise comparisons. Non-normal and homoscedastic data were compared with Kruskal-Wallis rank sum test and Dunn test. Correlation matrices were calculated using Sperman's nonparametric method. Statistical tests were performed using RStudio. Boxplots were calculated using Origin Pro23 (OriginLab Corp., Northampton, MA, USA).
Positive Matrix Factorization (PMF, Paatero and Tapper, 1994) is a factorization model for source apportionment. It has been developed for atmospheric aerosol but is widely used for different matrices (ashes, soils, road dust).
PMF is based on the mass conservation principle, thus for each sample the following equation applies:

$$x_{iJ} = \sum_{k=1}^{p} g_{ik} f_{jk} \quad i = 1,2,\dots,m \;\; j = 1,2,\dots,n$$

where x_{ij} is the i^{th} concentration of the species in the j^{th} sample, g_{ik} is the i^{th} contribution of the source k, and f_{jk} is the concentration of the species j in source k.

In this study, the PMF model was used to identify the main sources of REE in urban soils and to study the different dynamics of diverse elements. The program EPA PMF 5.0 (U.S. Environmental Protection Agency, 2014) was employed for the analysis of the dataset. To estimate the uncertainty of the species, the approach of Amato et al. (2009) was used.

For the base run, the selection of species was based on the S/N (signal to noise) ratio and on the percentage of data above detection limit (Amato et al. 2009).

A total of 25 species were selected for the analysis and the total mass was introduced as the total variable. Extra modeling uncertainty of 5% was added to account for unconsidered errors.

We explored solutions with different number of factors (3-7), and the six-factors solution was the one corresponding to meaningful sources. In the case of small datasets, the rotational ambiguity could strongly affect the modeling base solution. Thus, an exploration of the rotational ambiguity was made using the displacement (DISP) method (Paatero et al., 2014) embedded in the program on the 6-factor solution. Results indicated no significant rotational ambiguity, as the decrease in Q was lower than 1% and no factor swaps were observed for dQmax=4 and 8.

3.3. Results and discussion

3.3.1. Method development

A first extraction batch using all the defined methods (Table 3.3) was performed using the liquid to solid ratios described in literature. Results are reported in Table 3.5 for all the certified elements. The percentage yield is calculated from the total certified concentration obtained with HF. In method A and C higher recoveries were obtained for the agricultural soil (NIST SRM 2709) than for the calcareous one (ERM CC690) probably because of the presence of carbonates for the latter. Indeed, with methods B and D, using a higher amount of hydrochloric acid and a lower one of nitric acid, the differences between the certified soils are lower.

Table 3.5. Percentage extraction yields and RSD% obtained with the different methods tested, calculated over certified reference results obtained using HF extraction method.

Analyte_Isotope	METODO A NIST				METODO B NIST				METODO C NIST				METODO D NIST			
	NIST		ERM		NIST		ERM		NIST		ERM		NIST		ERM	
	Average %	RSD %	Average %	RSD %	Average %	RSD %	Average %	RSD %	Average %	RSD %	Average %	RSD %	Average %	RSD %	Average %	RSD %
Y_89	70.1	3.7	52.5	5.3	62.9	5.7	54.0	5.5	58.8	11.8	46.9	14.2	58.6	5.8	55.9	7.2
La_139	79.9	3.3	66.6	5.0	71.8	6.2	66.8	5.2	69.0	10.5	62.0	16.2	73.4	4.5	73.7	6.2
Ce_140	93.9	3.0	66.5	5.3	83.5	5.6	74.1	6.0	79.5	9.8	59.7	15.7	86.0	4.8	77.2	8.8
Nd_143	88.3	2.5	69.2	4.8	80.5	5.5	69.5	6.1	76.1	10.1	63.6	15.6	82.8	4.4	75.0	6.3
Nd_144	90.9	3.2	71.1	4.5	80.1	6.6	69.6	5.7	77.2	10.6	64.5	16.3	83.3	5.1	75.9	5.9
Nd_146	90.1	3.6	70.8	4.7	79.8	7.1	69.4	5.5	76.1	10.9	64.1	16.3	82.4	5.2	74.9	6.9
Sm_147	80.3	3.6	64.5	4.9	18.4	6.9	65.9	4.8	67.8	10.3	61.9	17.1	74.0	1.8	72.1	2.8
Sm_149	79.7	3.4	65.5	5.0	19.9	13.9	66.4	5.3	67.8	10.4	61.9	16.4	74.4	3.1	72.2	3.5
Eu_151	77.5	3.7	76.0	4.7	70.9	5.6	75.2	4.9	66.8	12.1	68.0	17.2	72.7	5.1	80.2	6.5
Eu_153	86.5	4.3	79.9	4.6	74.7	7.3	79.8	5.0	72.7	11.7	73.0	16.4	80.8	4.9	85.7	7.1
Gd_157	*n.c.*		75.9	5.7	*n.c.*		77.3	5.9	*n.c.*		67.4	16.1	*n.c.*		77.9	14.6
Gd_158	*n.c.*		65.7	5.8	*n.c.*		69.4	5.4	*n.c.*		61.8	15.3	*n.c.*		68.7	15.2
Tb_159	*n.c.*		60.7	4.8	*n.c.*		63.5	4.6	*n.c.*		55.6	14.5	*n.c.*		64.3	15.1
Dy_163	68.9	4.3	64.6	6.6	61.7	7.8	70.1	4.3	58.5	11.1	58.7	13.5	62.6	5.0	66.4	5.8
Ho_165	83.6	4.5	67.6	5.7	75.9	5.0	74.0	5.2	70.3	11.2	60.2	12.8	76.2	5.3	69.6	5.9
Tm_169	*n.c.*		56.9	5.9	*n.c.*		54.1	7.2	*n.c.*		50.3	13.4	*n.c.*		57.1	16.9
Yb_172	66.4	5.5	50.9	5.8	64.1	3.6	59.2	7.5	57.5	10.7	47.0	12.5	61.3	6.9	52.5	7.4
Yb_174	66.3	6.2	50.8	5.5	60.8	6.5	59.6	9.2	58.0	12.1	46.8	11.2	60.1	7.1	51.5	7.1
Average	**80**		**65**		**65**		**68**		**69**		**60**		**73**		**70**	

For NIST SRM 2709, the highest values were obtained with method A (80%), followed by method D (73%); both methods had the lowest extraction yields for Yb. Considering ERM CC690, the highest average recovery percentage were obtained with method D (70%) followed by method B (69%), the latter having lower recoveries for LREE. Even for the analytes certified only in ERM CC690, method D had the highest extraction recoveries. Methods A and D had also a better reproducibility, with relative standard deviations (RSD%) lower than 10%. These two promising methods were subsequently compared changing the sample/reagent ratio, by decreasing the quantity of digested samples from 1 g to 0.5 g of soil (Table 3.6). From the results obtained, method D presented the highest efficiency compared with method A for both CRMs and for all analytes in both cases (i.e., using a lower or a higher amount of sample). Method D showed higher extraction yield at the same mass-volume ratio. Subsequently, to further increase the yield for method D, we decreased the amount of soil to 0.1 g to reduce the weight-volume

ratio. The results obtained are shown in the Table 3.7. The chosen optimized method (8 ml *aqua regia*, 2 ml H_2O_2, 0.1 g of soil) exhibited an average recovery of 85% for the NIST sample and of 78% for ERM. For NIST, the analyte with the lowest recovery was Sm with the 53%, while for the ERM a lower extraction was observed for some of the HREE (e.g., Y, Tb, Tm, Yb) with an average value of 61%; probably because they are more associated with silicon oxides in soils.

Table 3.6. Percentage extraction yields obtained for method A and D weighing 0.5 g of samples

	METHOD A				METHOD D			
	NIST SRM 2709		ERM CC690		NIST SRM 2709		ERM CC690	
Analyte_Isotope	Average %	RSD %	Average %	RSD %	Average %	RSD %	Average %	RSD %
Y_89	62.72	7.0	56.77	4.4	68.88	2.8	54.28	6.7
La_139	71.48	4.3	65.82	7.7	81.47	1.8	71.58	8.0
Ce_140	85.78	3.6	64.73	8.8	96.28	1.2	74.66	9.4
Nd_143	85.2	4.9	68.84	10.8	90.89	2.5	74.23	8.4
Nd_144	82.01	5.7	67.9	9.7	88.62	2.0	73	8.5
Nd_146	82.06	3.1	69.78	8.4	89.85	2.7	73.46	6.9
Sm_147	43.42	4.9	39.81	6.6	48.45	2.4	72.73	8.7
Sm_149	43.64	3.6	39.65	8.6	49.56	3.3	73.01	7.3
Eu_151	74.3	3.4	76.6	9.4	81.47	2.6	80.67	8.0
Eu_153	86.74	5.7	83.95	8.2	90.46	1.8	84.05	7.9
Dy_163	62.74	3.0	64.61	9.2	68.98	3.2	67.21	7.7
Ho_165	77.27	4.5	69.84	8.4	86.16	4.5	72.04	8.7
Yb_172	62.22	4.9	53.11	8.6	68.89	3.6	55.23	9.6
Yb_174	61.58	4.5	52.4	9.9	67.58	3.5	54.25	8.8
Average	**69**		**62**		**77**		**70**	

Table 3.7 Percentage extraction yields obtained for method D weighing 0.1 g of sample

Analyte_Isotope	METODO D NIST		METODO D ERM	
	NIST SRM 2709		ERM CC690	
	Average %	RSD %	Average %	RSD %
Y_89	77.2	4.4	61.7	6.5
La_139	89.2	3.7	80.8	5.6
Ce_140	105.8	3.9	84.6	8.0
Nd_143	99.1	3.7	83.4	10.0
Nd_144	98.3	4.3	82.4	5.7
Nd_146	99.7	4.3	83.1	5.4
Sm_147	53.1	2.5	77.5	10.9
Sm_149	52.8	4.4	77.9	4.3
Eu_151	88.7	4.2	90.1	2.8
Eu_153	98.5	4.1	95.4	5.4
Gd_157	*n.c.*		99	5.4
Gd_158	*n.c.*		104	2.8
Tb_159	*n.c.*		69	10.3
Tm_169	*n.c.*		56	19.3
Dy_163	76.0	4.1	73.9	8.3
Ho_165	94.2	4.3	78.3	5.0
Yb_172	76.7	5.5	59.6	6.9
Yb_174	74.4	5.7	58.4	6.7
MEDIA	**85**		**79**	

3.3.2. REE pseudo-total concentration in urban soils

Urban soils exhibit significant heterogeneity, which can be partly attributed to their natural spatial variability, greatly intensified by human activities. Excavation, redistribution and mixing of the soil matrix, along with the addition of foreign materials, are common in the built environment because of the intensive and rapid changes in land use. These processes could result in the introduction of contaminants, including potentially toxic elements and less commonly monitored contaminants such as REE

The complexity and variability of urban soils make it difficult to identify relevant distribution patterns. However, some correlations between land use and REE concentrations could be identified.

Descriptive statistics of REE concentrations in the investigated soils divided by land use are reported in Table 3.8. The complete data are given in Table 3.9.

Table 3.8. Descriptive statistics of elemental concentrations of REE with the coefficient of variation in percent (CV%)

		Y	La	Ce	Pr	Nd	Sm	Eu	Gd	Tb	Dy	Ho	Er	Tm	Yb	Lu	∑REE
Agricultural	**Mean**	19.0	15.0	30.6	4.0	14.6	3.6	0.7	3.7	0.4	3.2	0.4	1.8	0.2	1.6	0.1	99
	Median	18.1	13.3	27.7	4.0	13.7	3.8	0.7	4.0	0.4	3.2	0.4	1.8	0.1	1.5	0.1	93
	RSD%	22.1	42.3	39.2	33.7	36.1	25.4	31.3	20.9	40.7	20.0	60.8	18.5	36.3	18.2	71.9	30
	Min	15.5	9.5	20.1	2.3	9.9	2.3	0.5	2.6	0.2	2.4	0.1	1.5	0.1	1.3	0.0	69
	Max	24.6	23.8	46.7	5.6	21.3	4.5	0.9	4.3	0.6	4.0	0.6	2.3	0.2	2.0	0.2	134
E-waste landfill	**Mean**	16.9	21.9	41.9	5.3	20.9	4.4	1.1	3.8	0.8	3.2	0.8	1.7	0.3	1.4	0.1	125
	Median	16.3	21.6	40.9	5.3	20.9	4.4	1.1	3.8	0.7	3.2	0.8	1.7	0.3	1.4	0.1	122
	RSD%	10.0	7.2	7.6	6.7	6.3	6.2	4.3	6.5	7.9	8.6	9.4	11.3	12.9	13.8	17.4	6
	Min	15.1	20.3	38.6	4.9	19.5	4.1	1.1	3.5	0.7	2.9	0.7	1.5	0.2	1.1	0.1	115
	Max	19.8	23.8	45.9	5.8	22.6	4.8	1.2	4.2	0.9	3.7	0.9	2.0	0.3	1.7	0.1	137
Industrial	**Mean**	15.7	15.5	33.5	3.9	16.0	2.9	0.8	3.1	0.5	2.4	0.5	1.2	0.2	1.0	0.1	97
	Median	12.1	13.8	28.1	3.4	13.9	2.9	0.7	2.9	0.4	2.3	0.4	1.1	0.2	1.0	0.1	84
	RSD%	60.7	42.9	51.4	46.8	45.8	31.0	40.9	25.9	40.1	19.1	28.2	16.4	21.5	17.0	9.6	46
	Min	10.6	9.0	18.2	2.3	9.2	1.5	0.5	2.3	0.4	2.0	0.4	1.1	0.1	0.9	0.1	61
	Max	37.1	28.9	70.1	7.7	31.2	4.0	1.5	4.6	0.9	3.4	0.8	1.6	0.2	1.4	0.2	194
Park	**Mean**	18.3	23.5	49.4	5.8	23.0	4.4	1.0	4.1	0.6	3.2	0.6	1.6	0.2	1.4	0.2	137
	Median	16.5	23.8	52.1	6.1	24.3	4.5	1.0	4.1	0.6	3.1	0.6	1.6	0.2	1.3	0.2	140
	RSD%	24.9	22.7	22.2	20.2	19.7	21.9	17.7	13.2	25.2	15.0	32.3	18.0	28.9	19.7	29.7	18
	Min	13.0	16.2	33.1	4.1	16.0	2.5	0.6	3.1	0.3	2.5	0.1	1.3	0.1	1.1	0.1	98
	Max	30.0	32.2	66.0	7.5	30.0	5.6	1.3	5.2	0.9	4.4	0.9	2.6	0.4	2.2	0.3	171
Roadside	**Mean**	16.4	17.5	36.4	4.5	17.1	3.6	0.8	3.6	0.5	2.7	0.4	1.4	0.2	1.2	0.1	106
	Median	15.9	17.9	36.4	4.5	17.9	3.8	0.9	3.7	0.5	2.6	0.5	1.3	0.2	1.1	0.1	107
	RSD%	26.2	26.2	25.4	19.5	24.5	26.9	14.7	18.7	19.3	17.0	32.5	19.7	24.3	21.4	26.9	21
	Min	10.3	9.6	19.4	3.1	9.3	1.4	0.6	2.4	0.2	2.1	0.1	1.1	0.1	0.9	0.1	68
	Max	26.3	24.5	49.9	5.9	22.5	4.7	1.0	4.5	0.6	3.9	0.7	2.1	0.2	1.8	0.2	137

The sum of the REE concentrations (∑REE) spans over a wide range, from 70 mg/kg to 202 mg/kg, with an average value of 126 mg/kg. Parks showed the highest average (147 mg/kg), followed by E-waste landfill (133 mg/kg), Roadside (117 mg/kg), Agricultural (110 mg/kg), and Industrial areas (106 mg/kg). However, the sample with the maximum value was in an industrial site (REEURB29), presenting higher concentrations than those found by Liu et al. (2023) in urban soils near industrial sites. REEURB29 site is in an intermodal combined transport area, which serves as a hub for incoming goods into the city. It has customs warehouses and a railway yard. This involves a heavy traffic of heavy vehicles. In addition, there is a waste-to-energy plant for municipal and non-hazardous waste in the immediate vicinity. Anthropogenic activities may have caused the high total REE

concentration (Funari et al., 2016; Mleczek et al., 2021; Yuksekdag et al., 2021).

Examining separately the LREE and HREE contents, LREE showed a higher contribution and variability than HREE for all land use types, ranging from 41 mg/kg to 143 mg/kg, with mean value decreasing in the following order: Park (107 mg/kg)> E-waste landfill (96 mg/kg)> Roadside (80 mg/kg)> Industrial (73 mg/kg)> Agricultural (68 mg/kg). The highest values were found at park sites adjacent to roads with high vehicle flows and at the site of an historic tire factory. In contrast, the HREE showed a lower variability between the different sites, with values from 18 mg/kg to 50 mg/kg. Among the land uses, the mean values were: Agricultural (30.4 mg/kg)> Park (30.2 mg/kg) > E-waste landfill (29 mg/kg)> Roadside (27 mg/kg)> Industrial (25 mg/kg). Naccarato et al. (2020) outlined the impact of agrochemical treatments in Italy, showing an accumulation of REE in soils linked mostly to continuous fertilizers application over time with values, for some HREE (Sm, Yb, Er, Tm, Gd, Dy and Y) 5-11 times greater than in the control. This is due to the presence, among P-fertilizers, of natural REE-rich phosphates, due to the high affinity of REE for P compounds (Martin and McCulloch, 1999). The agricultural site with the highest HREE values (REEURB1) is currently in use with possible fertilizer application.

The REEURB20 site, in the periurban area, showed also high concentrations (38 mg/kg) but the HREE presence could be due to a recycling center for scrap metal and steel products in the immediate vicinity. Supporting this hypothesis is the above average presence of HREE in sites near metallurgical industries, with no apparent relation to the current land use (sites REEURB4, REEURB22, REEURB25 and REEURB39, with 40 mg/kg, 38 mg/kg, 44 mg/kg, 50 mg/kg, 38 mg/kg, respectively).

Looking at the individual REE content, average and concentration ranges of all elements are reported in Table 3.8. Ce, compared to all other REE, had the highest concentrations on average, followed by La, Nd, Y. Parks had the highest concentrations of La, Ce, Pr, Nd, Gd, and Lu, followed by the E-waste landfill sites, having uppermost concentrations of Sm, Eu, Tb, Dy, Ho, and Tm. Finally, soils used for agricultural activities in peri-urban areas exhibited higher concentrations of Y, Er, and Yb.

Table 3.9. REE's pseudo-total concentrations and standard deviation among two replicates

ID	*Y*	*La*	*Ce*	*Pr*	*Nd*	*Sm*	*Eu*	*Gd*	*Tb*	*Dy*	*Ho*	*Er*	*Tm*	*Yb*	*Lu*
	mg/kg	*mg/kg*	*mg/kg*	*mg/kg*	*mg/kg*	*mg/kg*	*mg/kg*	*mg/kg*	*mg/kg*	*mg/kg*	*mg/kg*	*mg/kg*	*mg/kg*	*mg/kg*	*mg/kg*
REEURB1	*20.0*	*23.8*	*46.7*	*5.6*	*21.3*	*4.5*	*0.9*	*4.3*	*0.4*	*3.2*	*0.2*	*1.7*	*0.1*	*1.4*	*0.1*
± SD	*1.1*	*1.2*	*1.4*	*0.2*	*0.4*	*0.0*	*0.0*	*0.1*	*0.0*	*0.2*	*0.1*	*0.1*	*0.0*	*0.1*	*0.0*
REEURB2	*15.5*	*11.4*	*23.1*	*4.1*	*11.0*	*3.7*	*0.5*	*3.7*	*0.6*	*3.2*	*0.6*	*1.8*	*0.2*	*1.7*	*0.2*
± SD	*1.6*	*0.9*	*1.7*	*0.2*	*0.8*	*0.2*	*0.0*	*0.2*	*0.0*	*0.2*	*0.0*	*0.1*	*0.0*	*0.2*	*0.0*
REEURB3	*22.9*	*29.3*	*59.1*	*7.1*	*27.6*	*5.6*	*1.1*	*5.2*	*0.6*	*3.6*	*0.6*	*1.7*	*0.2*	*1.3*	*0.1*
± SD	*0.4*	*0.6*	*0.9*	*0.2*	*0.4*	*0.1*	*0.0*	*0.1*	*0.0*	*0.0*	*0.0*	*0.0*	*0.0*	*0.0*	*0.0*
REEURB4	*26.3*	*16.2*	*34.1*	*4.3*	*17.4*	*4.2*	*0.9*	*4.3*	*0.6*	*3.9*	*0.7*	*2.1*	*0.2*	*1.8*	*0.2*
± SD	*1.2*	*0.4*	*1.4*	*0.2*	*0.6*	*0.1*	*0.0*	*0.1*	*0.0*	*0.1*	*0.0*	*0.1*	*0.0*	*0.1*	*0.0*
REEURB5	*17.6*	*22.7*	*45.5*	*5.6*	*21.4*	*4.4*	*0.9*	*4.2*	*0.5*	*2.8*	*0.5*	*1.3*	*0.1*	*1.1*	*0.1*
± SD	*1.2*	*1.3*	*1.6*	*0.2*	*0.8*	*0.1*	*0.0*	*0.2*	*0.0*	*0.3*	*0.1*	*0.1*	*0.0*	*0.1*	*0.0*
REEURB6	*19.0*	*21.5*	*44.9*	*5.4*	*21.4*	*4.5*	*1.0*	*4.4*	*0.5*	*3.0*	*0.5*	*1.5*	*0.2*	*1.2*	*0.1*
± SD	*1.3*	*1.3*	*2.8*	*0.4*	*1.3*	*0.2*	*0.1*	*0.3*	*0.0*	*0.2*	*0.0*	*0.1*	*0.0*	*0.1*	*0.0*
REEURB7	*13.9*	*12.4*	*26.3*	*3.2*	*12.9*	*2.8*	*0.6*	*2.8*	*0.3*	*2.1*	*0.4*	*1.1*	*0.1*	*0.9*	*0.1*
± SD	*1.5*	*0.4*	*1.2*	*0.2*	*0.6*	*0.2*	*0.1*	*0.3*	*0.0*	*0.2*	*0.0*	*0.1*	*0.0*	*0.1*	*0.0*
REEURB8	*16.7*	*20.4*	*42.6*	*5.1*	*19.8*	*4.1*	*0.9*	*3.9*	*0.5*	*2.7*	*0.4*	*1.3*	*0.1*	*1.0*	*0.1*
± SD	*1.4*	*1.2*	*1.5*	*0.3*	*1.2*	*0.3*	*0.1*	*0.3*	*0.0*	*0.2*	*0.0*	*0.1*	*0.0*	*0.1*	*0.0*
REEURB9	*10.3*	*11.7*	*22.8*	*4.4*	*10.8*	*3.7*	*0.8*	*3.5*	*0.5*	*2.4*	*0.4*	*1.3*	*0.1*	*1.0*	*0.1*
± SD	*0.5*	*1.0*	*1.9*	*0.5*	*0.7*	*0.3*	*0.1*	*0.3*	*0.0*	*0.2*	*0.0*	*0.1*	*0.0*	*0.1*	*0.0*
REEURB10	*15.8*	*22.8*	*46.7*	*5.6*	*21.4*	*4.3*	*0.9*	*4.0*	*0.5*	*2.6*	*0.4*	*1.3*	*0.1*	*1.0*	*0.1*
± SD	*1.7*	*2.9*	*5.1*	*0.6*	*2.1*	*0.4*	*0.1*	*0.3*	*0.0*	*0.2*	*0.0*	*0.1*	*0.0*	*0.1*	*0.0*
REEURB11	*17.6*	*24.5*	*49.9*	*5.9*	*22.5*	*4.7*	*1.0*	*4.5*	*0.4*	*3.0*	*0.2*	*1.5*	*0.1*	*1.2*	*0.1*
± SD	*1.8*	*2.2*	*4.6*	*0.5*	*2.2*	*0.4*	*0.1*	*0.4*	*0.0*	*0.3*	*0.0*	*0.1*	*0.0*	*0.1*	*0.0*
REEURB12	*14.4*	*15.8*	*33.2*	*3.7*	*14.9*	*3.2*	*0.7*	*3.2*	*0.2*	*2.3*	*0.1*	*1.3*	*0.1*	*1.0*	*0.1*
± SD	*0.0*	*0.6*	*1.1*	*0.2*	*0.8*	*0.2*	*0.0*	*0.1*	*0.0*	*0.1*	*0.0*	*0.0*	*0.0*	*0.0*	*0.0*
REEURB13	*15.8*	*16.3*	*33.1*	*4.2*	*16.7*	*3.8*	*0.9*	*4.1*	*0.5*	*2.7*	*0.5*	*1.3*	*0.2*	*1.1*	*0.2*

± SD	0.3	0.4	0.9	0.2	1.0	0.3	0.1	0.2	0.0	0.0	0.0	0.0	0.0	0.0	0.0
REEURB14	15.7	17.4	35.2	4.1	16.0	3.4	0.6	3.3	0.3	2.5	0.1	1.3	0.1	1.2	0.1
± SD	1.9	1.8	3.1	0.3	0.8	0.2	0.0	0.3	0.0	0.3	0.1	0.2	0.0	0.1	0.0
REEURB15	13.2	16.9	34.1	4.3	16.5	3.6	0.8	3.9	0.5	2.3	0.4	1.1	0.1	0.9	0.1
± SD	0.9	0.6	1.1	0.1	0.3	0.1	0.0	0.1	0.0	0.1	0.0	0.1	0.0	0.0	0.0
REEURB16	16.0	20.6	41.1	4.9	19.2	4.1	0.9	3.9	0.3	2.7	0.2	1.4	0.1	1.1	0.1
± SD	1.3	1.7	2.7	0.4	1.5	0.3	0.1	0.2	0.1	0.3	0.1	0.1	0.0	0.1	0.0
REEURB17	22.3	19.2	40.8	4.8	18.9	4.2	0.9	4.3	0.4	3.6	0.4	2.0	0.2	1.7	0.1
± SD	0.6	1.2	2.1	0.3	0.9	0.1	0.0	0.2	0.1	0.1	0.1	0.0	0.0	0.0	0.0
REEURB18	11.3	9.6	19.4	4.0	9.3	3.5	0.8	3.5	0.5	2.8	0.5	1.5	0.2	1.2	0.1
± SD	0.4	0.3	0.8	0.3	0.4	0.3	0.0	0.2	0.0	0.0	0.0	0.0	0.0	0.0	0.0
REEURB19	16.1	9.5	20.1	2.3	9.9	2.3	0.5	2.6	0.2	2.4	0.1	1.5	0.1	1.3	0.1
± SD	4.2	2.4	5.0	0.6	2.5	0.6	0.2	0.7	0.1	0.7	0.1	0.4	0.0	0.3	0.0
REEURB20	24.6	15.3	32.3	4.0	16.5	3.9	0.9	4.3	0.5	4.0	0.5	2.3	0.1	2.0	<LOQ
± SD	1.3	0.3	0.1	0.1	0.0	0.0	0.0	0.0	0.0	0.1	0.0	0.1	0.0	0.1	
REEURB21	17.94	26.11	56.61	6.45	25.89	4.71	1.04	4.08	0.61	3.26	0.61	1.65	0.20	1.31	0.15
± SD	4.16	0.88	2.62	0.25	1.05	0.22	0.06	0.17	0.02	0.13	0.02	0.04	0.00	0.05	0.01
REEURB22	26.32	23.84	51.63	5.64	23.43	2.49	1.20	3.62	0.74	2.97	0.67	1.39	0.21	1.28	0.15
± SD	3.54	3.23	6.44	0.68	2.64	0.29	0.14	0.34	0.07	0.26	0.06	0.14	0.02	0.11	0.01
REEURB23	16.48	29.74	63.91	7.35	29.43	5.38	1.17	4.68	0.70	3.54	0.67	1.77	0.20	1.33	0.16
± SD	1.49	3.70	8.80	0.92	3.61	0.65	0.12	0.54	0.07	0.34	0.06	0.17	0.02	0.12	0.01
REEURB24	14.59	24.97	53.13	6.15	24.69	4.46	0.99	3.93	0.60	3.09	0.58	1.58	0.19	1.24	0.15
± SD	1.06	1.51	3.40	0.39	1.49	0.26	0.06	0.27	0.04	0.18	0.04	0.12	0.02	0.15	0.02
REEURB25	30.02	23.66	57.90	6.41	26.17	2.86	1.32	4.34	0.88	3.71	0.84	1.88	0.27	1.72	0.20
± SD	2.49	1.62	5.11	0.50	2.18	0.20	0.09	0.39	0.06	0.24	0.07	0.16	0.02	0.13	0.01
REEURB26	17.00	30.66	65.98	7.53	30.05	5.56	1.20	4.80	0.70	3.71	0.67	1.80	0.22	1.39	0.16
± SD	1.44	3.10	7.67	0.76	2.88	0.54	0.12	0.42	0.06	0.33	0.06	0.15	0.02	0.11	0.01
REEURB27	21.81	13.94	31.23	3.43	13.89	1.51	0.76	2.40	0.55	2.29	0.61	1.19	0.20	1.11	0.13
± SD	1.79	1.17	2.93	0.32	1.14	0.16	0.06	0.18	0.04	0.12	0.03	0.05	0.01	0.04	0.01

REEURB28	*13.37*	*20.69*	*44.56*	*5.13*	*20.68*	*3.71*	*0.86*	*3.37*	*0.52*	*2.73*	*0.52*	*1.40*	*0.17*	*1.11*	*0.13*
± SD	*0.99*	*1.59*	*3.37*	*0.38*	*1.39*	*0.24*	*0.03*	*0.21*	*0.04*	*0.22*	*0.04*	*0.11*	*0.01*	*0.07*	*0.01*
REEURB29	*37.09*	*28.91*	*70.15*	*7.68*	*31.19*	*3.98*	*1.53*	*4.65*	*0.94*	*3.39*	*0.79*	*1.60*	*0.24*	*1.38*	*0.16*
± SD	*21.26*	*3.83*	*9.83*	*0.78*	*3.56*	*1.20*	*0.18*	*0.56*	*0.11*	*0.45*	*0.08*	*0.13*	*0.02*	*0.21*	*0.02*
REEURB30	*12.98*	*16.18*	*34.39*	*4.06*	*16.81*	*3.17*	*0.77*	*3.05*	*0.48*	*2.61*	*0.50*	*1.37*	*0.16*	*1.10*	*0.13*
± SD	*1.25*	*3.38*	*7.72*	*0.89*	*3.62*	*0.63*	*0.12*	*0.49*	*0.06*	*0.27*	*0.05*	*0.14*	*0.02*	*0.10*	*0.01*
REEURB31	*15.88*	*12.01*	*27.13*	*3.10*	*12.67*	*1.43*	*0.60*	*2.50*	*0.50*	*2.55*	*0.58*	*1.43*	*0.20*	*1.42*	*0.17*
± SD	*1.16*	*0.88*	*1.96*	*0.22*	*0.46*	*0.10*	*0.05*	*0.09*	*0.02*	*0.12*	*0.04*	*0.04*	*0.01*	*0.05*	*0.01*
REEURB32	*15.28*	*17.61*	*39.98*	*4.85*	*19.75*	*4.32*	*0.92*	*3.67*	*0.55*	*2.99*	*0.59*	*1.60*	*0.21*	*1.28*	*0.17*
± SD	*0.99*	*3.44*	*0.36*	*0.07*	*0.16*	*0.10*	*0.02*	*0.09*	*0.02*	*0.13*	*0.03*	*0.08*	*0.02*	*0.07*	*0.01*
REEURB33	*10.57*	*12.73*	*28.10*	*3.19*	*13.34*	*1.49*	*0.83*	*2.33*	*0.53*	*2.12*	*0.53*	*1.07*	*0.17*	*1.01*	*0.13*
± SD	*1.02*	*1.68*	*3.71*	*0.46*	*1.77*	*0.22*	*0.06*	*0.27*	*0.05*	*0.22*	*0.03*	*0.09*	*0.01*	*0.07*	*0.01*
REEURB34	*12.94*	*18.91*	*38.75*	*4.62*	*18.35*	*3.82*	*0.71*	*3.11*	*0.46*	*2.56*	*0.48*	*1.34*	*0.18*	*1.12*	*0.15*
± SD	*0.63*	*2.15*	*3.92*	*0.50*	*1.83*	*0.31*	*0.04*	*0.19*	*0.01*	*0.09*	*0.02*	*0.09*	*0.01*	*0.07*	*0.01*
REEURB35	*17.30*	*27.85*	*56.04*	*6.56*	*25.50*	*5.14*	*0.91*	*4.19*	*0.62*	*3.42*	*0.66*	*1.78*	*0.24*	*1.53*	*0.20*
± SD	*2.21*	*4.31*	*8.80*	*1.03*	*4.04*	*0.78*	*0.13*	*0.60*	*0.08*	*0.40*	*0.07*	*0.20*	*0.03*	*0.17*	*0.02*
REEURB36	*15.28*	*25.58*	*52.12*	*6.19*	*24.30*	*4.98*	*0.99*	*4.02*	*0.59*	*3.11*	*0.59*	*1.57*	*0.21*	*1.27*	*0.17*
± SD	*0.69*	*1.98*	*4.05*	*0.49*	*1.72*	*0.27*	*0.04*	*0.20*	*0.02*	*0.12*	*0.03*	*0.07*	*0.01*	*0.06*	*0.01*
REEURB37	*12.13*	*13.78*	*27.95*	*3.42*	*13.88*	*2.92*	*0.65*	*2.59*	*0.40*	*2.30*	*0.46*	*1.25*	*0.17*	*1.09*	*0.15*
± SD	*1.48*	*1.74*	*3.05*	*0.33*	*1.26*	*0.25*	*0.06*	*0.24*	*0.04*	*0.23*	*0.06*	*0.14*	*0.02*	*0.13*	*0.02*
REEURB38	*10.71*	*18.60*	*37.48*	*4.63*	*18.29*	*3.94*	*0.82*	*3.10*	*0.43*	*2.32*	*0.43*	*1.13*	*0.15*	*0.93*	*0.13*
± SD	*1.25*	*0.92*	*2.16*	*0.26*	*1.23*	*0.51*	*0.11*	*0.31*	*0.03*	*0.19*	*0.03*	*0.07*	*0.01*	*0.06*	*0.01*
REEURB39	*22.15*	*20.37*	*42.86*	*5.61*	*22.45*	*4.96*	*0.90*	*4.56*	*0.76*	*4.40*	*0.91*	*2.58*	*0.37*	*2.20*	*0.32*
± SD	*2.19*	*2.19*	*2.19*	*2.19*	*2.19*	*2.19*	*2.19*	*2.19*	*2.19*	*2.19*	*2.19*	*2.19*	*2.19*	*2.19*	*2.19*
REEURB40	*15.70*	*32.18*	*59.36*	*6.77*	*26.09*	*5.08*	*1.11*	*4.22*	*0.59*	*3.09*	*0.59*	*1.52*	*0.20*	*1.27*	*0.17*
± SD	*0.60*	*0.41*	*1.13*	*0.14*	*0.51*	*0.05*	*0.03*	*0.07*	*0.02*	*0.11*	*0.03*	*0.06*	*0.01*	*0.05*	*0.01*
REEURB41	*19.5*	*17.8*	*36.8*	*4.3*	*17.7*	*4.0*	*0.9*	*4.2*	*0.6*	*3.3*	*0.6*	*1.7*	*0.2*	*1.5*	*0.2*
± SD	*1.6*	*1.0*	*2.4*	*0.4*	*1.2*	*0.3*	*0.1*	*0.3*	*0.1*	*0.3*	*0.1*	*0.1*	*0.0*	*0.1*	*0.0*
REEURB42	*11.9*	*9.0*	*18.2*	*2.3*	*9.2*	*2.2*	*0.5*	*2.5*	*0.4*	*2.0*	*0.4*	*1.1*	*0.1*	*0.9*	*0.1*

± SD	*1.1*	*0.4*	*0.8*	*0.1*	*0.6*	*0.1*	*0.0*	*0.2*	*0.0*	*0.2*	*0.0*	*0.1*	*0.0*	*0.1*	*0.0*
REEURB43	*15.1*	*10.6*	*22.6*	*2.5*	*11.1*	*2.6*	*0.6*	*2.9*	*0.4*	*2.4*	*0.4*	*1.3*	*0.2*	*1.2*	*0.2*
± SD	*3.1*	*2.1*	*4.3*	*0.5*	*2.1*	*0.5*	*0.1*	*0.6*	*0.1*	*0.5*	*0.1*	*0.3*	*0.0*	*0.2*	*0.0*
REEURB44	*12.6*	*15.0*	*30.1*	*3.7*	*14.7*	*3.2*	*0.7*	*3.4*	*0.5*	*2.2*	*0.4*	*1.1*	*0.1*	*0.9*	*0.1*
± SD	*0.4*	*1.0*	*2.3*	*0.3*	*1.3*	*0.3*	*0.1*	*0.3*	*0.0*	*0.1*	*0.0*	*0.0*	*0.0*	*0.0*	*0.0*
REEURB45	*15.14*	*23.80*	*45.86*	*5.74*	*22.21*	*4.61*	*1.19*	*3.81*	*0.74*	*2.93*	*0.72*	*1.46*	*0.23*	*1.12*	*0.11*
± SD	*1.46*	*1.04*	*1.58*	*0.23*	*0.91*	*0.15*	*0.07*	*0.19*	*0.05*	*0.25*	*0.07*	*0.12*	*0.02*	*0.09*	*0.01*
REEURB46	*19.79*	*23.81*	*45.70*	*5.77*	*22.58*	*4.77*	*1.17*	*4.21*	*0.88*	*3.71*	*0.92*	*2.02*	*0.33*	*1.66*	*0.09*
± SD	*2.03*	*1.09*	*1.35*	*0.17*	*0.83*	*0.21*	*0.07*	*0.24*	*0.12*	*0.14*	*0.09*	*0.13*	*0.01*	*0.08*	*0.01*
REEURB47	*17.81*	*20.54*	*39.30*	*5.00*	*19.52*	*4.08*	*1.07*	*3.61*	*0.75*	*3.29*	*0.82*	*1.75*	*0.28*	*1.42*	*0.14*
± SD	*0.67*	*2.21*	*4.12*	*0.53*	*1.93*	*0.36*	*0.07*	*0.26*	*0.03*	*0.11*	*0.03*	*0.04*	*0.00*	*0.01*	*0.01*
REEURB48	*16.51*	*21.03*	*40.23*	*5.23*	*20.55*	*4.35*	*1.09*	*3.72*	*0.73*	*3.19*	*0.77*	*1.63*	*0.27*	*1.35*	*0.14*
± SD	*2.92*	*3.89*	*6.65*	*0.88*	*3.44*	*0.68*	*0.16*	*0.56*	*0.15*	*0.48*	*0.13*	*0.23*	*0.03*	*0.18*	*0.02*
REEURB49	*16.06*	*22.07*	*41.56*	*5.40*	*21.24*	*4.47*	*1.17*	*3.91*	*0.80*	*3.30*	*0.81*	*1.70*	*0.27*	*1.36*	*0.14*
± SD	*1.34*	*1.60*	*3.02*	*0.41*	*1.65*	*0.33*	*0.09*	*0.26*	*0.06*	*0.22*	*0.06*	*0.14*	*0.02*	*0.11*	*0.01*
REEURB50	*15.89*	*20.25*	*38.60*	*4.93*	*19.50*	*4.11*	*1.12*	*3.51*	*0.71*	*2.98*	*0.74*	*1.56*	*0.24*	*1.22*	*0.13*
± SD	*1.12*	*0.78*	*1.25*	*0.21*	*0.85*	*0.19*	*0.05*	*0.16*	*0.04*	*0.21*	*0.07*	*0.11*	*0.02*	*0.09*	*0.01*

High concentrations in urban parks have already been observed while studying potentially toxic metals; this condition was likely explained by the lower frequency of reworking and land use changes, allowing the accumulation of contaminants over time through wet and dry atmospheric deposition. This hypothesis for REE is supported by Shajib et al. (2020), whom reported a strong influence of antecedent dry days on the La, Ce, Pr and Nd concentrations in the runoff of a low trafficked urban area. The parks with the highest concentrations are those located near industrial areas. According to Liu et al. (2023), the number of industrial enterprises is an important factor contributing to the variability of REE presence: high concentrations were found in Bejing urban park soils located near industrial area. In our study, industrial sites showed the highest coefficients of variation (CV%) for most REE. REE were found to be the most used in the metallurgical, glass and catalyst industries (Lima and Ottosen, 2021). Although these industries do not directly produce REE, the extensive use in additives, catalysts, alloys, polishing compounds and oil refinery releases large amounts of REE into the environment (Gwenzi et al., 2018; Pagano et al., 2019).

3.3.3. Soil contamination assessment

Several parameters (i.e., EFs, REE-normalized patterns and fractionation) representative of soil contamination processes were used to assess REE anomalies in an urban area affected by anthropogenic impact. They are conventionally used as environmental tracers to assess whether these anomalies are related to anthropogenic contamination or abundance in the parent material.

3.3.4. Enrichment factors (EFs)

Enrichment Factors (EFs) are commonly used to evaluate the intensity of soil contamination, as they allow to hypothesize the natural or anthropogenic origin of a contaminant by comparing its concentrations with those of a reference element and with background values. The reference element is assumed as immobile in soils, and not affected by contamination. For the present study, Al was chosen as the reference element and Upper Continental Crust (UCC) as background values. EFs results are shown in Table 3.10. On average, no REE exceeded moderate enrichment values. Gd, Tb, Ho and Yb displayed maximum values with significant enrichment at the roadside site REEURB31. Gd, on the other hand, showed moderate to significant enrichment in almost all samples considered. Deserving attention are the results from the e-waste landfill site, revealing modest Eu, Gd, Tb, Dy and Ho enrichments. Similar levels were also found at some industrial and roadside sites located near industrial areas. Overall, enrichment emerges in areas affected by industrial activities and high vehicular flow, but REE EFs do

not delineate a critical REE contamination. However, more accurate results could be obtained with are-specific background values.

Table 3.10. REE enrichment factors (EF) calculated using Al as a reference element and UCC as background values.

ID	Y	La	Ce	Pr	Nd	Sm	Eu	Gd	Tb	Dy	Ho	Er	Tm	Yb	Lu
REEURB1	2	1	1	2	1	2	2	3	1	2	1	1	0	2	1
REEURB2	1	1	1	1	1	1	1	2	2	2	2	1	1	2	1
REEURB3	2	1	1	2	2	2	2	3	2	2	2	1	1	1	1
REEURB4	3	1	1	2	2	2	2	4	3	4	3	2	1	3	2
REEURB5	2	2	2	2	2	2	2	4	3	3	2	1	1	2	1
REEURB6	3	2	2	2	2	3	3	4	3	3	2	1	1	2	1
REEURB7	3	1	2	2	2	2	2	4	3	3	2	1	1	2	1
REEURB8	2	1	1	2	2	2	2	3	2	2	2	1	1	2	1
REEURB9	1	1	1	2	1	2	2	3	2	2	2	1	1	2	1
REEURB10	2	2	2	2	2	2	2	3	2	2	2	1	1	1	1
REEURB11	2	1	1	2	2	2	2	3	1	2	1	1	0	1	1
REEURB12	2	1	1	2	1	2	2	3	1	2	0	1	0	2	1
REEURB13	2	1	1	1	1	2	2	3	2	2	2	1	1	2	1
REEURB14	2	2	2	2	2	2	2	3	2	3	1	1	1	2	1
REEURB15	1	1	1	1	1	2	2	3	2	2	2	1	1	1	1
REEURB16	1	1	1	1	1	2	2	3	1	2	1	1	0	1	1
REEURB17	2	1	1	1	1	2	2	3	2	2	1	1	1	2	1
REEURB18	1	1	1	1	1	2	2	3	2	2	2	1	1	2	1
REEURB19	2	1	1	1	1	1	1	3	1	2	1	1	1	2	1
REEURB20	2	1	1	1	1	1	2	3	2	2	1	1	0	2	0
REEURB21	2	2	2	2	2	2	2	3	3	2	2	1	1	2	1
REEURB22	3	2	2	2	2	1	3	3	4	3	3	1	1	2	1
REEURB23	2	2	2	3	3	3	3	4	3	3	3	1	1	2	1
REEURB24	2	2	2	2	2	2	2	3	3	2	2	1	1	2	1
REEURB25	3	2	2	2	2	1	3	3	4	3	3	1	1	2	1
REEURB26	2	2	2	2	2	2	2	3	3	3	2	1	1	2	1
REEURB27	4	2	2	2	2	1	3	3	4	3	4	1	2	3	2
REEURB28	2	2	2	2	2	2	3	4	3	3	3	1	1	2	1
REEURB29	4	2	2	3	3	2	3	4	4	3	3	1	1	2	1
REEURB30	2	1	2	2	2	2	2	3	3	3	2	1	1	2	1
REEURB31	4	2	2	3	2	2	3	5	5	4	5	2	2	5	3
REEURB32	1	1	1	2	2	2	2	3	2	2	2	1	1	2	1
REEURB33	2	1	2	2	2	1	3	3	4	3	3	1	1	2	2
REEURB34	2	2	2	3	3	3	3	4	3	3	3	1	1	3	2
REEURB35	2	2	2	3	3	3	3	4	3	3	3	1	1	3	2
REEURB36	2	2	2	2	2	3	2	4	3	3	2	1	1	2	1
REEURB37	2	2	2	2	2	2	3	4	3	3	3	1	1	3	2
REEURB38	2	2	2	2	2	3	3	4	3	3	2	1	1	2	1
REEURB39	3	2	2	2	2	3	2	4	4	4	4	2	2	4	3
REEURB40	2	3	3	3	3	3	3	4	3	3	3	1	1	2	2
REEURB41	3	2	2	2	2	2	2	4	3	3	3	1	1	3	2
REEURB42	2	1	1	1	1	2	2	4	3	3	3	1	1	2	2
REEURB43	3	1	1	2	2	2	2	4	3	3	3	1	1	3	2
REEURB44	2	1	1	2	2	2	2	3	2	2	2	1	1	2	1
REEURB45	2	2	2	2	2	2	3	3	4	2	3	1	1	2	1
REEURB46	2	2	2	2	2	2	3	3	4	3	3	1	1	3	1
REEURB47	2	2	2	2	2	2	3	3	4	3	4	1	2	3	1
REEURB48	2	2	2	2	2	3	3	4	4	3	4	1	2	3	1
REEURB49	2	2	2	2	2	3	3	4	4	3	4	1	1	2	1
REEURB50	2	1	1	2	2	2	3	3	3	2	3	1	1	2	1

3.3.5. REE-normalized patterns and fractionation

To discriminate between natural REE variation and anthropogenic impacts on the urban soils considered, the determined REE concentrations were normalized for the REE concentrations in the UCC. Normalization is used to eliminate the marked change in concentrations between lanthanides with even or odd atomic numbers, as their distribution respects the abundance of the elements indicated by the Oddo-Harkins rule (Harkins, 1917; Oddo, 1914). REE-normalized concentrations highlight the enrichment (if the number is above 1) or depletion of one group or individual REE relatively to others. From this we could derive insights into REE partitioning (Coppin et al., 2002; Laveuf and Cornu, 2009).

The REE-normalized concentrations and related descriptive statistics are reported in Table 3.11 (a-b). These data are also usually represented in order of increasing atomic number (REE patterns). The resulting graphs is shown in Figure 3.2 (a-b).

In general, examining the REE-normalized mean value pattern (Figure 3.2a) reveals a depletion trend from Y to Sm, and from Dy to Lu across all land uses in comparison to UCC. Eu and Tb anomalies could be due to their presence in optoelectronic materials (e.g., cathode-ray tubes and magneto-optical disks. Tb and Eu positive anomalies have also been reported for airborne particulate matter, inducing higher diffuse concentrations in urban areas (Suzuki et al., 2011, 2010; Yan et al., 2020). The normalization does not display a flat or characteristic/representative pattern for Turin soils. Instead, it has a very heterogeneous shape even between neighboring sites, revealing a distinct lanthanide pattern signature between the land uses. This could be justified both by the anthropogenic contribution and by the frequent use changes to which urban soils are subjected, with possible introduction of extraneous materials during their use. The urban context is the result of a mix of sources: contemporary vehicular traffic and the extensive industrial activity in the metallurgical-mechanical sector that characterized Turin in the 1900s. This period involved the massive use of coal as a fuel, which likely contributed to the presence of REEs (Dai et al., 2016).

Table 3.11 (a-b). REE concentrations in Turin urban soils normalized to Upper Continental Crust (UCC) values (a) and related descriptive statistics (b).

a)

ID	Soil type	La/La$_{UCC}$	Ce/Ce $_{UCC}$	Pr/Pr$_{UCC}$	Nd/Nd $_{UCC}$	Sm/Sm$_{UCC}$	Eu/Eu$_{UCC}$	Gd/Gd$_{UCC}$	Tb/Tb$_{UCC}$	Dy/Dy$_{UCC}$	Ho/Ho$_{UCC}$	Er/Er$_{UCC}$	Tm/Tm$_{UCC}$	Yb/Yb$_{UCC}$	Lu/Lu$_{UCC}$
REEURB1	A	0.8	0.7	0.8	0.9	1.0	1.0	1.1	0.6	0.9	0.3	0.7	0.4	0.6	0.4
REEURB2	A	0.4	0.4	0.6	0.4	0.8	0.6	1.0	0.9	0.9	0.8	0.8	0.7	0.8	0.6
REEURB3	P	1.0	0.9	1.0	1.1	1.3	1.3	1.4	1.0	1.0	0.7	0.8	0.5	0.6	0.4
REEURB4	R	0.5	0.5	0.6	0.7	0.9	1.0	1.1	0.9	1.1	0.9	0.9	0.7	0.8	0.6
REEURB5	R	0.8	0.7	0.8	0.9	1.0	1.0	1.1	0.8	0.8	0.6	0.6	0.5	0.5	0.3
REEURB6	R	0.7	0.7	0.8	0.9	1.0	1.1	1.1	0.8	0.9	0.6	0.6	0.5	0.5	0.3
REEURB7	R	0.4	0.4	0.5	0.5	0.6	0.6	0.7	0.5	0.6	0.4	0.5	0.3	0.4	0.2
REEURB8	R	0.7	0.7	0.7	0.8	0.9	1.0	1.0	0.7	0.8	0.5	0.6	0.4	0.5	0.3
REEURB9	R	0.4	0.4	0.6	0.4	0.8	0.9	0.9	0.7	0.7	0.5	0.5	0.4	0.5	0.4
REEURB10	R	0.8	0.7	0.8	0.9	1.0	1.0	1.1	0.7	0.7	0.5	0.5	0.4	0.4	0.2
REEURB11	R	0.8	0.8	0.8	0.9	1.1	1.1	1.2	0.6	0.9	0.3	0.7	0.3	0.6	0.3
REEURB12	R	0.5	0.5	0.5	0.6	0.7	0.8	0.8	0.4	0.7	0.1	0.5	0.3	0.5	0.3
REEURB13	P	0.5	0.5	0.6	0.7	0.8	1.0	1.1	0.9	0.8	0.6	0.6	0.5	0.5	0.5
REEURB14	P	0.6	0.6	0.6	0.6	0.8	0.7	0.9	0.4	0.7	0.2	0.6	0.3	0.5	0.3
REEURB15	R	0.6	0.5	0.6	0.7	0.8	1.0	1.0	0.8	0.7	0.5	0.5	0.4	0.4	0.4
REEURB16	P	0.7	0.6	0.7	0.8	0.9	1.0	1.0	0.5	0.8	0.2	0.6	0.3	0.5	0.3
REEURB17	R	0.6	0.6	0.7	0.8	0.9	1.0	1.1	0.7	1.0	0.5	0.9	0.5	0.8	0.5
REEURB18	R	0.3	0.3	0.6	0.4	0.8	0.9	0.9	0.8	0.8	0.6	0.6	0.5	0.5	0.4
REEURB19	A	0.3	0.3	0.3	0.4	0.5	0.5	0.7	0.3	0.7	0.2	0.6	0.4	0.6	0.4
REEURB20	A	0.5	0.5	0.6	0.7	0.9	1.0	1.1	0.7	1.1	0.6	1.0	0.4	0.9	0.0
REEURB21	P	0.9	0.9	0.9	1.0	1.0	1.2	1.1	0.9	0.9	0.8	0.7	0.6	0.6	0.5
REEURB22	P	0.8	0.8	0.8	0.9	0.6	1.4	1.0	1.2	0.8	0.8	0.6	0.6	0.6	0.5
REEURB23	P	1.0	1.0	1.0	1.2	1.2	1.3	1.2	1.1	1.0	0.8	0.8	0.6	0.6	0.5

REEURB24	P	0.8	0.8	0.9	1.0	1.0	1.1	1.0	0.9	0.9	0.7	0.7	0.6	0.6	0.5
REEURB25	P	0.8	0.9	0.9	1.0	0.6	1.5	1.1	1.4	1.1	1.0	0.8	0.8	0.8	0.6
REEURB26	P	1.0	1.0	1.1	1.2	1.2	1.4	1.3	1.1	1.1	0.8	0.8	0.7	0.6	0.5
REEURB27	R	0.5	0.5	0.5	0.6	0.3	0.9	0.6	0.9	0.7	0.8	0.5	0.6	0.5	0.4
REEURB28	R	0.7	0.7	0.7	0.8	0.8	1.0	0.9	0.8	0.8	0.7	0.6	0.5	0.5	0.4
REEURB29	I	1.0	1.1	1.1	1.2	0.9	1.7	1.2	1.5	1.0	1.0	0.7	0.7	0.6	0.5
REEURB30	P	0.5	0.5	0.6	0.7	0.7	0.9	0.8	0.7	0.7	0.6	0.6	0.5	0.5	0.4
REEURB31	R	0.4	0.4	0.4	0.5	0.3	0.7	0.7	0.8	0.7	0.7	0.6	0.6	0.6	0.5
REEURB32	P	0.6	0.6	0.7	0.8	1.0	1.0	1.0	0.9	0.9	0.7	0.7	0.6	0.6	0.5
REEURB33	I	0.4	0.4	0.4	0.5	0.3	0.9	0.6	0.8	0.6	0.7	0.5	0.5	0.5	0.4
REEURB34	R	0.6	0.6	0.7	0.7	0.8	0.8	0.8	0.7	0.7	0.6	0.6	0.5	0.5	0.5
REEURB35	P	0.9	0.9	0.9	1.0	1.1	1.0	1.1	1.0	1.0	0.8	0.8	0.7	0.7	0.6
REEURB36	P	0.9	0.8	0.9	1.0	1.1	1.1	1.1	0.9	0.9	0.7	0.7	0.6	0.6	0.5
REEURB37	I	0.5	0.4	0.5	0.6	0.6	0.7	0.7	0.6	0.7	0.6	0.5	0.5	0.5	0.5
REEURB38	I	0.6	0.6	0.7	0.7	0.9	0.9	0.8	0.7	0.7	0.5	0.5	0.5	0.4	0.4
REEURB39	P	0.7	0.7	0.8	0.9	1.1	1.0	1.2	1.2	1.3	1.1	1.1	1.1	1.0	1.0
REEURB40	P	1.1	0.9	1.0	1.0	1.1	1.3	1.1	0.9	0.9	0.7	0.7	0.6	0.6	0.5
REEURB41	P	0.6	0.6	0.6	0.7	0.9	1.0	1.1	0.9	0.9	0.7	0.8	0.6	0.7	0.6
REEURB42	I	0.3	0.3	0.3	0.4	0.5	0.6	0.6	0.6	0.6	0.5	0.5	0.4	0.4	0.4
REEURB43	I	0.4	0.4	0.4	0.4	0.6	0.7	0.8	0.6	0.7	0.5	0.6	0.5	0.5	0.5
REEURB44	I	0.5	0.5	0.5	0.6	0.7	0.9	0.9	0.7	0.6	0.5	0.5	0.4	0.4	0.4
REEURB45	E	0.8	0.7	0.8	0.9	1.0	1.3	1.0	1.2	0.8	0.9	0.6	0.7	0.5	0.4
REEURB46	E	0.8	0.7	0.8	0.9	1.1	1.3	1.1	1.4	1.1	1.2	0.9	1.0	0.8	0.3
REEURB47	E	0.7	0.6	0.7	0.8	0.9	1.2	1.0	1.2	0.9	1.0	0.8	0.9	0.6	0.5
REEURB48	E	0.7	0.6	0.7	0.8	1.0	1.2	1.0	1.1	0.9	1.0	0.7	0.8	0.6	0.4
REEURB49	E	0.7	0.6	0.8	0.8	1.0	1.3	1.0	1.2	0.9	1.0	0.7	0.8	0.6	0.4
REEURB50	E	0.7	0.6	0.7	0.8	0.9	1.3	0.9	1.1	0.9	0.9	0.7	0.7	0.6	0.4

A=Agricultural, P=Park, R=Roadside, E=E-waste landfill

b)

		La	Ce	Pr	Nd	Sm	Eu	Gd	Tb	Dy	Ho	Er	Tm	Yb	Lu
Agricultural	Mean	0.50	0.48	0.56	0.59	0.80	0.79	0.98	0.62	0.92	0.46	0.79	0.48	0.72	0.35
	Median	0.44	0.43	0.57	0.55	0.85	0.78	1.05	0.66	0.92	0.46	0.77	0.41	0.70	0.38
	RSD%	42.3	39.2	33.7	36.1	25.4	31.3	20.9	40.7	20.0	60.8	18.5	36.3	18.2	30.5
	Min	0.32	0.31	0.32	0.39	0.52	0.55	0.69	0.29	0.69	0.16	0.63	0.38	0.59	0.01
	Max	0.79	0.73	0.79	0.85	0.99	1.02	1.13	0.88	1.14	0.77	0.98	0.75	0.89	0.63
E-waste landfill	Mean	0.73	0.65	0.75	0.84	0.98	1.29	1.00	1.20	0.92	1.00	0.73	0.82	0.62	0.39
	Median	0.72	0.64	0.75	0.84	0.98	1.30	0.99	1.17	0.93	0.99	0.72	0.81	0.62	0.42
	RSD%	7.2	7.6	6.7	6.3	6.2	4.3	6.5	7.9	8.6	9.4	11.3	12.9	13.8	17.4
	Min	0.68	0.60	0.69	0.78	0.91	1.21	0.92	1.11	0.84	0.90	0.64	0.68	0.51	0.27
	Max	0.79	0.72	0.81	0.90	1.06	1.35	1.11	1.37	1.06	1.16	0.88	0.99	0.76	0.45
Industrial	Mean	0.52	0.52	0.55	0.64	0.65	0.93	0.81	0.78	0.69	0.61	0.53	0.50	0.48	0.44
	Median	0.46	0.44	0.48	0.56	0.65	0.85	0.77	0.67	0.66	0.55	0.49	0.46	0.46	0.42
	RSD%	42.9	51.4	46.8	45.8	31.0	40.9	25.9	40.1	19.1	28.2	16.4	21.5	17.0	9.6
	Min	0.30	0.28	0.32	0.37	0.33	0.61	0.61	0.57	0.57	0.48	0.46	0.42	0.40	0.40
	Max	0.96	1.10	1.08	1.25	0.88	1.74	1.22	1.46	0.97	0.99	0.70	0.73	0.63	0.51
Park	Mean	0.78	0.77	0.81	0.92	0.97	1.13	1.08	0.93	0.92	0.73	0.72	0.62	0.62	0.52
	Median	0.79	0.81	0.87	0.97	0.99	1.12	1.09	0.93	0.89	0.74	0.70	0.61	0.58	0.51
	RSD%	22.7	22.2	20.2	19.7	21.9	17.7	13.2	25.2	15.0	32.3	18.0	28.9	19.7	29.7
	Min	0.54	0.52	0.57	0.64	0.55	0.74	0.80	0.40	0.71	0.18	0.58	0.31	0.50	0.31
	Max	1.07	1.03	1.06	1.20	1.25	1.49	1.38	1.38	1.26	1.14	1.12	1.12	1.00	0.99

Roadside	Mean	0.58	0.57	0.64	0.68	0.80	0.91	0.95	0.73	0.78	0.56	0.61	0.47	0.53	0.38
	Median	0.60	0.57	0.63	0.72	0.84	0.97	0.97	0.75	0.76	0.57	0.58	0.46	0.50	0.39
	RSD%	26.2	25.4	19.5	24.5	26.9	14.7	18.7	19.3	17.0	32.5	19.7	24.3	21.4	26.9
	Min	0.32	0.30	0.44	0.37	0.32	0.65	0.63	0.36	0.61	0.13	0.48	0.29	0.41	0.23
	Max	0.82	0.78	0.83	0.90	1.05	1.11	1.18	0.95	1.11	0.87	0.92	0.73	0.80	0.56

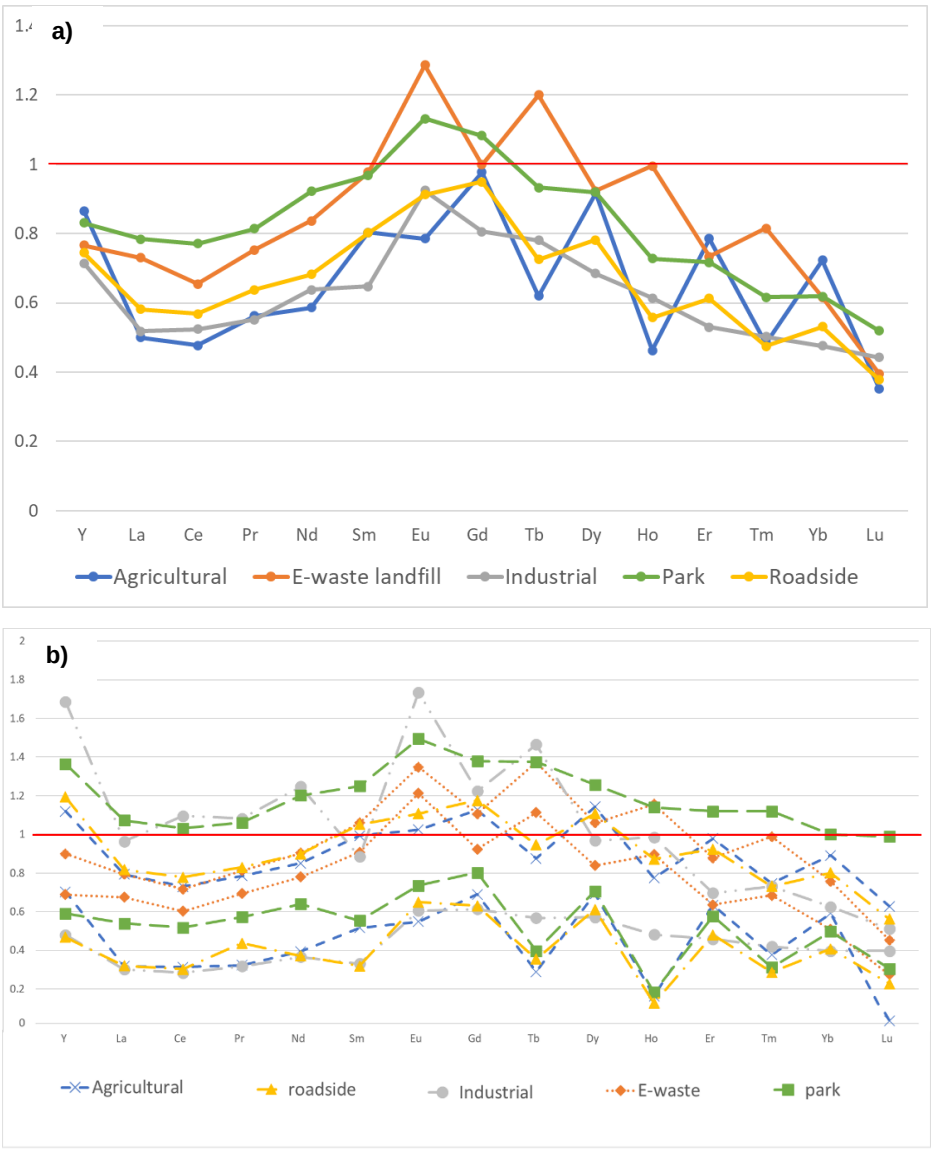

Figure 3.2. The REE-normalized average a) patterns and maximum and minimum values b) in urban soils in a historically industrial city calculated using Upper Continental Crust (UCC) among land used.

Figure 3.2b shows the maximum and minimum values in the different land uses. In an urban context, it is important to point out that average values often hides anomalies due to point or diffuse pollution phenomena characterizing a localized area. It is therefore more

appropriate to observe the minimum and maximum values in the area under consideration.

It immediately emerges how maximum REE/UCCs values in industrial and park areas reached values appreciably higher than 1 (Table 3.10b). In roadside and agricultural sites, a higher presence than in UCC was also observed for Gd, Dy, and Eu. Finally, in e-waste landfill sites the maximum and minimum values do not differ much from each other.

The maximums pattern for parks showed an intermediate trend between industrial and roadside sites; while the minimums pattern appeared similar to roadside one. The results are in line with what found by Liu et al. (2023) in Beijing urban park soils, where REE accumulation was affected by both industrial and traffic emissions, demonstrated by micro morphology and chemical components detected by SEM-EDS.

Conventionally, the ternary Ce-La-Sm diagram has been used to distinguish the REE distribution in minerals and rocks. More recently, this has also been used in environmental studies to show the geochemical patterns of REE (Moreno et al 2008, 2010), and it can be used to discriminate natural variation in REE concentrations from non-geological sources influencing REE levels. The diagram for all samples is presented in Figure 3.3. The UCC point is in the center of the triangle. Most of the samples cluster into a group with a composition comparable to that of the UCC, while a few of them were distributed discretely, indicating a diversity in REE sources (Hou et al., 2017). In particular, the REEURB25, REEURB29, REEURB22, REEURB27, REEURB33 and REEURB31 samples were found to have a higher abundance of La and Ce and a lower concentration of Sm. The peculiarity of these sites is their proximity to industrial sites. Therefore, it is possible an in industrial emission of La and Ce for the sites (Gwenzi et al., 2018; Gao et al., 2020). Samples with a higher presence of Sm but lower presence of La are REEURB9, REEURB2 and REEURB18. These, on the other hand, are characterized by their proximity to heavily trafficked areas.

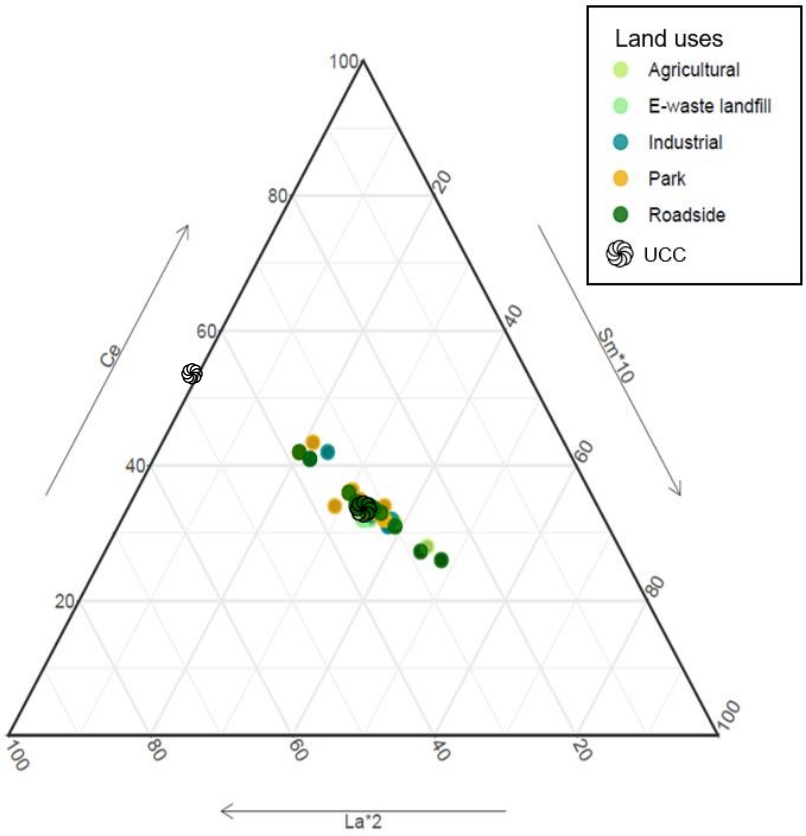

Figure 3.3. The ternary Ce-La-Sm diagram

3.3.6. Association and sources of REE in a historically industrial city

Matrix Factorization (PMF) is a statistical tool for deconvoluting the complex compositional patterns of soil pollutants. Through PMF analysis, we identified six distinct factors contributing to soil contamination (Figure 3.4), each with specific characteristics and sources. The first factor, characterized by the co-occurrence of cadmium (Cd) with rare earth elements, is likely attributed to the addition of fertilizers containing phosphorus in agricultural soils, as well as gypsum, a byproduct of phosphoric acid production from fluorapatites; these minerals are associated with both rare earth elements and cadmium (Jalali et al., 2020; Salem et al., 2019; Wang et al., 2019; Broom-Fendley et al., 2021). Considering the share of the apportioned mass analysis within each land use category (Figure 3.5), this factor predominantly impacts on agricultural and roadside soils, highlighting the

importance of agricultural practices and soil disturbance as the addition of construction materials (such as bricks and gypsum) to urban soils (Howard and Orlicki, 2015). The second factor contain mostly LREE and is more prevalent in park soils and e-waste landfill areas, emphasizing both widespread contamination and the potential impact of electronic waste disposal practices on soil contamination. The third factor, dominated by HREE, shares similarities with the second factor, but weighs more heavily in agricultural soils. In general, it has a higher contribution in all soil categories examined, highlighting the widespread distribution and importance of HREE presence in urban environments. The fourth factor, identified with the diffuse sources of urban contamination, accounted for the levels of Cu, Zn, Pb, and Cd, commonly associated with anthropogenic activities such as traffic and industrial processes (Giordano et al., 2024).

Considering its importance in the sites, this factor has a greater and almost constant influence in all urban sites (parks, roadside areas, and industrial zones), emphasizing the extensive impact of urban diffuse contamination in all urban soils. The fifth factor is associated with serpentinite, as it explain most of the variability of Cr, Ni, and Co, and showed a similar contribution across all sites with a peack in industrial areas, highlighting both the impact of chromium plating processes in industrial areas, and suggesting the importance of geological sources in the distribution of elements in soil (Ajmone-Marsan and Biasioli, 2010, ARPA Piemonte, 2020). Lastly, the sixth factor exclusively represented lead (Pb) contamination, reflecting historical and ongoing pollution sources, particularly evident in roadside and industrial soils. The share of the apportioned mass indicated that this factor has a lower contribution compared to others, but is mainly represented in roadside and industrial soils, emphasizing the persistent legacy of lead contamination in these areas. In conclusion, the results obtained through the analysis of PMF provide an important framework for understanding the distribution, association, and potential sources of contamination of rare earth elements, which represent emerging contaminants of growing interest. However, it is important to emphasize that these results are not definitive and require further investigation and assessment. The statistical processing conducted merits to provide an overview of the potential distributions of rare earth elements in the urban soils of a post-industrial city like Turin, but continuous effort is necessary for a deeper understanding.

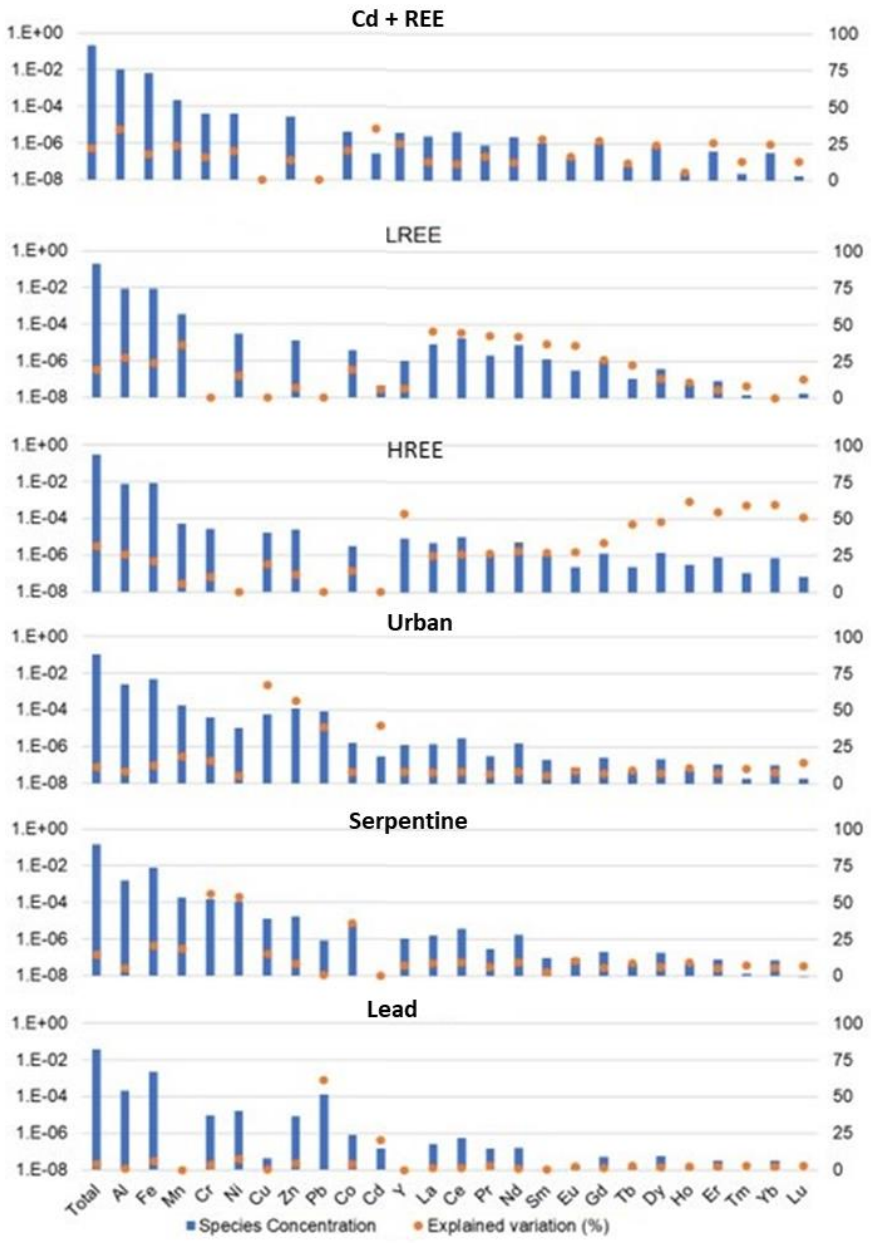

Figure 3.4. Representation of factors obtained through Positive Matrix Factorization (PMF) analysis depicting the concentration of species and the explained variation percentage.

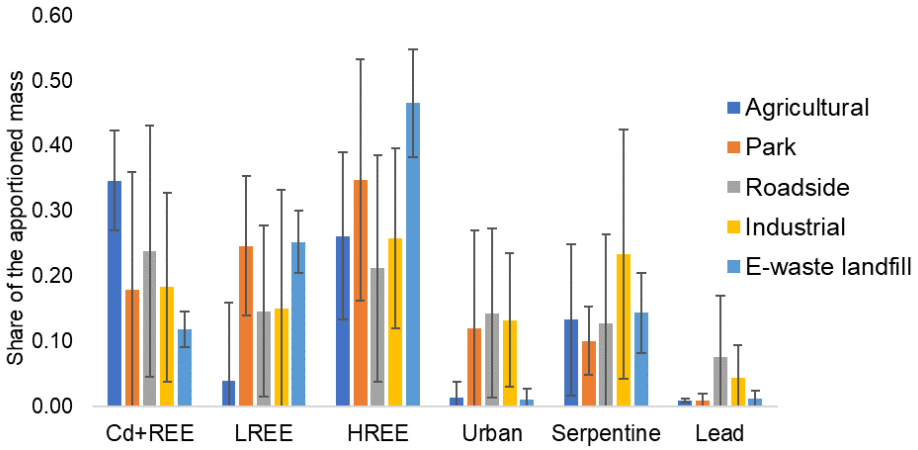

Figure 3.5. Representation of the Share of the Apportioned Mass for the factors identified through Positive Matrix Factorization (PMF) analysis.

CHAPTER 4

Release of PTE and REE under pre-definite redox conditions in urban soils.

4.1. Introduction

The complexity of assessing risk conditions induced by natural events in urbanised areas is strongly influenced not only by the local geomorphology, but also by extensive anthropization (Ortega et al., 2014). This is the case of large urban settlements such as the city of Turin, which, due to its position and conformation, is affected by lowland phenomena: during persistent rainfall or violent rainstorms, flooding phenomena, even major ones, may occur in the rivers of these areas. These phenomena can lead to even very serious effects in heavily urbanized areas, such as altered mobility patterns of contaminants that could intensify risks to ecosystems and human health (Ajmone-Marsan et al., 2019; Cao et al., 2001; Du Laing et al., 2009; Li et al., 2022; Shaheen et al., 2016). Shaheen et al. (2014) showed how periodic inundation of contaminated flood soils alters the temporal dynamics of various metals due to changes in environmental factors such as pH, dissolved organic carbon and the chemistry of elements such as iron, manganese and sulphur. This increased mobility of metals in flooded urban soils was also observed by (Florido et al., 2011), and attributed to the dissolution of iron and manganese oxides. Studies have indicated that organic matter can sequester REE, the fate of which is influenced by soil components and organic matter dynamics, which in turn are dictated by redox conditions. Research by Šmuc et al. (2012) and Chen et al. (2014) on contaminated rice field soils revealed an increase in REE concentrations mainly related to organic matter. Sequential extractions on wetland soils show that REE are mainly found in the residual fraction with minimal amounts in the exchangeable fraction (Davranche et al., 2016; Mihajlovic et al., 2014). However, under reducing conditions, the solubilization of organic phases releases REE into the liquid fraction of the soil, which prompts the investigation of their bioavailability in relation to organic ligands (Wang et al., 2017).

Understanding the behavior and fate of contaminants in soil is essential for an adequate risk assessment of contaminated sites. Therefore, we set out to assess the effects of changing redox conditions caused by flooding on the potential release of PTE and REE from contaminated soils near rivers. Upon controlling the redox conditions applied to soils we studied the impact of specific E_H conditions on the release mechanism of dissolved REE and to elucidate the underlying redox-

driven processes, including the role played by pH, Fe, Al, Mn, DOC, DIC and SO_4^{2-} in flooded soils.

4.2. Materials and methods

4.2.1. Study area

The city of Turin (45°04′ N; 7°41′ E) is situated in northern Italy within a narrow strip of the western Po Valley, primarily formed by a succession of fluvio-glacial and fluvial sediments linked to alpine tributary watercourses, constituting a series of partially coalescing alluvial cones. These formations, shaped by significant watercourses including the River Po and its tributaries Sangone, Dora Riparia, and Stura di Lanzo, are characterized by Quaternary deposits of fluvial and fluvioglacial origin, comprising clayey, sandy, and gravelly deposits (Bini, 2013). The hydrogeological significance of these deposits lies in their alternation between coarse, permeable layers and fine, impermeable, or semi-permeable sediments, forming a multifold system that represents the most exploited water resource in the Turin area.

Subsurface water resources, particularly abundant in the Turin plain, consist mainly of two primary flow circuits: a superficial one, commonly referred to as the "shallow aquifer," directly connected to surface water bodies and a deeper one. The geological characteristics of the Turin area are influenced by each of these elements, with precise significance in recent geological evolution derived from the geomorphological processes that have shaped it and the lithological and structural characteristics of the geological materials comprising it (Borghi et al., 2014).

The geological composition of the extensive Turin city plain belongs to the large alluvial cone, with its vast sedimentary body consisting of deposits from watercourses constantly flowing from the front of the alpine valley glacier during its repeated advance phases until its valley outlet. The alpine reliefs comprise metamorphic rocks of pre-Triassic age, attributable to continental margin units (Dora Maira Massif and Sesia-Lanzo Zone) and oceanic basin units (Lanzo Ultrabasic Complex and Piedmont Zone). Lithologically, these include various types of gneisses, mica schists, quartzites, serpentinites, amphibolites, prasinites, granites, porphyries, and their metamorphic derivatives (De Luca et al., 2020). This mineral heritage has led to a history of extensive extraction activity, particularly for the significant litho-applicative characteristics of the present geomaterials, which are important raw materials not only industrially but also for construction purposes (Borghi et al., 2014).

The extension of the plain areas, characterized by predominantly gravelly constitution and extremely modest inclination, has over time favored the progressive development of industrial areas - driven by the metalworking sector - and the expansion of the urban fabric. Profound urban transformations and large infrastructure projects have required more construction materials and the production of significant amounts of excavated earth and rocks (Dino et al., 2015), which have led to efforts for an increased use of residual lithoid materials as by-products and/or recycled materials used as a supplement to quarry resources for civil purposes (Legislative Decree 152/2006 and 117/2008).

The significant anthropogenic pressure exerted on the territory has inevitably impacted pollution levels, leading to environmental contamination across various matrices (Giordano et al., 2024). The pollutant typology observed in environmental matrices within the territory of the province of Turin is typical of industrialized areas, with a predominance of metals.

The morphological aspects of the plain area are generally affected by anthropogenic remodeling, particularly pronounced in extensive urban areas. In a heavily urbanized territory like the metropolitan area of Turin, the natural landscape component is closely interconnected with the anthropogenic one. The occurrence of phenomena such as river overflow and urban drainage networks during persistent rains or violent downpours, particularly along riverbanks, highlights potential damage scenarios for adjacent urban areas (Hirabayashi and Kanae, 2009). The depressed areas developed along watercourses, corresponding to the most vulnerable bands of fluvial activity, host extensive public river parks, mitigating some impacts of urbanization on natural environments. Nonetheless, like any heavily urbanized area, occasional unauthorized settlements persist for varying durations within the city context, such as the shantytowns developed along the Stura River.

4.2.2. Sampling sites: recreational and abusive urban settings

The urban park arises to offer citizens spaces typically located on the city peripheries for walking, while also embodying the concept of a consumable object and social functioning, thus representing a necessity for daily human life. In this study, four different sites were selected (Figure 4.1), representing places where the daily life of citizens coexists with the potential health risks caused by direct exposure to emissions of metallic contaminants accumulated during years of intense industrialization. The selected sites include green or residential land use categories, as these may pose the most direct risk to human health.

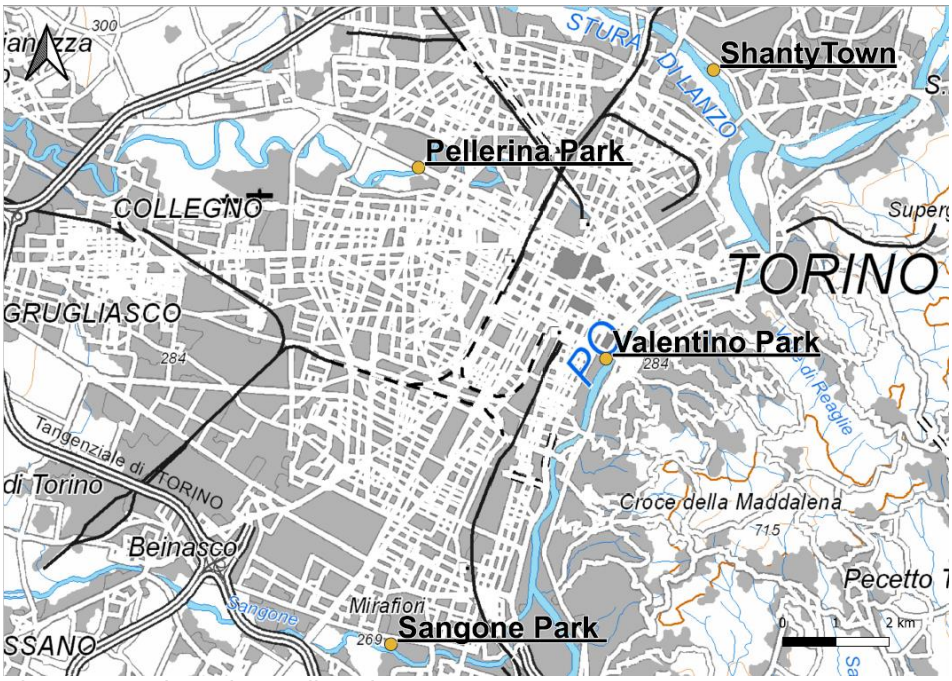

Figure 4.1 Selected sampling sites

Valentino Park settled prominently as it is known today in the 19th century, representing a moment of novelty and experimentation, and is the city's most famous and oldest public park. Completed in 1870, it featured a green area equipped for recreational activities and sports for the citizens, with hygienic and recreational purposes. It became the venue for hosting international exhibitions, through which it acquired a new function as a public space, expanding to 421,000 m^2; however, this led to an imbalance between asphalted and green areas due to the addition of internal vehicular pathways.

The Pellerina Park, spanning approximately 837,000 m^2, is diagonally crossed by the Dora Riparia River. The park's construction took place in 1934 with the acquisition of some areas where the current hills were built, using rubble from demolished buildings along the old Via Roma. After World War II, the accumulation of debris from buildings damaged by air bombings continued. In 1970, the park was expanded to include the first square for traveling shows and an additional area previously dominated by deposits of ferrous materials from adjacent foundries.

The Sangone Park is the most recent park among those studied, situated on the banks of the Sangone River to promote the recovery of post-industrial areas. Specifically, the area is located in the immediate vicinity of a large Fiat automobiles factory plant, one of Italy's largest industrial entities, which played a pivotal role in establishing Turin as

Italy's industrial capital in the 20th century. The economic downturn resulting from deindustrialization in the former Fiat area prompted authorities to seek new economic and environmental solutions to transform brownfields into attractive areas. In the Sangone River park, a newly regenerated soil was tested, obtained by mixing materials from deep urban construction excavations, compost, zeolite, and biotic compounds to stimulate mycorrhizal growth. This initiative aimed to provide fertile soil for parks and green areas, promoting the recovery of post-industrial areas through the use of nature-based solutions (Dogan et al., 2023; Fan et al., 2017).

The Shanty Town settlement stands on the banks of the Stura River at its confluence with the Po River; it is an illegal settlement built with makeshift houses accommodating several families, lacking connections to sewerage networks and proper hygiene conditions. The lands have been allocated for illicit vegetable gardens. The hallmark of these places is their unsustainable waste management practices, with waste often abandoned and left on adjacent lands or disposed of through uncontrolled open-air burning. This has inevitably led to the degradation of the area, causing discontent and concern due to the continuous detection of foul odors and fumes from fires of various materials such as tires, metal scraps, and plastics. Residues from combustion persist on the ground for extended periods and may be exposed to river or meteoric waters.

4.2.3. Soil sampling and characterization

Four soil samples (0-20 cm) were selected from the urban area of Turin near the rivers (Po, Dora Riparia, Sangone, and Stura). Each soil sample was obtained from composite samples of five soil aliquots from different random points mixed to form a single representative sample of the area under consideration. The samples were air-dried, and then sieved <2 mm with a plastic sieve and ceramic mortar. A small aliquot, obtained after quartering, was ground with an agate mortar and plastic sieve to obtain a portion of soil ground to 0.5 mm and another portion ground to 0.15 mm for carrying out chemical-physical analyses for basic soil properties analysis and pseudo-total content of the elements of interest, respectively.

Surface layers are those directly exposed to the input of anthropogenic metals (Cicchella et al., 2016). Considering both surface and deep layers together would likely introduce uncontrollable variables, such as the time effect, the different proportions of anthropogenic elements, and especially the vertical heterogeneity in the parameters of undisturbed soils.

In more detail, the following chemical-physical analyses were performed on all samples: pH (1:2.5, soil: water) after agitation on a horizontal mechanical shaker for 2 hours, carbonates (volumetric method, ISO 10693:1995), total carbon and nitrogen through elemental analysis (UNICUBE, Elementar Analyses System GmbH, Langensbold, Germany), texture was measured using the pipette method. The chemical-physical characterization and sampling coordinates are reported in Table 4.1.

Table 4.1 Chemical-physical characterization and sampling coordinates of the selected sites

Site	Coordinates		Depth	pH	$CaCO_3$	OC	Sand	Silt	Clay
	LAT	LONG	cm	[H2O]	%	%	%	%	%
Valentino (V)	45.057	7.690	0-20	7.7	2.1	3.4	56	40	4
Pellerina (E)	45.089	7.645	0-20	7.7	8.0	3.3	64	29	7
Sangone (S)	45.009	7.640	0-20	8.0	2.3	2.4	55	36	9
ShantyTown (T)	45.106	7.715	0-20	7.4	5.1	8.1	82	15	3

The pseudo-total content of Al, Cr, Cu, Fe, Mn, Ni, Pb, S, and Zn was obtained after acid digestion with *aqua regia* assisted with microwaves (Milestone ethos D, ISO 54321:2020) and analyzed using inductively coupled plasma optical emission spectroscopy (ICP-OES, Horiba Jobin Yvon, Uterhaching, Germany). The results in mg/kg are reported in Table 4.2.

The pseudo-total content of REE was obtained using the D method optimized in Chapter 3, and analyzed using Inductively coupled plasma mass spectrometry (ICP-QQQ-MS, Agilent Technologies 8900) the results obtained are shown in Table 4.3

Table 4.2 Fe, Mn, Al and potentially toxic elements' pseudo-total concentrations

Soil	Al mg/kg	Cr mg/kg	Cu mg/kg	Fe mg/kg	Mn mg/kg	Ni mg/kg	Pb mg/kg	S mg/kg	Zn mg/kg
Valentino (V)	20832	346	93	29136	934.1	200	148	364	250
±SD	1252	18	0.3	1436	28.8	11	4	9	7
Pellerina (E)	24859	300	86	33796	1037	167	136	322	316
±SD	4226	3	4	2049	24	11	10	14	4
Sangone (S)	23890	225	116	30518	867	158	155	237	241
±SD	2264	32	5	2978	81	16	12	21	4
ShantyTown (T)	27772	478	367	35063	861	394	1222	2961	1518
±SD	3242	8	195	3986	13	17	439	404	158

Table 4.3 Rare Earth Elements' pseudo-total concentrations

Soil	Y mg/kg	La mg/kg	Ce mg/kg	Pr mg/kg	Nd mg/kg	Sm mg/kg	Eu mg/kg	Gd mg/kg	Tb mg/kg	Dy mg/kg	Ho mg/kg	Er mg/kg	Tm mg/kg	Yb mg/kg	Lu mg/kg
Valentino (V)	13.3	20.4	42.6	5.1	20.0	4.1	0.8	3.6	0.5	2.8	0.5	1.4	0.2	1.2	0.2
±SD	0.6	0.9	1.6	0.2	0.9	0.2	0.02	0.1	0.02	0.1	0.02	0.1	0.01	0.1	0.01
Pellerina (E)	12.7	23.7	48.9	5.8	22.7	4.6	0.9	3.7	0.5	2.8	0.5	1.3	0.2	1.0	0.2
±SD	0.5	1.3	2.5	0.2	0.8	0.2	0.1	0.1	0.02	0.1	0.02	0.03	0.01	0.04	0.005
Sangone (S)	15.3	24.6	51.5	6.2	24.2	4.9	0.9	4.1	0.6	3.1	0.6	1.6	0.2	1.3	0.2
±SD	1.1	1.6	4.5	0.5	1.9	0.2	0.03	0.2	0.03	0.2	0.04	0.1	0.01	0.1	0.01
ShantyTown (T)	19.0	11.5	25.2	3.2	13.5	3.2	0.8	3.6	0.6	3.5	0.7	2.0	0.3	1.6	0.3
±SD	1.4	0.9	2.1	0.2	0.9	0.2	0.1	0.2	0.02	0.2	0.03	0.1	0.02	0.2	0.03

The examined soils are moderately alkaline, consistently with the characteristics of urban soils, as showed in previous studies (Padoan et al., 2017; Poggio et al., 2009; Yan et al., 2021), which report high pH values probably due to the addition of foreign materials during the parks' construction (building debris, pieces of mortar, cement, and other waste materials). This common practice could justify, in addition to the characteristic lithological origin, also the texture observed for these soils, which have a high sand content, with Shanty Town having the highest sand content (82%) and Sangone the lowest (55%). The average Organic Carbon content is 4.3%; noteworthy is the organic carbon content present in Shanty Town (8.1%), while other sites have more

common values for urban soils, with values due to the permanent grass cover. In urban areas, however, certainly not to be excluded is the anthropic contribution deriving from lubricating oils, coal, petroleum, fertilizers, and herbicides (Hagmann et al., 2019), especially for the Shanty Town site where the illegal settlement has most likely contributed significantly to the high OC content. Also, the carbonate content varies greatly among the different sites examined, Pellerina being the one with the highest content at 8%, followed by Shanty Town at 5.1%, with very similar values for Sangone and Valentino, at 2.3% and 2.1%, respectively. As the Pellerina park was built on demolition rubbles, the values derived from the calcareous building waste (Jim, 1998).

Analysis of soil data revealed a variety of metal concentrations at different locations. Elements with the highest concentrations include sulfur (S) with an average of 2961 mg/kg and lead (Pb) with an average of 1222 mg/kg, both of which are mainly found in the ShantyTown (T) location. This location shows a significantly higher concentration of Pb than the others, which might suggest the presence of specific sources of contamination in this area. In addition, it is important to note that according to D.Lgs 152/2006 regarding soils in residential areas, concentrations of chromium (Cr), copper (Cu), nickel (Ni), lead (Pb), and zinc (Zn) exceed legal limits in several locations. For example, chromium (Cr) and lead (Pb) exceed the legal limit at all locations, with maximum values observed at the ShantyTown location.

The results indicate significant variations in the concentrations of the elements among different locations. In addition to Ce, which emerges as the most abundant element at all locations with average concentrations exceeding 40 mg/kg, other elements show significant variations. For example, Nd shows significantly higher values, compared to other locations, in Pellerina (E) and Sangone (S), with averages of 22.7 mg/kg and 24.2 mg/kg, respectively. Lutetium and Yb show relatively low concentrations at all locations, with averages below 1.6 mg/kg. This observation could be indicative of differences in the sources of contamination or in the specific geochemical processes that influence the distribution of this element in the analyzed soils. Further investigations are needed to fully understand the causes of these differences and the implications for soil and environmental quality in these areas.

4.2.4. The microcosm experiment

4.2.4.1. Setup of the microcosm and experimental conditions

To simulate laboratory-scale flooding of urban soils following intense precipitation and observe the consequent biogeochemical processes occurring during changes in the redox conditions governing the behavior of contaminants, an advanced automated microcosm (MC) was utilized. Its operation is detailed in Yu and Rinklebe (2011) and depicted in Figure 4.2. The MC has been employed in various studies (El-Naggar et al., 2019; Mihajlovic et al., 2017; Rinklebe et al., 2016; Shaheen et al., 2018, 2017), proving to be an effective tool for investigating redox-induced trends of trace elements, as it can reproduce natural conditions in a controlled manner on a laboratory scale (Rupp et al., 2010), allowing the observation of parameters that most influence the behavior of potentially toxic metals.

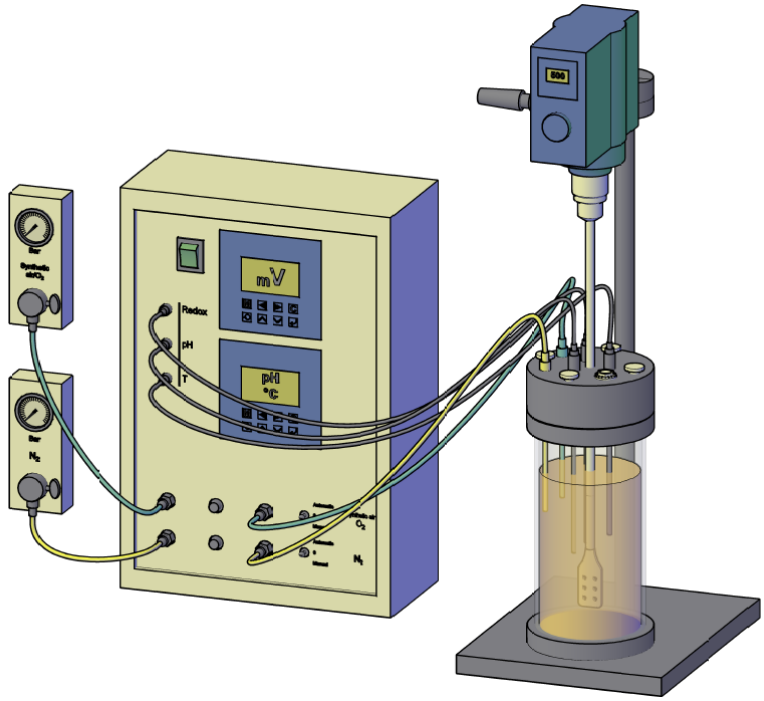

Figure 4.2 Schematic diagram of the automated microcosm system

For this experiment, a total of 16 automatic MC systems were used: 4 replicates were performed for each urban soil under investigation. In each vessel, 210 g of dry soil and 2 g of fresh soil were added after sieving at 2 mm; the latter acted as an inoculum for autochthonous microorganisms. To achieve a soil:water ratio of 1:8, 1.68 L of tap water

was added. To support microbial activity (no C-limited system), both readily available carbon sources and slow-release carbon sources were added: 10 g of glucose, 15 g of wheat straw, and 2 g of local vegetation. The latter was obtained by mixing equal parts of vegetation collected from the respective sites under investigation, dried, ground, and well homogenized, to add the same type of vegetation to all soils, making the carbon source comparable for different soil types and avoiding the introduction of an additional variable into an already complex system.

Once everything was added, the vessel was hermetically sealed and covered with aluminum foil to shield the system from exposure to sunlight; the suspension was constantly stirred to ensure homogeneity. The redox potential, pH, and temperature were recorded throughout the incubation period every 10 minutes in the soil slurry. Once a stable minimum redox potential was reached - achieved through insufflation of gaseous N_2 and microbial activity- the redox potential was sequentially increased by 100 mV +/- 10 mV. The desired redox windows were maintained stable through the automatic system of insufflation of synthetic air and gaseous N_2. A total of eight distinct levels of redox potentials were obtained in this experiment: E_H -200 mV, -100 mV, 0 mV, +100 mV, +200 mV, +300 mV, +400 mV, +500 mV.

4.2.4.2. Sampling

The first sampling, representative of the initial point, was carried out after two hours from the start of the incubation. The subsequent eight samplings, instead, were performed after maintaining the desired redox window for at least 48 hours. For each sampling, 65 mL of soil slurry was collected. This was immediately centrifuged at 5000 rpm for 10 minutes. Within an anaerobic chamber (Don Whitley Scientific, Shipley, United Kingdom), the supernatant was filtered using a 0.45 µm membrane filter (Whatman Inc., Maidstone, UK); thus, for each sampling, the liquid phase (containing the dissolved component) and the sedimented phase were obtained. From the liquid phase, sub-samples were prepared for the determination of dissolved concentrations of PTE (Cr, Cu, Ni, Pb, Zn), REE, Fe, ferrous ion (Fe(II)), Mn, Ca, Mg, K, P, anions (sulfate SO_4^{2-}, phosphate PO_4^{3-}), dissolved organic carbon (DOC), Specific Ultraviolet Absorbance (SUVA), dissolved inorganic carbon (DIC). The sub-sample for the metal analysis was stored in the refrigerator after addition of 1% HNO_3; the two sub-samples for the determination of anions and DOC were stored in a freezer at -20°C. These were analyzed at a later time. Instead, Fe(II) and SUVA determination was carried out immediately after filtration.

4.2.4.3. Analysis

The determination of ferrous ions (Fe(II)) was carried out via colorimetry using the phenanthroline method at 510 nm. Sample preparation occurred inside the anaerobic chamber to prevent oxidation to Fe^{3+}; readings were taken with a spectrophotometer (HACH 5000series) at 510 nm. Meanwhile, Specific UV Absorbance (SUVA) was measured using a quartz cuvette at 254 nm and calculated by normalizing to the DOC concentration following the method of Weishaar et al., (2003). Anion analysis was conducted via ion chromatography. DOC and DIC concentrations were obtained using a C/N analyzer (multi N/C 2100 S, Analytik Jena, Germany).

4.3. Results and discussion

Electrochemical properties of the soil that are affected by flooding are oxidation-reduction potential or redox potential (E_H), pH, and ionic strength (electrical conductivity) of soil pore water. The redox potential of soil is measured using a platinum electrode with a standard calomel reference electrode. The E_H of soil is determined by the concentration (activities) of oxidants and reductants. Oxidants include oxygen, nitrate, nitrite, manganese, iron, sulfate, and carbon dioxide, while reductants include various organic substrates and reduced inorganic compounds.

4.3.1. Dynamic of E_H and pH

The Figure 4.3 (a-d) illustrate the E_H e pH dynamic obtained from the different experimental replicates for each soil. The graph depicts the temporal evolution, where the black line represents the redox potential recorded during the experiment (y-axis on the left), the red line indicates the pH value (y-axis on the right). The green dots denote the sampling times, considering the sampling redox potential as the average of the preceding 6 hours, a method chosen for its high correlation coefficients between E_H/pH and elements in solution within the MC system (Frohne et al., 2014; Mihajlovic et al., 2017).

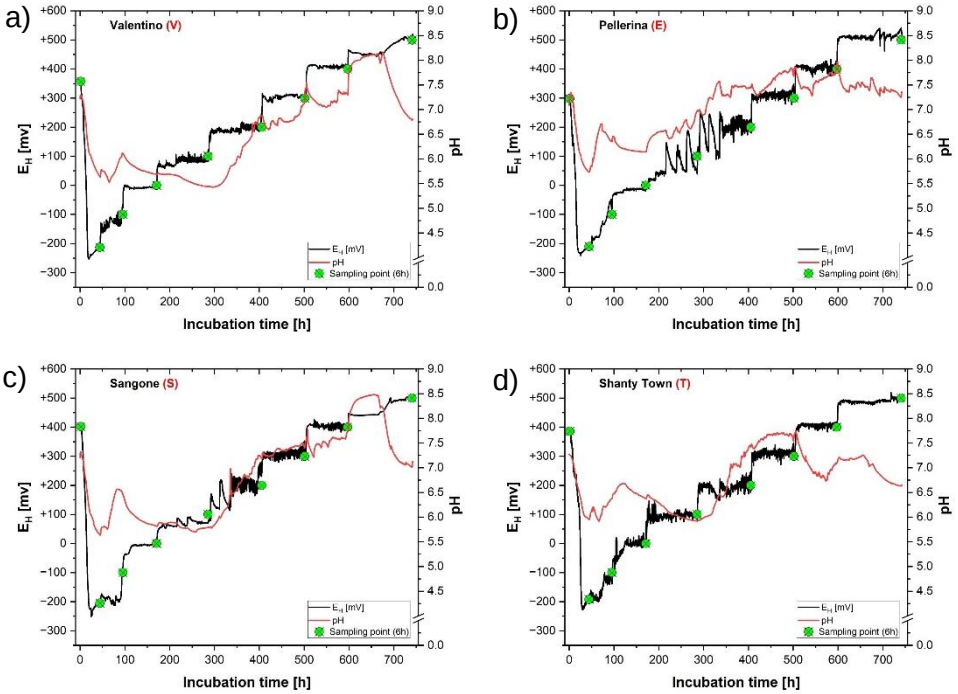

Figure 4.3. Temporal evolution of pH and E_H values for the selected soils. The black line represents the redox potential (y-axis on the left), the red line indicates the pH value (y-axis on the right); green dots denote the sampling times. Valentino (a), Pellerina (b), Sangone (c), and Shanty Town (d).

E_H values ranged from -245 to +542 mV at sampling times, typical for flooding soils under natural conditions (Table 4.4). The minimum was observed in Sangone, while the maximum was in Pellerina. The mean E_H varied from +148 mV for Valentino to +157 mV for Pellerina among individual soils, with an overall mean of +153 mV.

Table 4.4 Minimum, maximum and mean values of E_H (6h), pH (6h) at sampling point

Parameter	Soil	Minimum	Maximum	Mean
E_H [mV]	**V**	-237	524	148
	E	-244	**542**	157
	S	**-245**	526	154
	T	-205	511	152
	All soils	-245	542	153
pH	**V**	**5.2**	8.1	6.4
	E	5.7	8.1	6.9
	S	5.4	**8.2**	6.7
	T	5.9	7.8	6.7
	All soils	5.2	8.2	6.7

pH values ranged between 5.2 in Valentino soil and 8.2 in Sangone soil, showing a significant positive correlation with E_H at the sampling point. Particularly, Pellerina exhibited the highest correlation coefficient between E_H and pH (0.81), followed by Sangone (0.75), Valentino (0.62), and ShantyTown (0.56) (Table 4.5).

Table 4.5 Correlation coefficient (Spearman); ** significant at 0.01 level

Parameter	Soil	E_H	pH
E_H [mV]	**V**	1	0.62**
	E	1	0.81**
	S	1	0.75**
	T	1	0.56**
	All soils	1	0.69**
pH	**V**	0.62**	1
	E	0.81**	1
	S	0.75**	1
	T	0.56**	1
	All soils	0.69**	1

Initial E_H ranged around +400 mV for Sangone and Shanty Town, about +350 mV for Valentino, and +300 mV for Pellerina. E_H decreased rapidly during simulated flooding, with Valentino and Sangone soils reaching the lowest E_H values more rapidly compared to Pellerina and ShantyTown.

At the lowest E_H Sangone and Shanty Town showed greater stability at these redox potentials than Valentino and Pellerina. Starting from the -100 mV redox window, Valentino showed the most stability throughout the experiment.

Pellerina exhibited a different behavior, showing initial difficulty in reaching E_H of +100 mV and subsequently, high sensitivity to oxygen, resulting in significant fluctuations around the target value; without oxygen insufflation, the potential tended to decrease again. This sensitivity to oxygen within the E_H range of 0 to +150 mV was maintained for a limited time, after which the E_H tended to increase. This trend was observed, though less pronounced, in Sangone soil at the beginning of the +200 mV redox window, where it showed marked sensitivity to oxygen that diminished after about 50 hours. ShantyTown easily reached the preset +200 mV potential but struggled to maintain it after about 50 hours, eventually stabilizing at the desired value. However, after about a hundred hours from the start, potential fluctuations increased, indicating instability. Valentino exhibited slight fluctuations within the +200 mV redox window, gaining higher stability in subsequent windows. In the +300 mV and +400 mV redox windows, all soils achieved greater stability compared to the previous target potentials. In the +500 mV redox window, soils exhibited different behaviors: ShantyTown and Pellerina immediately reached the set redox potential, with ShantyTown showing greater long-term stability than Pellerina. Conversely, Valentino and Sangone struggled to increase E_H to the target potential, taking about 50 hours to reach it.

Redox potential variations are correlated with pH changes (Table 4.5). Observing the red line depicted in Figure 4.3, a distinct trend can be observed for each soil, characteristic of its composition. The pH range recorded for Valentino varies from 5.2 to 8.1, with an average value of 6.4; Pellerina ranges from 5.7 to 8.1, with an average value of 6.9; Sangone has a range of 5.4 to 8.2, with an average value of 6.7, and finally, ShantyTown ranges from 5.9 to 7.8, with an average value of 6.7.

The initial soil pH was consistently basic: Valentino pH 7.5, Pellerina pH 7.3, Sangone 7.5, Shanty Town 7.5. At the beginning of the microcosm,

for all soils, a decrease in pH is observed as acidity coincides with E_H reduction, reaching the first peak of minimum: Valentino pH 5.7, Pellerina pH 5.8, Sangone pH 5.7, and ShantyTown pH 6.0. Subsequently, pH increases, registering a peak maximum: Valentino 6.1, Pellerina 6.4, Sangone 6.5, and Shanty Town 6.4; it is observed that for the soils of Valentino, Sangone, and ShantyTown, pH variations correspond to E_H changes. At 100 hours from the beginning of the experiment, in the +0 mV redox window, corresponding to E_H stabilization, pH decreases, returning to acidic levels and starting the descent to reach another minimum peak corresponding to the +100 mV redox window. For Valentino, the pH decrease is linear with a single minimum peak; Sangone presents a rounded first maximum peak in the -100 mV redox window but subsequently decreases similarly to Valentino. For Pellerina and Shanty Town, the pH decrease is less steep.

As the E_H increases in the +200 mV redox window, a progressive rise in pH towards basic conditions is observed, reaching the first positive peak: pH 6.8 for Valentino, pH 7.3 for Pellerina, pH 7.3 for Sangone, and 7.5 for Shanty Town. The attainment of the peak differs within the soils: for Valentino, the increase remains very linear, ranging from pH 5.5 to 6.8 (Δ= 1.3), stabilizing when E_H stabilizes. Sangone shows a similar pattern but with fluctuations following those of E_H, ranging from a minimum of 5.8 to 7.3 (Δ= 1.5). For Pellerina, this fluctuating trend is accentuated, with decreases in EH corresponding to decreases in pH and vice versa; the attainment of stability in both parameters also corresponds. Shanty Town ranges from pH 6.0 to 7.5 (Δ= 1.5), characterized by a very irregular trend with a brief stabilization at pH 7.2 and subsequent increase to pH 7.5.

As soon as the desired potential of the +300 mV redox window is reached, in the Valentino soil, pH shows a decreasing trend, then changes direction at the end of the redox window and goes from 6.8 to 7.5; there is also a peak when O_2 is added to the system to reach the +400 mV window. Upon reaching the desired potential of the +400 mV redox window, the pH of Valentino tends to decrease from 7.5 to 7.0, before starting to increase again.

4.3.2. Correlation of E_H and pH with release of DOC, SUVA, Fe, Mn and SO_4^{2-}

The pH in soils is influenced by various intricate processes. For further interpretation, it is useful to look at the parameters that might influence pH, such as Dissolved Organic Carbon (DOC), Specific ultraviolet Absorbance (SUVA), Dissolved Inorganic Carbon (DIC), Fe, Fe(II), Mn,

and SO_4^{2-}. Table 4.6 provides the minimum, maximum, and average values of these parameters for individual soils as well as all soils. Figure 4.4 displays histograms for each redox window of the experiment, illustrating the concentrations in solution (mg/L) of DOC, Fe, Mn, and SO_4^{2-}, along with SUVA values expressed in $cm^{-1}mg^{-1}L$. Regarding SUVA, it should be specified that the value of SUVA determined by spectrophotometer at 254 nm was normalized for the concentration of DOC because this parameter indicates DOC's chemical composition, specifically for estimating Dissolved aromatic compounds. In Table 4.8, the Spearman correlation coefficients for the parameters represented in the histograms are reported.

To better understand these processes, we must take in consideration soil microbes' respiration. It involves the oxidation of organic matter, acting as a major controller of many biogeochemical reactions in soils and as main electron donor. Unless these electrons are removed, they accumulate in the system, creating an electron pressure or intensity. In the presence of oxygen, electrons are easily removed, preventing the buildup of significant electron pressure. Under flooding conditions, aerobic organisms become quiescent or die, and facultative and obligate anaerobic bacteria take over (Stotzky, 2016).

Table 4.6 Minimum, maximum, and average values of Dissolved Organic Carbon (DOC), Specific Ultraviolet Absorbance (SUVA), Dissolved Inorganic Carbon (DIC), SO_4^{2-}, Fe, Mn, and Fe(II)

Parameter	Soil	Minimum	Maximum	Mean
DOC [mg/L]	V	62	2170	1009
	E	53	2129	957
	S	59	2343	1149
	T	69	2259	904
	All soils	53	2343	1001
SUVA [cm^{-1} mg^{-1} L]	V	0.002	0.03	0.01
	E	0.002	0.03	0.01
	S	0.001	0.03	0.01
	T	0.001	0.03	0.01
	All soils	0.001	0.03	0.01
DIC [mg/L]	V	0.3	92	37
	E	4	84	35
	S	0.1	78	36
	T	2	74	42
	All soils	0.1	92	36
SO_4^{2-} [mg/L]	V	1	208	47
	E	4	175	48
	S	3	171	48
	T	1052	1896	1490
	All soils	1	1896	357
Fe (II) [mg/L]	V	11	122	54
	E	0.4	24	13
	S	7	49	27
	T	2	10	5
	All soils	0.4	122	27
Fe [mg/L]	V	0.1	87	20
	E	0.1	15	4
	S	0.1	49	11
	T	0.1	8	2
	All soils	0.1	87	10
Mn [mg/L]	V	0.1	53	26
	E	0.03	36	18
	S	0.01	53	22
	T	1	24	10
	All soils	0.01	54	19

The metabolic activities of anaerobic bacteria depend from different electron acceptors (oxidized forms of nitrogen, iron, manganese, and sulfur). In the absence of oxygen, but with the presence of nitrate, a slightly higher electron pressure develops. Once nitrate is depleted,

further electron pressure builds up, facilitating the reduction of manganic manganese by manganese reducers (Stotzky, 2016). When the slurry soil reaches the critical reducing conditions, defined by the range of redox potentials required for the reduction of Fe and Mn, soil redox-active species are transformed into their reduced form. Similarly, ferric iron sulfate and CO_2 serve as electron acceptors in sequence as the electron pressure increases. Additionally, it should be also considered consider that the types of microorganisms selected during the incubation may vary from one soil to another (Luo et al., 2021).

Figure 4.4 Histograms representing Dissolved Organic Carbon (DOC), Specific Ultraviolet Absorbance (SUVA), Dissolved Inorganic Carbon (DIC), SO_4^{2-}, Fe, Mn, and Fe(II) concentrations at the sampling points. The individual values are shown in the table 4.7

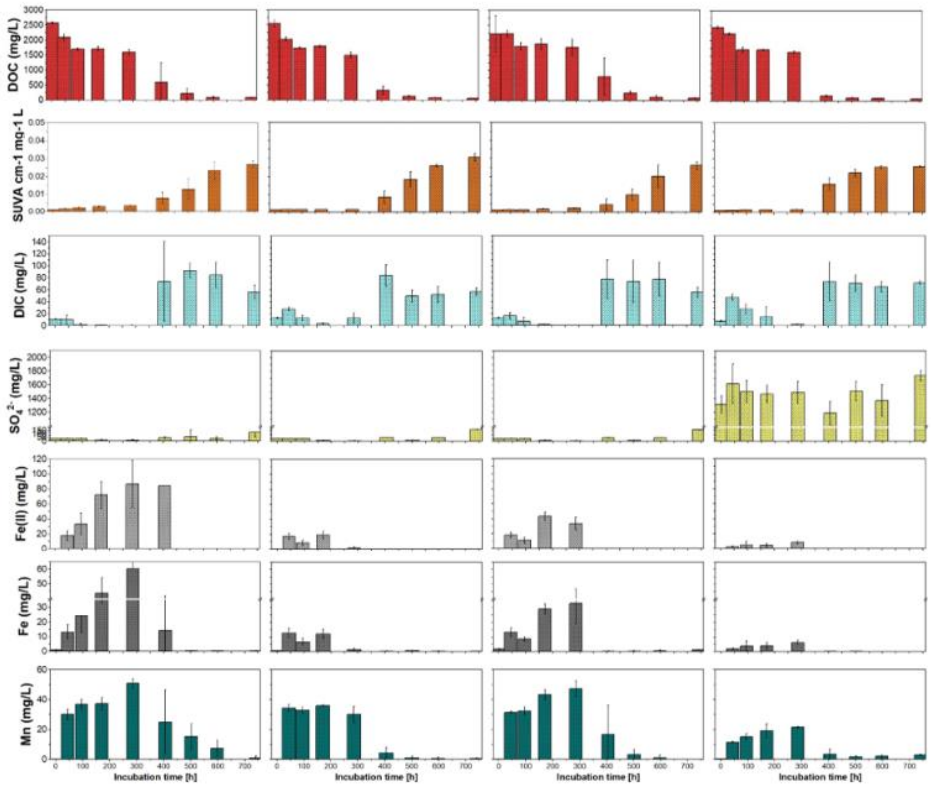

Table 4.7 Concentrations of Dissolved Organic Carbon (DOC), Specific Ultraviolet Absorbance (SUVA), Dissolved Inorganic Carbon (DIC), SO_4^{2-}, Fe, Mn, and Fe(II) parameters in the liquid fraction of soil at different sampling points

Soil	E_H windows	E_H(6 h)	pH (6 h)		SUVA	DOC	DIC	SO_4^{2-}	Fe(II)	Fe	Mn
					cm-1 mg-1 L	mg/L	mg/L	mg/L	mg/L	mg/L	mg/L
Valentino	initial point	357	7.3		0.001	2575	11	36	<LOD	1.0	0.2
				±SD	0.0001	30	1	1	<LOD	0.4	0.02
	-200	-213	5.7		0.002	2088	10	38	17.7	13	30.2
				±SD	0.0003	107	7	4	6.3	5	3.3
	-100	-109	6.1		0.003	1696	2	36	33.2	24	36.9
				±SD	0.001	35	2	7	14.8	11	3.2
	0	-7	5.7		0.003	1709	1	15	72.1	44	37.4
				±SD	0.001	74	1	11	17.9	11	4.2
	100	86	5.4		0.004	1595	0.3	11	86.6	60	50.9
				±SD	0.001	85	0.3	7	31.3	22	2.9
	200	212	6.9		0.008	593	74	46	84.1	14	25.1
				±SD	0.003	657	66	17		28	21.3
	300	307	7.1		0.013	215	92	65	<LOD	0.3	15.3
				±SD	0.006	177	12	96		0.2	8.6
	400	411	7.3		0.023	92	85	37	<LOD	0.2	7.4
				±SD	0.005	28	21	23		0.1	5.5
	500	494	6.8		0.027	84	56	132	<LOD	0.3	1.1
				±SD	0.002	19	11	73		0.2	1.1
Pellerina	initial point	298	7.3		0.002	2553	13	39	<LOD	0.6	0.2
				±SD	0.0001	110	1	1		0.1	0.01
	-200	-210	5.8		0.002	2035	28	37	17.1	13	34.5
				±SD	0.0001	63	3	2	4.0	3	2.2
	-100	-63	6.4		0.002	1730	13	36	8.6	7	32.9
				±SD	0.0001	39	4	2	3.5	3	2.2
	0	-14	6.1		0.002	1802	4	12	18.9	12	35.9
				±SD	0.0000	39	1	1	5.1	3	0.6
	100	57	6.9		0.002	1499	13.1	7	1.5	1	30.0
				±SD	0.0001	104	8.4	2	1.6	1	5.3
	200	204	7.4		0.008	327	84	55	<LOD	0.3	4.5
				±SD	0.004	135	18	1		0.2	3.4
	300	329	7.8		0.018	125	49	16	<LOD	0.7	1.0
				±SD	0.004	34	10	1		0.1	1.0
	400	418	7.8		0.026	80	52	50	<LOD	0.3	0.7
				±SD	0.001	4	13	1		0.2	0.7
	500	533	7.3		0.031	58	57	173	<LOD	0.2	0.6
				±SD	0.002	4	6	2		0.02	0.7
Sangone	initial point	402	7.3		0.001	2212	13	36	<LOD	1.6	0.2
				±SD	0.00002	605	1	3		0.5	0.04
	-200	-205	5.7		0.002	2217	16	41	18.2	14	31.4
				±SD	0.0002	117	5	3	3.3	3	0.8
	-100	-142	6.5		0.002	1798	7	36	11.4	9	32.4
				±SD	0.0001	121	7	4	4.1	2	2.6

	0	-1	5.8		0.002	1878	1	14	43.0	29	43.3
				±SD	0.0002	184	1	5	5.5	4	3.4
	100	72	5.8		0.002	1765	0.1	6	33.4	33	47.4
				±SD	0.0002	278	0.1	5	8.5	14	5.3
	200	262	7.2		0.004	794	77	52	<LOD	0.2	16.8
				±SD	0.003	624	33	7		0.1	19.3
	300	335	7.5		0.011	204	78	17	<LOD	0.4	3.3
				±SD	0.004	93	26	0		0.3	3.1
	400	401	7.7		0.020	109	77	49	<LOD	0.5	1.3
				±SD	0.006	55	28	1		0.6	1.8
	500	509	7.0		0.026	79	56	169	<LOD	1.3	0.1
				±SD	0.002	14	8	2		0.2	0.1
Shanty Town	initial point	386	7.3		0.001	2445	8	1317	<LOD	0.1	0.5
				±SD	0.0001	41	1	131		0.01	0.05
	-200	-192	6.0		0.001	2230	48	1619	2.7	2	11.5
				±SD	0.00005	41	5	287	0.6	0.5	0.4
	-100	-125	6.4		0.002	1698	28	1508	5.1	4	15.2
				±SD	0.0001	88	8	161	4.1	3	2.3
	0	-1	6.4		0.002	1697	15	1474	4.4	4	19.2
				±SD	0.0001	22	17	128	2.3	2	4.6
	100	97	5.9		0.002	1619	2.3	1494	8.1	6	21.6
				±SD	0.0001	40	0.4	159	2.1	1	0.4
	200	206	7.4		0.016	171	74	1192	<LOD	0.2	3.5
				±SD	0.003	28	32	170		0.01	3.3
	300	324	7.6		0.022	102	71	1512	<LOD	0.2	1.8
				±SD	0.002	16	14	138		0.1	0.5
	400	408	7.1		0.026	85	65	1377	<LOD	0.1	2.0
				±SD	0.001	6	9	230		0.05	0.9
	500	499	6.6		0.026	71	72	1742	<LOD	0.1	3.1
				±SD	0.0004	2	3	73		0.02	0.4

Table 4.8 Spermann correlation coefficients of Dissolved Organic Carbon (DOC), Specific ultraviolet Absorbance (SUVA), Dissolved Inorganic Carbon (DIC), Fe, Mn, and SO_4^{2-} versus E_H and pH

	Soil	DOC	SUVA	DIC	SO_4^{2-}	Fe (II)	Fe	Mn
E_H	**V**	-0.96**	0.97**	0.61**	n.c.	-0.65**	-0.63**	-0.68**
	E	-0.96**	0.88**	0.62**	n.c.	-0.83**	-0.84**	-0.87**
	S	-0.94**	0.94**	0.62**	n.c.	-0.72**	-0.65**	-0.72**
	T	-0.97**	0.96**	0.63**	n.c.	-0.75**	-0.78**	-0.63**
	All soils	-0.95**	0.91**	0.63**	n.c.	-0.76**	-0.74**	-0.73**
pH	**V**	-0.67**	0.62**	0.76**	n.c.	-0.89**	-0.84**	-0.83**
	E	-0.82**	0.71**	0.64**	n.c.	-0.89**	-0.77**	-0.85**
	S	-0.80**	0.61**	0.71**	n.c.	-0.85**	-0.79**	-0.78**
	T	-0.53**	0.57**	0.60**	n.c.	-0.79**	-0.63**	-0.77**
	All soils	-0.72**	0.60**	0.71**	n.c.	-0.88**	-0.79**	-0.81**

4.3.2.1. Dissolved Organic Carbon (DOC)

Under reducing conditions, the concentrations of Dissolved Organic Carbon (DOC) were consistently higher compared to oxidizing conditions across all treatments. Initially, DOC concentrations ranged from approximately 2000 mg/L at the start of the experiment (under the most reducing conditions) to 60 mg/L at the end of the experiment (under the most oxidizing conditions). This decrease in DOC concentration coincided with a reduction in E_H and pH during the early stages of the experiment. For all soils, DOC reached its highest values in the initial redox windows (-200 mV, -100 mV, 0 mV, +100 mV), showing a stepwise decrease trend, stabilizing at around 1500 mg/L during the windows with E_H at -100 mV, 0 mV, and +100 mV.

The Spearman correlation coefficient in Table 4.8 indicates a significant negative correlation for DOC with both E_H and pH across all four soils. The correlations with E_H are as follows: Shanty Town -0.97**, Valentino and Pellerina -0.96**, and Sangone -0.94**. The minimal differences observed among the four sampled soils are likely due to the high levels of DOC resulting from adding glucose, local vegetation, and straw to all soils to ensure the experiment was not limited by carbon availability. Given that E_H conditions were predetermined and imposed on all soils, we can conclude that the dynamics of DOC in solution are reproducible across the four soils and are inversely correlated with E_H.

pH exhibits a negative correlation with DOC, stronger for Pellerina (0.82**), Sangone (0.80**) soils and weaker in Valentino (-0.67**), Shanty Town (-0.53**). Thus, the higher the DOC concentration, the lower the pH recorded during the experiment. From +200 mV, DOC tends to decrease significantly, especially for Pellerina and Shanty Town, where a more pronounced increase in pH is observed as the system shifts from the +100 mV window to the +200 mV window.

The respiratory processes of soil microorganisms continually produce CO_2, which lowers the pH and alters the solubility of many elements (Stotzky, 2016). The equilibrium reactions governing various carbonate species are summarized as follows:

$$CO_2\ (g) + H_2O <-> H_2CO_3°$$

$$H_2CO_3° <-> H^+ + HCO_3^-$$

$$HCO_3^- <-> H^+ + CO_3^{2-}$$

$$CO_{2(g)} + H_2O <-> H^+ + HCO_3^-$$

$$CO_{2(g)} + H_2O <-> 2H^+ + CO_3^{2-}$$

Very high pressures of CO_2 arise in flooded soils because it can slowly escape from the soil only in percolating water and by diffusion in the soil solution to the floodwater and atmosphere. The pressure of CO_2 influences the rate of movement of soil acidity. A high value results in a high concentration of H_2CO_3 in the soil solution, and consequently, pH changes in one soil portion may be propagated rapidly to others as HCO_3^- ions diffuse from regions with higher pH.

At high CO_2 pressures, which are likely to be found in flooded soils (Stotzky, 2016), very high soil acidity diffusion coefficients arise: above neutral pH, $[HCO_3^-]_L$ is high and the contribution of the H_2CO_3– HCO_3^- pair dominates soil acidity movement even at quite low pH. In alkaline soils, CO_2 accumulation lowers the pH. When a reduced alkaline soil is dried and oxidized, the pH will tend to increase as dissolved CO_2 escapes from the soil. If the same soil is oxidized without drying, the CO_2 does not escape, and the pH may fall as acidity is produced in oxidation reactions, as predicted by the model. A higher pH results in a higher rate of neutralization of acidity generated by oxidation, and a smaller lowering of pH in the oxidation region. Microbial activities and organic matter (OM) decomposition contribute to CO_2 and organic acid production (Tranvik, 1998), explaining the lower pH observed during reducing conditions. Although other acids like succinic, lactic, butyric, and propionic acids are produced, their concentrations are generally lower than acetic acid, making it the major contributor to pH reduction (Gupta et al., 2018). This decrease in pH is also partly due to the breakdown of glucose. Glucose can undergo both oxidative and reductive reactions, resulting in various products such as carbon dioxide, oxalate, formate, acetaldehyde, acetylene, ethylene, methanol, ethanol, and methane. The transformation of glucose into acetic acid, a common intermediate in anaerobic respiration, does not involve a net transfer of electrons. During decomposition, all forms of organic matter, including carbohydrates, fats, and amino acids, are converted to acetic acid (Gupta et al., 2018).

Consequently, the increase in DOC under reducing conditions can be explained with two processes:

1. the production of dissolved organic metabolites by reducing bacteria before fermentation.

2. the solubilization of OM originally bound onto Fe- and Mn-oxyhydroxides. Fe- and Mn- oxyhydroxides strongly adsorb OM. When

soil becomes water-saturated, microorganisms that normally use oxygen as the terminal electron acceptor for OM oxidation will change to other electron acceptors such as Fe and Mn. This shift results in the reductive dissolution of Fe- and Mn- oxyhydroxides, followed by a release of associated substances including OM (Zhang et al., 2014).

In oxidizing conditions, the decrease in DOC could be explained by the increase of oxygen availability that might accelerate the aerobically microbial mineralization of organic compounds (Hanke et al., 2013), thereby decreasing the concentration of DOC or the microbial utilization of DOC throughout the experiment (Shaheen et al., 2016; Yu et al., 2007).

4.3.2.2. Specific Ultra Violet Adsorbance (SUVA)

The Specific Ultraviolet Absorbance (SUVA) values in this experiment increased with rising E_H and pH, showing a consistent upward trend throughout the experiment. The correlation matrix revealed a significant positive correlation (>0.9) between SUVA and E_H. Conversely, the correlation between SUVA and pH was positive but considerably lower (<0.7).

These findings suggest that low molecular weight and labile organic carbon (C) were more readily decomposed under reducing conditions (Yang et al., 2016). At low pH levels in our soils, protonated hydroxyl groups on mineral surfaces may have induced a positive charge, promoting the adsorption of negatively charged organic molecules and facilitating their surface complex formation.

Under oxidizing conditions, aromatic carbon compounds exhibited greater resistance and accumulation. As pH increased, the deprotonation of hydroxyl groups reduced the positive net surface charge, making organic molecules more electronegative. Consequently, mineral surfaces and organic matter repelled each other, limiting surface complex formation.

The aromaticity values lend support to the hypothesis of increased DOC under reducing conditions due to the production of soluble organic metabolites by soil microbial biomass. Microbial metabolites, which are low molecular weight compounds, are associated with low aromaticity, aligning with the observed trends in SUVA.

4.3.2.3. Dissolved Inorganic carbon

As described in the previous section, an increase in pH occurs in the -100 mV and +200 mV redox windows, with the latter exhibiting a faster increase compared to the former.

The pH elevation is attributed to the continuous consumption of H^+ during carbonate dissolution. In alkaline soils, CO_3^{2-} reaches levels where many metal carbonates can form, thereby increasing the concentration of many carbonate minerals, which, in turn, impose limits on the solubility of many metal ions and govern soil pH even under flooded conditions. Carbonate dissolution increases pH according to the following reaction:

$$CO_3^{2-} + 2H_2O <-> H_2CO_3 + 2OH^-$$

As evident from Figure 4.4, the presence of DIC in solution for all four soils seems to justify the pH increase. Spearman correlation coefficients calculated for DIC relative to E_H are: Valentino 0.62**, Pellerina 0.62**, Sangone 0.62**, Shanty Town 0.63**; while for pH: Valentino 0.77**, Pellerina 0.64**, Sangone 0.71**, Shanty Town 0.60**.

All soils exhibit varying degrees of DIC increase in solution in the lowest redox window, -200 mV, in decreasing order: ShantyTown 47.6 mg/L, Pellerina 27.9 mg/L, Sangone 16.1 mg/L, and Valentino 10.1 mg/L. These concentrations, as observed in the trend graphs extensively discussed in Section 4.3.1, coincide with the first noticeable pH increase around 100 hours from the incubation time, corresponding to the -100 mV redox window. The DIC likely originates from the dissolution of calcium and magnesium carbonates, which also justifies the concurrent increase in calcium and magnesium in solution. Only in Shanty Town, in the +0 mV redox window, is there still a significant presence of DIC in solution, justifying a slower pH decrease. In the +100 mV redox window, only Pellerina exhibits a considerable concentration of DIC in solution concurrent with a pH increase.

Subsequently, after an almost complete absence of DIC in solution, an increase in DIC concentration and pH is observed in all soils in the +200 mV redox window. Particularly, in the +200 mV window, Pellerina exhibits 84.1 mg/L in solution, followed by Sangone with 77.1 mg/L, Valentino with 74.2 mg/L, and finally Shanty Town with 73.6 mg/L.

In the subsequent redox windows, the soils of Valentino and Sangone maintain a high IC concentration until the +400 mV redox window, before decreasing in the +500 mV window to 56.3 mg/L and 55.9 mg/L, respectively. Meanwhile, both soils exhibit an increase in pH followed by a subsequent decrease.

For Shanty Town, however, DIC remains high until the +500 mV redox window, along with calcium and magnesium, unlike the other soils. Nevertheless, the pH decreases, likely due to the presence of other species in solution counteracting the pH-raising effect of carbonates.

In contrast, Pellerina exhibits a different behavior compared to the other soils: from the +300 mV redox window, it shows a halving of DIC concentration in solution, decreasing from 84.1 mg/L to 49.3 mg/L and remaining around 50 mg/L until the end of the incubation.

4.3.2.4. Fe and Mn minerals

The solubility of Fe and Mn exhibited significant negative correlations with soil E_H and pH across all soils. Fe(II) and Fe showed highly similar correlation coefficients to Mn, with negative correlations ranging from -0.6** for Mn in Shanty Town to -0.87** for Mn in Pellerina. Similarly, the correlation with pH varied from -0.63** for Fe in Shanty Town to -0.89** for Fe(II) in both Valentino and Pellerina.

As observed in all soils, albeit with varying intensities, the behavior of Fe and Mn appeared very similar. Concentrations of Fe and Mn in all soils ranged from 0.071 mg/L to 86.8 mg/L for Fe and from 0.005 mg/L to 53.4 mg/L for Mn.

In the Valentino soil, exhibiting the highest concentration of both elements, Fe, Fe(II), and Mn began to be present in solution from the -100 mV window. The concentration of Mn in solution remained fairly stable in the windows from -200 mV to 0 mV. The maximum values were recorded in the +100 mV window, where the lowest pH was recorded (5.4), and were: Fe(II) 87 mg/L, Fe 60 mg/L, and Mn 50 mg/L. Fe(II) remained high even at 200 mV (84 mg/L), while Fe and Mn decreased drastically. Compared to Fe, Mn continued to have a significant presence even in the redox windows from +200 mV to +400 mV, where the pH gradually increased from 6.9 to 7.3.

Pellerina, exhibited lower concentrations of Fe and Mn compared to Valentino. The highest values were found at 0 mV (Fe(II) 19 mg/L, Fe 12 mg/L, and Mn 36 mg/L), with pH 6.1, and at -200 mV (Fe(II) 17, Fe 13, Mn 34 mg/L), with pH 5.8. The concentration of Mn in solution remained around 30 mg/L from the -200 mV to +100 mV window and decreased drastically from +200 mV, where the pH reached 7.4.

Similar to Valentino, Sangone exhibited higher values of Fe and Mn in the 0 mV and +100 mV windows, characterized by a pH of 5.8. Significant concentrations could be observed in the -200 mV window

(pH=5.7). Mn maintained a high concentration in solution from -200 mV to 100 mV, before decreasing at +200 mV but remaining appreciable. Fe, on the other hand, exhibited a drastic decrease at +200 mV with a pH of 7.2.

Shanty Town showed maximum concentrations at +100 mV, pH 5.9, which were much lower compared to the other soils. Starting from -200 mV, pH 6.0, there was a noticeable increasing trend for both Mn (11.5 - 21.6 mg/L) and Fe (1.9 - 6.1 mg/L). At +200 mV, pH 7.4, both Fe and Mn decreased drastically: 0.2 and 3.5 mg/L, respectively.

At -200 mV, the pH decrease caused by OM decomposition likely facilitates the dissolution of minerals in solution. in the form of hydroxides and bicarbonates, which counteract the pH decrease. Indeed, for all soils, a temporary pH increase is observed in the -100 mV redox window, probably due to both carbonates and the redox chemistry of Fe and Mn, which can abiotically accept electrons. This finding might be tied to the redox chemistry of Fe- and Mn- hydroxides, which could accept electrons abiotically and biotically from chemical donors. The abiotic reduction of Mn and Fe can occur under low redox potential conditions, with adequate availability of reducing agents (organic or inorganic compounds) and/or the presence of electrons, and is favored under neutral to slightly acidic pH conditions (Aeppli et al., 2019; Reddy and DeLaune, 2008; Xiao et al., 2018).

The reduction of Fe^{3+} to Fe^{2+} and Mn^{4+} to Mn^{2+} can occur according to the following reactions:

$Fe(OH)_3 + 3H^+ + e^- <-> Fe^{2+} + 3H_2O$

$Fe_2O_3 + 6H^+ + 2e^- <-> Fe^{2+} + 3H_20$

$MnO_2 + 4H^+ + 2e^- <-> Mn^{2+} + 2H_2O$

The increase in pH under weakly acidic conditions could also be due to the dissolution of hydroxides.

In the +0 mV redox window, the phenomenon of pH decrease, favored by the conditions of the window, in addition to attributing it to the DOC as described in the previous paragraph, is probably partly due to the hydrolysis of Fe and Mn species.

Another potential source of protons that could influence the pH decrease to a lesser extent might be the oxygen insufflated to reach the next redox window in the presence of Fe(II) in solution, according to the following reaction:

$4Fe^{2+} + 0_2 + 10H_2O = 4Fe(OH)_3 + 8H^+$

This reaction may have been more favored in the soils of Pellerina, Sangone, and Shanty Town, which reached higher pH levels (Figure 4.3), resulting in the precipitation of hydroxides. This could be one of the reasons why the iron concentration in solution in the soils of Pellerina, Sangone, and Shanty Town is much lower compared to Valentino.

The amount of iron available depends primarily from factors such as organic carbon content, soil acidity, temperature, and the 'active' iron content per se (Ponnamperuma, 1972; Reddy et al., 1986). This leads to an increase in pH, as observed in the soils of Valentino, Sangone, and Shanty Town after maintaining a stable +100 mV redox window. Valentino shows lower pH values for a longer time, possibly due to the higher presence of Fe and Mn with a potential for greater hydrolysis.

The lower concentrations of Fe in the +100 mV redox window for the Pellerina soil may be due to the instability of that EH window. In the case of Shanty Town, the very low concentrations of Fe in solution could be explained by the elevated sulfate (SO_4^{2-}) levels in solution, which competitively inhibit the reduction of Fe^{3+} by reductants, as sulfate reduction is favored at pH >5 (Blodau, 2006).

In the +200 mV redox window, the continued consumption of protons during Mn reduction may contribute to the increase in pH. In subsequent redox windows, only Valentino and Sangone continue to show a significant concentration of Mn in solution. The actual dissolution reaction can be complex and involve a series of chemical and biological processes, as seen in the preceding paragraphs.

At the beginning of the +200 mV redox window, Sangone and Pellerina exhibit instability. This might stem from the fact that they are parks formed from excavation soils and rocks, composed of a variety of minerals that can present different aggregation structures and also manganese and iron oxides in various aggregation states. Therefore, the instability could be caused by bacteria using Fe or Mn as proton acceptors, which are more or less exposed and readily available on the surface of the aggregates present (Zhang et al., 2014).

Regarding Fe, only Valentino continues to have a soluble Fe concentration even in the +200 mV redox window. For the other soils, the concentration in solution is below detectable limits, possibly due to the slightly higher pH recorded in the soils of Pellerina, Sangone, and Shanty Town, leading to Fe immobilization via precipitation into oxyhydroxides. It can be hypothesized that a mixture of Fe^{2+} and Fe^{3+}

oxides likely precipitates in the soils when they are highly reduced and that the amorphous form produced is less soluble than fresh precipitated $Fe_3(OH)_8$ (Graf, 1980).

An abrupt decrease in dissolved Mn was noticed at +300 mV, where the increase in pH may have led to Mn immobilization via precipitation as oxyhydroxides. In fact, in the soils of Pellerina and Shanty Town, the decrease in Mn solution occurs earlier compared to Valentino and Sangone, which have lower pH values.

Under oxidizing conditions, both Fe and Mn in all soils have negligible concentrations in solution, probably due to precipitation.

4.3.2.5. Sulfates

The concentrations of SO_4^{2-} in the liquid phase were much higher in Shanty Town compared to the soils of Valentino, Pellerina, and Sangone. The concentration ranges are as follows: Valentino 10.9-131.99 mg/L, Pellerina 6.67-172.51 mg/L, Sangone 5.96-169.14 mg/L, and Shanty Town 1191.88-1741.84 mg/L.

Probably, in the latter area, the lack of an adequate sewage system results in the direct disposal of wastewater into the soil, carrying various contaminants such as detergents and cleaning products. Additionally, the combustion of materials such as wood, coal, or solid waste can produce sulfur gases that contaminate the soil.

On the other hand, sulfate could derive from gypsum (calcium sulfate dihydrate, $CaSO_4*2H_2O$), which is often deliberately added to reconstituted soils to reduce alkalinity, provide calcium and sulfur, and improve soil structure. Gypsum can come from various sources: residual material recovered from cement production; byproduct of the rock phosphate fertilizer production process; byproduct of sulfuric acid production; in some cases, it can be recovered as part of the waste recycling process, especially industrial waste and demolition residues (Abel et al., 2015).

SO_4^{2-} did not show significant correlations in any of the soils. The concentration of SO_4^{2-} in the liquid phase is often a poor indicator of reduction due to the rapid internal sulfur cycling in wetland soils (Du Laing et al., 2009; Shaheen et al., 2014; Rinklebe et al., 2016a).

The oxidation-reduction reactions involving sulfate are more intricate than their acid-base interactions due to the various oxidation states sulfur can assume, ranging from +2 to +6. Sulfate is weakly retained by soils and can be divided into the following categories: easily soluble

sulfate, adsorbed sulfate, and insoluble sulfate. In calcareous soils, co-precipitation with $CaCO_3$ is possible. Sulfate is the predominant form of sulfur over most of the pH and E_H range encountered in natural waters.

In natural systems, redox reactions with sulfate are typically slow unless facilitated by microorganisms. Very little sulfate reduction occurs without specific bacteria species, as *Desulfovibrio desulfuricans*, the predominant sulfate reducer in waterlogged soils and freshwater sediments, an obligate anaerobe, like other sulfate-reducing bacteria. These bacteria thrive within a narrow pH range, with no growth observed below pH 5.5 (Wind et al., 1999).

The presence of SO_4^{2-} in the liquid fraction of submerged soil may contribute to soil acidification, although it is not the predominant factor. Under specific conditions, sulfates can react with other compounds; for example, the oxidation of sulfides can produce sulfuric acid (H_2SO_4), leading to a decrease in pH. The acidification effect caused by sulfates might be less significant compared to other factors such as OM decomposition and hydrogen sulfide production in anaerobic soil conditions. Moreover, the net effect will depend on the sulfate concentration and the presence of other factors that can influence pH. Therefore, although sulfates may contribute to soil acidification under certain conditions, their overall influence on soil acidity can vary depending on specific soil factors and the surrounding environment, such as soil buffering capacity and overall chemical balance. It can thus be hypothesized that the pH reduction in the +100 mV redox window for all soils is partly due to the presence of SO_4^{2-} in the liquid fraction.

4.3.3. PTE mobilization dynamics

4.3.3.1. Zinc (Zn)

Zinc, a versatile chemical element, retains its relevance across diverse industrial sectors. Its applications range from galvanization for corrosion protection of iron and steel to battery manufacturing, pharmaceuticals, rubber vulcanization, pigment production, and agricultural fertilizers (including ZnEDTA and $ZnSO_4$ in organic and inorganic forms). Moreover, zinc plays a crucial role in water treatment processes. Additional sources of zinc pollution encompass fossil fuel emissions, non-ferrous metal smelting, sewage sludge, and animal excreta from feed additives containing zinc sulfate. Hence, zinc (alongside copper) is found, often in significant amounts, in animal excreta, as animals assimilate only small percentages of the metals in their feed, resulting in highly enriched feces (Pinto et al., 2018).

In natural settings, zinc primarily exists in sulfide, carbonate, silicate, and oxide forms. In the soils of the Turin Plain, Zn associates with various minerals primarily linked to sedimentary and metamorphic rocks. (*Environmental Inorganic Chemistry*, 1988; Graf, 1980).

The only oxidation state of significance for zinc under environmental conditions is +2. However, the speciation of ligands that react with Zn^{2+} (e.g., sulfur) can be influenced by E_H. The precipitation of sulfide is a crucial factor controlling the mobility of zinc in reducing environments. Metallic zinc (crystalline) forms only in highly reducing environments.

The solubility of zinc in soil water is linked to soil-Zn adsorption equilibria. Several factors notably influence zinc's solubility, including pH, redox potential, temperature, and the presence of complexing ligands, competing ions, and precipitating agents.

Zinc exhibits negligible hydrolysis below pH 6, but significant hydrolysis occurs above pH 7, leading to the formation of aqueous hydrolysis products. In most natural waters, zinc is readily transported, especially in neutral and acidic solutions, due to the solubility of its species formed with common ligands, making it one of the most mobile PTE. The predominant species in solution varies with pH: below 7.7, Zn^{2+} prevails; between 7.7 and 9, $ZnOH^{+}$ predominates; and above 9, neutral $Zn(OH)_2$ becomes prevalent. Other complexes like $ZnSO_4$ and $ZnHPO_4$ can also contribute significantly to the zinc content in solution.

Organic ligands typically present in aqueous systems have minimal impact on zinc speciation. However, in polluted areas, organic materials can alter the chemical form of zinc. Non-complexing monovalent anions (NO_3^-, Cl^-, ClO_4^-) have limited influence on zinc sorption, while multivalent anions (e.g., SO_4^{-2}, CrO4-², PO_4^{-3}) may enhance zinc sorption by Fe oxides, likely by reducing surface particle charge.

The sorption of zinc on soil and sediments profoundly affects its environmental mobility. Various sorbents, including hydrous iron and manganese oxides, clay minerals, carbonate minerals, and organic matter, significantly impact zinc behavior in soil and sediments. Specific adsorption, co-precipitation, and ion exchange processes contribute to zinc sorption on soils and sediments.

The concentrations found in solution for zinc in different redox windows are reported in Table 4.9 and represented in Figure 4.5.

For all soils, a higher presence in solution is observed under reducing conditions compared to oxidizing ones. Indeed, zinc showed significant

negative correlations with E_H in all soils (Table 4.10).: Valentino -0.62**, Pellerina -0.87**, Sangone -0.78**, and Shanty Town -0.62**. The highest concentrations were observed in the Shanty Town soil (8.25 mg/L at +100 mV) while the lowest in Pellerina. All the soils showed the highest concentration when reached the lowest pH of the trial.

Moreover, pH is negatively correlated with Zn in all soils, confirming the established role played by acidity in promoting the release of metallic components: Valentino -0.90**, Pellerina -0.88**, Sangone -0.89**, and Shanty Town -0.84**.

With increasing pH, zinc can undergo hydrolysis and form insoluble zinc hydroxides, represented by the following reaction:

$$Zn^{2+} + 2H_2O \rightarrow Zn(OH)_2\downarrow + 2H^+$$

The zinc hydroxide formed is generally insoluble in water, especially at high pH levels. The formation of insoluble hydroxides may lead to zinc precipitation in the soil, reducing its bioavailability and influencing the biogeochemical cycle in the environment. However, it's important to note that the solubility and stability of Zn hydroxides can vary depending on factors such as zinc ion concentration, pH, temperature, and the presence of other ions in the soil.

Table 4.9 Concentrations of Cr, Cu, Ni, Pb, and Zn in the liquid fraction of soil at different sampling points

	E_H windows	E_H (6 h)	pH (6 h)		Cr	Cu	Ni	Pb	Zn
					mg/L	mg/L	mg/L	mg/L	mg/L
Valentino	initial point	357	7.3		0.01	0.15	0.1	<LOD	0.05
				±SD	0.001	0.01	0.004		0.01
	-200	-213	5.7		0.02	0.02	0.2	<LOD	0.3
				±SD	0.003	0.004	0.04		0.09
	-100	-109	6.1		0.03	0.02	0.3	<LOD	0.2
				±SD	0.01	0.001	0.05		0.08
	0	-7	5.7		0.03	0.01	0.3	<LOD	0.40
				±SD	0.01	0.001	0.1		0.07
	100	86	5.4		0.04	0.01	0.5	<LOD	0.8
				±SD	0.01	0.002	0.1		0.3
	200	212	6.9		0.03	0.03	0.2	<LOD	0.3
				±SD	0.01	0.02	0.2		0.5
	300	307	7.1		0.02	0.09	0.1	<LOD	0.01
				±SD	0.003	0.01	0.03		0.003
	400	411	7.3		0.01	0.10	0.1	<LOD	0.02
				±SD	0.001	0.01	0.02		0.01
	500	494	6.8		0.02	0.10	0.1	<LOD	0.03
				±SD	0.003	0.02	0.01		0.01
Pellerina	initial point	298	7.3		0.07	0.13	0.04	<LOD	0.05
				±SD	0.001	0.00	0.003		0.01
	-200	-210	5.8		0.01	0.01	0.2	<LOD	0.6
				±SD	0.002	0.001	0.02		0.06
	-100	-63	6.4		0.02	0.02	0.2	<LOD	0.2
				±SD	0.003	0.002	0.01		0.03
	0	-14	6.1		0.02	0.01	0.2	<LOD	0.3
				±SD	0.01	0.002	0.02		0.02
	100	57	6.9		0.02	0.01	0.1	<LOD	0.09
				±SD	0.003	0.004	0.01		0.04
	200	204	7.4		0.02	0.02	0.1	<LOD	0.02
				±SD	0.01	0.01	0.01		0.01
	300	329	7.8		0.01	0.08	0.1	<LOD	0.02
				±SD	0.007	0.01	0.002		0.008
	400	418	7.8		0.01	0.07	0.1	<LOD	0.02
				±SD	0.004	0.01	0.005		0.01
	500	533	7.3		0.01	0.06	0.1	<LOD	0.02
				±SD	0.002	0.001	0.004		0.01
Sangone	initial point	402	7.3		0.01	0.20	0.04	<LOD	0.04
				±SD	0.003	0.01	0.002		0.00
	-200	-205	5.7		0.02	0.03	0.2	<LOD	0.4
				±SD	0.003	0.003	0.01		0.05
	-100	-142	6.5		0.02	0.02	0.2	<LOD	0.2
				±SD	0.004	0.005	0.05		0.06
	0	-1	5.8		0.02	0.01	0.2	<LOD	0.2
				±SD	0.00	0.004	0.03		0.06
	100	72	5.8		0.03	0.01	0.3	<LOD	0.5
				±SD	0.004	0.002	0.1		0.3
	200	262	7.2		0.02	0.03	0.1	<LOD	0.04
				±SD	0.01	0.02	0.05		0.02
	300	335	7.5		0.01	0.12	0.1	<LOD	0.01
				±SD	0.004	0.03	0.03		0.02
	400	401	7.7		0.01	0.14	0.1	<LOD	0.01
				±SD	0.001	0.01	0.02		0.002
	500	509	7.0		0.02	0.16	0.1	<LOD	0.02
				±SD	0.002	0.03	0.03		0.01

Shanty Town	initial point	386	7.3		0.01	0.27	0.1	<LOD	0.3
				±SD	0.000	0.02	0.007		0.03
	-200	-192	6.0		0.02	0.06	0.2	0.05	5
				±SD	0.002	0.007	0.01	0.01	0.5
	-100	-125	6.4		0.03	0.05	0.3	0.05	6
				±SD	0.01	0.01	0.07	0.01	3
	0	-1	6.4		0.03	0.04	0.3	0.06	5
				±SD	0.01	0.006	0.1	0.01	3
	100	97	5.9		0.03	0.04	0.4	0.09	8
				±SD	0.00	0.008	0.02	0.01	0.3
	200	206	7.4		0.02	0.06	0.2	<LOD	0.1
				±SD	0.00	0.01	0.00		0.02
	300	324	7.6		0.03	0.20	0.1	0.06	0.2
				±SD	0.017	0.03	0.01	0.0001	0.0
	400	408	7.1		0.01	0.21	0.1	0.06	0.3
				±SD	0.003	0.04	0.01	0.0001	0.2
	500	499	6.6		0.02	0.25	0.2	0.04	1
				±SD	0.003	0.02	0.02	0.002	0.2

The highest concentrations of Zn were found under the same conditions where the highest concentrations of dissolved organic carbon (DOC) were observed, suggesting DOC can also act as a carrier for these elements, thereby increasing their mobility. Zn can also be associated with organic matter (OM) present in the soil, as fulvic and humic acids, proteins, and polysaccharides; confirmed from the correlations among these parameters in all soils (Table 4.10). These organo-metallic compounds can be formed through processes of adsorption, complexation, and ion exchange between Zn ions and functional groups present in soil organic matter. Soil submersion may facilitate the mobilization of elements from the solid fraction to the liquid phase of the soil, leading to the release of organo-metallic compounds into the liquid fraction, which can influence water quality and aquatic system ecology.

DIC shows a negative correlation with zinc: Valentino -0.80**, Pellerina -0.69**, Sangone -0.80**, and Shanty Town -0.74**. Under high pH conditions, Zn may react with carbonate ions present in the soil to form insoluble Zn carbonate ($ZnCO_3$) precipitates. If Zn is present in the form of Zn^{2+} ions, it can also compete with other cations, such as Ca^{2+} and Mg^{2+}, for adsorption sites on mineral surfaces, including carbonates. Depending on specific conditions, the adsorption capacity of carbonates for Zn can vary (Antoniadis et al., 2018). Another phenomenon between Zn and carbonates, albeit to a lesser extent, may occur at acidic pH where the solubilization of Zn carbonates and subsequent release may have occurred.

Strong positive correlations between Zn, and Fe and Mn suggest that those elements might be affected by the behavior and dynamics of Fe and Mn transformation. Specifically, between Zn and Fe: Valentino

0.88**, Pellerina 0.83*, Sangone 0.84**, and Shanty Town 0.82**; between Zn and Fe(II): Valentino 0.92**, Pellerina 0.89**, Sangone 0.85**, and Shanty Town 0.91**; between Zn and Mn: Valentino 0.86**, Pellerina 0.87**, Sangone 0.84**, and Shanty Town 0.89**. Therefore, when Fe and Mn oxides and hydroxides undergo abiotic and biotic reduction processes, converting to reduced forms, they may lead to the release of previously adsorbed metal ions, including Zn. The reduction of oxides and hydroxides can influence the mobility and availability of Zn, making it more easily transportable with potential subsequent contamination of groundwater and surface waters.

The adsorption of metallic cations on Fe and Mn oxides and hydroxides is also influenced by two processes that may have partly contributed to the dynamics of Zn in solution. The first factor is the surface charge of Fe and Mn oxides and hydroxides, which is highly dependent on pH. The second process happen at pH >7 under oxidizing conditions with the formation of high-valence Fe and Mn oxides and hydroxides, which immobilize Zn in the soil. Therefore, under oxidizing conditions, the dissolved Zn concentration in the soil tends to be lower compared to that under reducing conditions, as Zn ions are less mobile and more readily adsorbed by soil minerals. Zn does not appear to show correlations with sulfate ions.

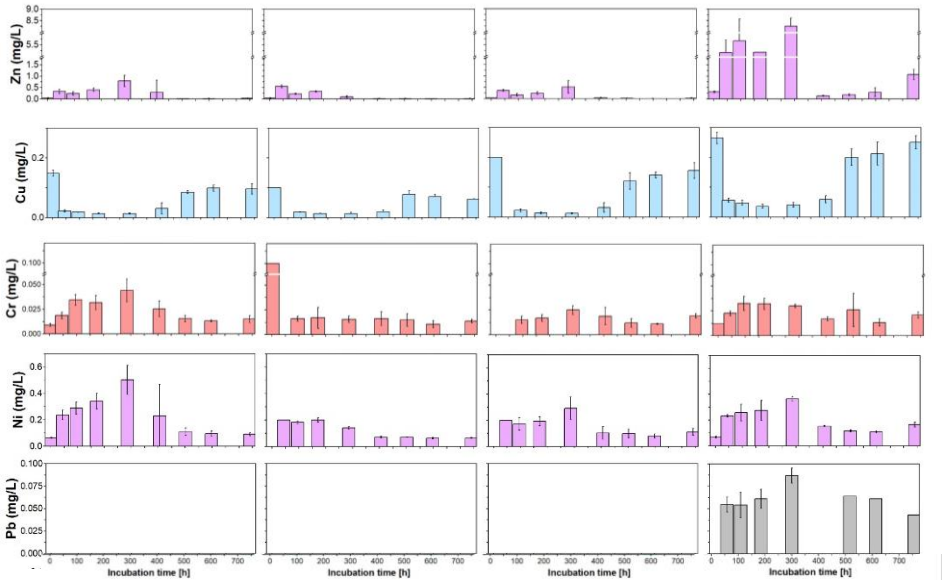

Figure 4.5. Histograms representing Zn, Cu, Ni, and Pb concentrations in liquid fraction at the sampling points. The individual values are shown in the table 4.9

In conclusion, the most important soil parameters regulating the bioavailability and mobility of Zn are pH, the content of OM, and the presence of iron and manganese-hydrated oxides or, to a lesser extent, clays. The bioavailability of Zn decreases as the concentration of H^+ ions decrease. The adsorption or fixation capacity of Zn by clays varies with the cation exchange capacity of the specific surface and the structure of these minerals. Irreversible fixation may also occur due to penetration into the crystal lattice. In alkaline and carbonate soils, Zn fixation is due to the precipitation of Zn hydroxides or carbonates.

4.3.3.2. Chromium (Cr)

The primary sources of Cr pollution are represented by atmospheric deposition caused by emissions from metallurgical industries, especially steelworks or facilities that extract and process Fe. Large quantities of chromite are used in the steel industry to produce ferroalloys that are resistant to corrosion, oxidation, and stress. Cr is also used in the production of stainless steel, refractory bricks (heat-resistant and chemically resistant), pigments, electroplating, and in the dye, tanning, textile, and chemical industries.

Table 4.10 Spermann correlation coefficients. ***significant at 0.01 level*

V	E_H	pH	DOC	DIC	SO_4^{2-}	Fe(II)	Cr	Cu	Fe	Mn	Ni	Pb	Zn
E_H	1	0.61**	-0.95**	0.61**	n.c.	-0.65**	-0.59**	0.68**	-0.63**	-0.68**	-0.66**	n.c.	-0.62**
pH		1	-0.66**	0.76**	n.c.	-0.89**	-0.72**	0.80**	-0.84**	-0.83**	-0.85**	n.c.	-0.91**
DOC			1	-0.61**	n.c.	0.68**	0.59**	-0.70**	0.68**	0.68**	0.67**	n.c.	0.67**
DIC				1	n.c.	-0.89**	-0.76**	0.78**	-0.89**	-0.76**	-0.77**	n.c.	-0.80**
SO_4^{2-}					1	-0.55**	n.c.	n.c.	-0.51**	-0.56**	-0.53**	n.c.	n.c.
Fe(II)						1	0.86**	-0.91**	0.95**	0.93**	0.94**	n.c.	0.92**
Cr							1	-0.83**	0.86**	0.90**	0.90**	n.c.	0.82**
Cu								1	-0.87**	-0.88**	-0.85**	n.c.	-0.81**
Fe									1	0.86**	0.86**	n.c.	0.88**
Mn										1	0.98**	n.c.	0.86**
Ni											1	n.c.	0.91**
Pb												1	n.c.
Zn													1
E													
E_H	1	0.81**	-0.96**	0.62**	n.c.	-0.83**	n.c.	0.70**	-0.84**	-0.87**	-0.88**	n.c.	-0.87**
pH		1	-0.82**	0.64**	n.c.	-0.89**	n.c.	0.72**	-0.77**	-0.85**	-0.85**	n.c.	-0.88**
DOC			1	-0.67**	-0.52**	0.87**	n.c.	-0.74**	0.87**	0.90**	0.91**	n.c.	0.86**
DIC				1	0.75**	-0.76**	n.c.	0.52**	-0.76**	-0.71**	-0.74**	n.c.	-0.69**
SO_4^{2-}					1	n.c.	n.c.	n.c.	-0.60**	-0.55**	-0.57**	n.c.	n.c.
Fe(II)						1	n.c.	-0.65**	0.90**	0.88**	0.90**	n.c.	0.89**
Cr							1	n.c.	n.c.	n.c.	n.c.	n.c.	n.c.
Cu								1	-0.51**	-0.79**	-0.73**	n.c.	-0.71**
Fe									1	0.83**	0.89**	n.c.	0.83**
Mn										1	0.95**	n.c.	0.87**
Ni											1	n.c.	0.84**
Pb												1	n.c.
Zn													1

S													
E_H	1	0.75**	-0.94**	0.62**	n.c.	-0.72**	n.c.	n.c.	-0.65**	-0.72**	-0.71**	n.c.	-0.78**
pH		1	-0.80**	0.71**	n.c.	-0.85**	n.c.	0.54**	-0.79**	-0.78**	-0.82**	n.c.	-0.88**
DOC			1	-0.68**	-0.56**	0.77**	n.c.	n.c.	0.74**	0.74**	0.79**	n.c.	0.84**
DIC				1	0.73**	-0.87**	n.c.	0.74**	-0.86**	-0.81**	-0.82**	n.c.	-0.80**
SO_4^{2-}					1	-0.68**	n.c.	n.c.	-0.67**	-0.74**	-0.62**	n.c.	-0.52**
Fe(II)						1	n.c.	-0.69**	0.92**	0.85**	0.84**	n.c.	0.85**
Cr							1	n.c.	0.56**	0.51**	0.59**	n.c.	0.51**
Cu								1	-0.51**	-0.69**	-0.51**	n.c.	-0.50**
Fe									1	0.78**	0.86**	n.c.	0.84**
Mn										1	0.86**	n.c.	0.84**
Ni											1	n.c.	0.90**
Pb												1	n.c.
Zn													1
T													
E_H	1	0.56**	-0.97**	0.63**	n.c.	-0.75**	-0.52**	0.70**	-0.78**	-0.63**	-0.69**	n.c.	-0.62**
pH		1	-0.53**	0.60**	n.c.	-0.79**	n.c.	0.49**	-0.63**	-0.77**	-0.81**	n.c.	-0.82**
DOC			1	-0.64**	n.c.	0.77**	0.54**	-0.74**	0.83**	0.67**	0.70**	n.c.	0.63**
DIC				1	n.c.	-0.85**	-0.50**	0.87**	-0.76**	-0.71**	-0.74**	-0.51**	-0.74**
SO_4^{2-}					1	n.c.	n.c.	n.c.	n.c.	n.c.	n.c.	n.c.	n.c.
Fe(II)						1	0.74**	-0.78**	0.93**	0.90**	0.91**	0.67**	0.91**
Cr							1	-0.54**	0.79**	0.80**	0.72**	0.64**	0.75**
Cu								1	-0.80**	-0.71**	-0.75**	n.c.	-0.56**
Fe									1	0.85**	0.88**	0.70**	0.81**
Mn										1	0.93**	0.66**	0.89**
Ni											1	0.58**	0.88**
Pb												1	0.70**
Zn													1

However, chromium is a relatively common element in the Earth's crust and can be present in various minerals. Anthropogenic soil contamination overlaps a high natural background, as the Turin plains are composed of sediments derived from the upland serpentinitic areas widely distributed in the Alps (Cr-spinels, such as chromites, magnesium chromites, and Cr-magnetite) (Bonifacio et al., 2010; Rinklebe et al., 2016; Tassi et al., 2018). Although the weathering of indigenous Cr minerals contributes to the geogenic sources of Cr in soils, the majority of Cr could be derived from industrial activities.

Cr can have different oxidation states (Cr^{3+} cation, CrO^{2-} anion, hexavalent with $Cr_2O_7^{2-}$ and CrO_4 anions), but in soils, it generally occurs as trivalent (Cr^{3+}). Cromium(VI) occurs in anionic form, is highly soluble even at relatively low pH levels, easily extractable from soils and sediments, and is also the most toxic form, posing a potential hazard for water environments and humans (Shaheen et al., 2018). The oxidation of Cr^{3+} to Cr^{6+} has been observed in soils with pH above 5 and seems to be strongly favored by the presence of Mn oxides. Therefore, as soil pH increases, the toxicity of Cr also increases, probably due to the increase in the Cr^{6+} species.

Previous research has indicated that Cr in polluted soils is primarily linked with Fe phases, as Fe (oxy)hydroxides act as crucial scavengers owing to their prevalence in the environment and large surface area (Rinklebe et al., 2016; Shi et al., 2020). Fe oxides, sulfides, or dissolved organic substances can convert Cr^{5+} to Cr^{3+} (Yu et al., 2020). Thus, to evaluate the potential harmful effects of Cr, it's imperative not only to ascertain the oxidation states of these elements but also their interaction with soil components that could alter their chemical characteristics. Cr may be conserved within original minerals, co-precipitated with Fe, adsorbed onto soil particles, and complexed with organic entities, the latter of which can undergo alterations under diverse environmental conditions (Xia et al., 2020).

The sorption of Cr^{3+} and Cr^{6+} is complicated by redox fluctuations that can transpire in soil surroundings. Chromate (CrO_4^{2-}) and dichromate ($Cr_2O_7^{-2}$) ions form numerous soluble salts and hence represent the mobile and potentially hazardous forms in soils. In anaerobic conditions, these species are promptly reduced to Cr^{3+} and precipitated. As soil conditions approach neutrality, the formation of dichromate is minimized. The adsorption of Cr^{3+} intensifies with rising pH, leading to precipitation as $Cr(OH)_3$ (Reddy and DeLaune, 2008).

At low concentrations and acidic pH levels, where Cr^{3+} solubility is heightened, significant specific adsorption occurs on Fe and Mn oxides. The creation of soluble organic complexes diminishes the extent of adsorption. Hexavalent chromium exhibits negligible sorption by clays or hydrous metal oxides. Adsorption of Cr^{6+} by hydrous metal oxides and soil diminishes as pH increases. Some adsorption occurs on Mn and Fe oxides. The presence of anions (e.g., sulfate and phosphate) substantially impacts the extent of adsorption by competing for adsorption sites. The formation of ion pairs, such as dissolved calcium chromate, can also diminish adsorption.

OM in soils can catalyze the spontaneous reduction of Cr^{6+} to Cr^{3+}, even under alkaline conditions, and it may serve as a significant adsorbent in soil; slight enrichment of chromium occurs in the humic acid fraction of sediments.

The concentrations of Cr in the liquid fraction in the four soils exhibit reduced concentrations with a small range of variation (Table 4.9, Figure 4.5): Valentino 0.01 – 0.04 mg/L, Pellerina 0.01 – 0.2 mg/L, Sangone 0.01 – 0.03 mg/L, Shanty Town 0.01 – 0.03 mg/L.

Cr shows a significant but weak negative correlation with E_H only for the soils of Valentino (-0.59**) and Sangone (-0.52**), while with pH it shows a strong negative correlation only for Valentino (-0.72**). Also, for the other key factors, Cr shows significant correlations only for Valentino and Shanty Town soils. More specifically, the correlations with dissolved OM are not as strong: Valentino 0.59**; Shanty Town 0.54**. Dissolved OM can act as a ligand for chromium, through complexation processes or the formation of chromium organic complexes, increasing its solubility and presence in the soil liquid fraction.

For DIC, only Valentino shows a significant negative correlation (-0.76**).

Regarding Fe(II), Fe, and Mn, the correlations shown by Valentino (respectively 0.86**, 0.86**, and 0.90**) and Shanty Town (respectively 0.74**, 0.79**, and 0.80**) highlight a relationship between reduction, co-precipitation, and adsorption of Fe and Mn minerals.

For the other soils, Pellerina and Sangone, no significant correlations are evident for Cr in the liquid fraction: the mixing of backfill materials from different sources may have homogenized the distribution and absorption of chromium, reducing the possibility of finding correlations with other variables in the liquid fraction.

4.3.3.3. Nickel (Ni)

Possible sources of Ni pollution include the metallurgical industry, which uses it in the production of metal alloys and employs compounds such as nickel sulfate ($NiSO_4$) and nickel chloride ($NiCl_2$). Vehicle transport releases nickel into the environment through exhaust gases and wear particles from brakes and tires, which contain $Ni(OH)_2$, NiS, and $NiCO_3$. Urban solid waste may contain Ni from consumer products and packaging, such as nickel nitrate ($Ni(NO_3)_2$) from spent batteries and nickel carbonate ($NiCO_3$) from paints and pigments. Furthermore, the use of products such as fertilizers, pesticides, and those containing compounds like Ni acetate ($Ni(CH_3COO)_2$) can result in the release of nickel into the surrounding environment.

Ni ores primarily occur in the form of oxides, silicates, and sulfides and are typically associated with other sulfides and silicates.

The only oxidation state of significance in environmental conditions is Ni^{2+}, although Ni can exhibit valences of +1, +3, or +4 in certain compounds. Ni in soil solution may exist either as free ions or complexed ions with other ligands, both organic and inorganic. Aquo-Ni ions behave as acids when in water. Aqueous Ni does not readily undergo hydrolysis to form hydroxide under typical environmental conditions; instead, the presence of other ligands results in the formation of various Ni species. Significant formation of hydroxide complexes occurs only under basic conditions (pH>7) (Lindsay, 1979). In the presence of sulfur and highly reducing environments, extremely insoluble nickel sulfide solids may form. Under aerobic conditions and below pH 9, Ni forms complexes with carbonate, sulfate, hydroxide, and other naturally occurring ligands.

The sorption mechanisms may include specific adsorption, ion exchange, and/or co-precipitation. Fe and Mn oxides, clay minerals, and (to some extent OM) are believed to play significant roles as sorbents for Ni in soil. Ni sorption on Fe and Mn oxides is pH-dependent, likely because $NiOH^+$ is preferentially sorbed and because the surface charge on sorbents is influenced by pH. Its solid-liquid partitioning appears to be more dependent on pH than soil composition.

The environmentally important relatively insoluble compounds of Ni include sulfide, hydroxide, and carbonate. Given that the solubility product of Ni hydroxide is much lower than that of Ni carbonate, the precipitation of the latter is highly unlikely under typical environmental conditions. Under aerobic conditions and at normal pH values,

complexation reduces the activity of free aqueous Ni ions, thereby discouraging precipitation reactions.

Nickel is the PTE that exhibits the highest concentrations in the liquid fraction after Zn. Across all soils, Ni concentrations are higher under reducing conditions and at low pH, while they decrease under oxidizing conditions at higher pH levels. Indeed, Ni shows significant negative correlations with E_H (Valentino -0.66**, Pellerina -0.88**, Sangone -0.71**, Shanty Town -0.69**) and with pH (Valentino -0.85**, Pellerina -0.85**, Sangone -0.83**, and Shanty Town -0.82** (Table 4.10).

As depicted in Figure 4.5, the concentrations range found in solution are, in descending order: Valentino 0.5 – 0.1 mg/L, Shanty Town 0.4 – 0.1 mg/L, Sangone 0.29 – 0.08 mg/L, Pellerina 0.2 – 0.06 mg/L.

The presence of significant correlations between Ni and various components in the liquid fraction of submerged urban soils provides important insights into the dynamics of this metal. For all soils, OM shows a positive correlation: Valentino 0.67**, Pellerina 0.91**, Sangone 0.79**, and Shanty Town 0.70**; suggesting that organic compounds may mobilize Ni species, facilitating dispersion in the soil. Additionally, organic compounds such as humic acids may form complexes with Ni, influencing its availability and reactivity in the liquid fraction in reducing conditions.

Conversely, a negative correlation was observed between Ni and DIC: Valentino -0.77**, Pellerina -0.74**, Sangone -0.82**, and Shanty Town -0.74**. This may indicate competition between nickel and DIC for adsorption sites in the soil. DIC, like carbonates, may be preferentially adsorbed over Ni, thus reducing its concentration in the liquid fraction of submerged urban soil. It's also worth considering that a negative correlation with DIC may indirectly result from an increase in pH due to carbonate dissolution, leading to the precipitation of Ni with other soil components.

For all soils, Ni also shows a strong positive correlation with Fe(II), Fe, and Mn, respectively: Valentino 0.94**, 0.86**, 0.99**; Pellerina 0.90**, 0.89**, 0.95**; Sangone 0.85**, 0.86**, 0.86**; Shanty Town 0.91**, 0.88**, 0.93** (Table 4.10). This suggests a possible association between Ni and heavy metal mobilization processes. Iron and manganese may act as carriers for Ni in the soil, as they are frequently co-transported through reduction-oxidation and complexation processes.

Unlike Cr, Ni exhibits a moderate negative correlation with sulfate for Valentino (-0.53**), Pellerina (-0.57**), and Sangone soils (-0.62**). This

suggests an interaction between nickel and sulfates in the soil, probably due to the formation of insoluble compounds with sulfates present in the soil or competitive processes for adsorption sites between Ni and sulfates.

4.3.3.4. Copper (Cu)

The presence of Cu in soils can be attributed to a series of anthropogenic activities involving the direct use of Cu compounds or their release as by-products of various anthropogenic activities.

A significant source of Cu in urban soils is represented using pesticides and fertilizers, such as Cu sulfate and Cu powder. Vehicle traffic represents another significant source of Cu in urban soils: particles from tire abrasion, brake wear, and vehicle exhaust can contain traces of Cu, which deposit on soils along roads and in adjacent urban areas. Finally, industry plays an important role in releasing Cu into the urban environment, through Cu processing, the production of electronic materials, and the manufacturing of Cu-based chemical products. Commonly used compounds include sulfate ($CuSO_4$), oxalate (CuC_2O_4), nitrate ($Cu(NO_3)_2$), and other organic and inorganic compounds.

Quantities of Cu can also be found in sewage sludge and the excrement of animals fed with feeds supplemented with Cu sulfate, as it has proven to be a valid food supplement.

Cu can generate various sulfate and oxysulfate minerals and various complexes with inorganic substances, including chlorides, sulfates, and carbonates, which are significant in soil. Sorption is the primary mechanism governing Cu mobility in the environment: organic complexation, specific adsorption, precipitation, and ion exchange, particularly with hydrous Fe and Mn oxides. pH plays a crucial role in sorption dynamics by affecting surface charge and sorptive capacity.

Generally, the quantity of Cu complexed organically and found in solution increases as pH rises above 7 due to the direct correlation between the solubility of organic matter and pH. Under oxidizing conditions, Cu exists mainly as oxides and hydroxides, whereas under anaerobic conditions, sulfur-containing species such as copper sulfide and cuprous oxide may prevail.

Below pH 6.9, Cu primarily exists as Cu^{2+} but may undergo reduction to Cu^{1+} or even Cu^0 in reducing environments. Above pH 6.9, $Cu(OH)_2°$ predominates in solution, while hydrolysis species such as $CuOH^+$ become significant around pH 7. Species like $Cu(OH)^{3-}$, $Cu(OH)_4^{2-}$, and $Cu_2(OH)_2^{2+}$ are insignificant in soils (Graf, 1980; Lindsay, 1979).

Shanty Town soil exhibits the highest concentrations of Cu in the liquid fraction. Specifically, concentration ranges are as follows: Valentino 0.1 – 0.01 mg/L, Pellerina 0.08 – 0.01 mg/L at 0 mV, Sangone 0.16 – 0.01 mg/L, Shanty Town 0.25 – 0.06 mg/L.

Unlike other trace elements under examination, Cu exhibits greater mobility under oxidizing conditions and less under reducing conditions. Indeed, it is the only one showing positive correlations with E_H: Valentino 0.68**, Pellerina 0.70**, and Shanty Town 0.70**; for Sangone soil, however, correlations did not show a significant relationship with E_H.

Correlations between pH and Cu, compared to other trace elements, also show a positive trend: Valentino 0.79**, Pellerina 0.73**, and Sangone 0.53**; in the case of Shanty Town, no significant correlation was observed. This positive correlation may be indirectly influenced by carbonate dissolution, resulting in Cu release. It is likely that in Shanty Town soil, Cu mobility is predominantly governed by other factors as OM presence or Cu forms.

Significant and relevant negative correlations were observed between DOC and Cu for Valentino (-0.70**), Pellerina (-0.74), and Shanty Town (-0.74**), while for Sangone, there was a low correlation (-0.46*) probably because of a lower OM content compared to other soils, as OM may act as a binder for copper, reducing its mobility.

Positive correlations were observed between DIC and Cu: Valentino 0.78**, Pellerina 0.52**, Sangone 0.74**, Shanty Town 0.87**. Copper may be bound to IC-containing minerals present in the soil, increasing its concentration in the liquid fraction.

Significant negative correlations were found for Cu with Fe(II), Fe, and Mn, higher for Valentino soil compared to others-0.91**, -0.87**, -0.88**; Pellerina -0.66**, -0.51**, -0.79**; Sangone -0.69**, -0.51**, -0.69**; Shanty Town -0.78**, -0.80, -0.71**. This data could result from competitive adsorption, precipitation, or complexation processes affecting the relative availability of these metals in the soil solution.

Although Cu does not show strong correlations with sulfates, it could be hypothesized that these factors justify a possible indirect correlation with E_H. Under reducing conditions, Cu may react with sulfide ions (S^{2-}) present in the soil solution to form insoluble copper sulfide compounds (CuS), thereby decreasing its concentration in the liquid fraction through precipitation or adsorption processes. Under oxidizing conditions, it is more likely that, through reaction with sulfate ions (SO_4^{2-}), soluble copper sulfate compounds ($CuSO_4$) would form.

4.3.3.5. Lead (Pb)

One of the main anthropogenic contributions of Pb into the environment may stem from improper waste disposal, including lead-acid batteries containing lead sulfate ($PbSO_4$), paints containing lead dioxide (PbO_2) or tetraethyl lead ($Pb(C_2H_5)4$), and coatings of electrical cables. Uncontrolled waste incineration may also contribute to contamination, releasing into the environment in the form of fine particles and exhaust gases from the combustion of lead-containing materials.

In the context of the soils of the Turin plain, the presence of Pb from geogenic sources is generally low, as minerals associated with Pb, such as galena (PbS), cerussite ($PbCO_3$), anglesite ($PbSO_4$), and pyromorphite ($Pb_5(PO_4)_3Cl$), are not common. Therefore, the main source of Pb in Turin soils is more likely from anthropogenic contamination. Aqueous-lead ions function as acids when dissolved in water. The prevailing species in acidic environments, where no other complexing agents are present, is Pb^2, although $PbOH^+$ becomes dominant within the typical pH range encountered. Pb can exhibit oxidation states of 0, +2, and +4. Pb^{4+} is only present in extremely oxidizing conditions rarely encountered within typical environmental pH and redox parameters (*Environmental Inorganic Chemistry*, 1988). Stability regions for PbO_2 and Pb^0 are very limited, with the former occurring solely in highly oxidizing environments and the latter in extremely reduced conditions. Pb^{2+} remains stable under most circumstances as both Pb^{2+} and hydroxy complexes of Pb^{2+}.

Increasing the OM content reduces the mobility of Pb since it tends to form insoluble complexes with it. It should be noted, however, that the fraction of OM that contributes most to Pb fixation is defined as high molecular weight humus (humic acids).

Complexes formed with fulvic acids are much more mobile, as they can flocculate only with high concentrations of electrolytes. Furthermore, fulvic acids become more soluble as pH values increase.

Considering that Pb is very similar to Zn (both divalent and chalcophilic), the predominant influence for Pb appears to be OM through the formation of soluble complexes with fulvic acids (Grybos et al., 2007).

During the experiment, Pb was mobile only in the soil of Shanty Town, while in others the concentrations were under the limit of detection. Mobile concentrations in the liquid fraction show the following range: 0.09 mg/L at 100 mV, pH 5.9 to 0.04 mg/L at +500 mV, pH 6.6; in other redox windows, it remains stable with slight variation.

However, it cannot be excluded that the mobile Pb in Valentino, Pellerina, and Sangone soils was associated with the colloidal part of the liquid fraction, which was not evaluated as filtration at 0.45 μm was performed.

As the soil of Shanty Town Pb is the only one enriched in Pb, the mobility can be justified by considering the dynamics of soil contamination. Here a more recent contamination is probable, due to improper waste disposal practices and the use of building materials not compliant with regulations; Pb may be present in more soluble and therefore more mobile forms, such as $PbCl_2$, $Pb(NO_3)_2$, having not had the time to transform into more stable and less mobile forms, such as lead oxides or sulfates, typical of older contaminations. In soils with more historical contamination, Pb is often concentrated in the residual fraction, bound to soil minerals or OM.

The graphs in Figure 4.5 highlight that, in Shanty Town soils, E_H and pH may have a small direct impact on Pb mobility. However, it does not seem to have a higher mobility at oxidizing comparing to reducing environments. In fact, it does not show significant correlations with E_H, while shows a weak correlation with pH and DIC. A small influence of pH on Pb mobility should not be excluded. The correlation with DIC is probably due to the formation of insoluble lead carbonate complexes, such as cerussite ($PbCO_3$), which can precipitate in the liquid fraction of the soil, thus reducing the concentration of dissolved Pb.

Positive correlations for Shanty Town have also been observed for Fe(II), Fe, and Mn. The reported mechanisms for sorption of lead onto soils and sediments are specific adsorption, co-precipitation with hydrous oxides, and incorporation into cationic lattice sites in crystalline sediments; OM and oxides of manganese and iron are important sorbents of lead in soils, and the extent of sorption appears to increase with increasing pH. Soil systems contain many anions that may influence the sorption of lead.

4.3.4. Rare Earth Elements (REE)

Rare earth elements (REE) are often associated with a variety of minerals, including monazite ($(Ce,La,Nd,Th)PO_4$), bastnasite ($(Ce,La)(CO_3)F$), and xenotime (YPO_4). These minerals, known for their relative abundance in REE, serve as natural reservoirs of these elements in the Earth's crust. However, in the specific context of Turin soils, the presence of geogenic REE is generally limited, as geological characteristics do not favor the formation or significant accumulation of these minerals.

Nevertheless, it is important to consider that urban soils can be influenced by anthropogenic processes that lead to the introduction of anthropogenic REE. In particular, the widespread use of phosphate fertilizers may contribute to the release of REE into soils, as these fertilizers may contain impurities of REE as byproducts of the production process. Similarly, the chemical, electronic, and semiconductor industries can be significant sources of REE in urban soils, as these sectors utilize them in various applications, including automotive catalysts for the reduction of vehicle emissions: cerium is often used as an active component for the selective catalytic reduction of nitrogen oxides, thus contributing to the reduction of the environmental impact of vehicle exhaust gases.

Additionally, REE may also be present in vehicle tires and braking systems. For example, neodymium-iron-boron (NdFeB) magnets, which contain REE such as neodymium and dysprosium, may be used in small quantities within tire pressure monitoring systems. During tire and brake usage, friction and wear can lead to the release of particles containing REE into the surrounding environment, thus contributing to contamination in urban soils.

Another potential source of introduction of REE into urban soils is represented by building materials, such as bricks and ceramics. In particular, the practice of using rubble as fill material, as in the case of Pellerina and Sangone parks in Turin, may have contributed to the accumulation of REE in the soils of these parks.

As observed from the graphs in Figure 4.6, most of the REE exhibit greater mobility under reducing conditions and acidic pH, and lower mobility under oxidizing conditions and basic pH. Table 4.12 shows the Spearman correlation coefficients, highlighting a significant negative correlation for E_H and pH. However, not all soils show a negative correlation for all REE. In fact, Valentino does not exhibit correlations with E_H and pH for Y, La, Ce, and Pr.

Among the four soils, the concentrations in the liquid fraction of Shanty Town are the lowest for all REE. Among all REE, those showing higher mobility are Nd, Y, Ce, Gd, and Dy. However, compared to PTE, the concentrations are lower, ranging in the order of µg/L. The REE with lower concentrations are La, Pr, Tb, Ho, Tm, and Lu, mostly <0.1 µg/L.

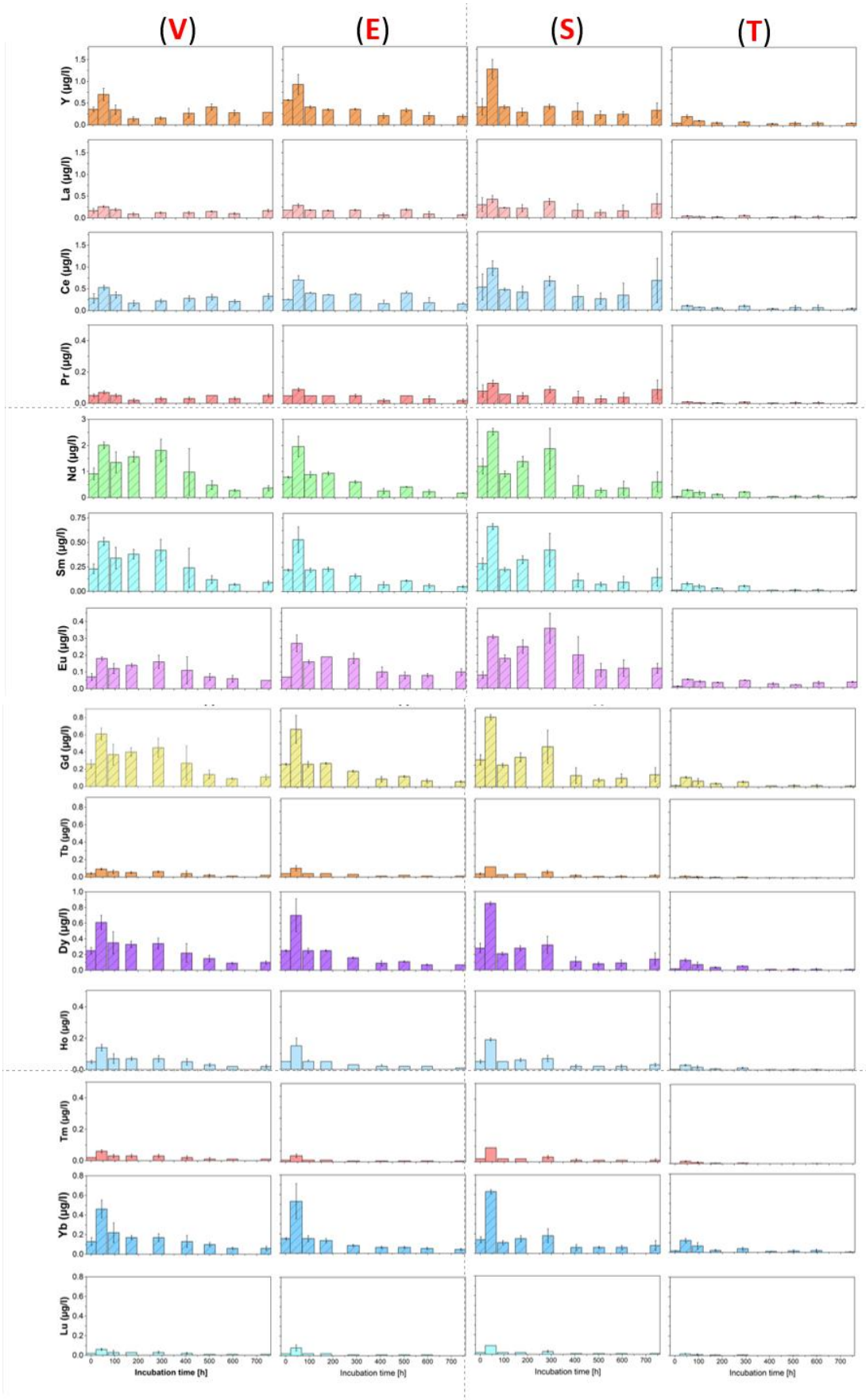
(V)
(E)
(S)
(T)
Y (µg/l)
La (µg/l)
Ce (µg/l)
Pr (µg/l)
Nd (µg/l)
Sm (µg/l)
Eu (µg/l)
Gd (µg/l)
Tb (µg/l)
Dy (µg/l)
Ho (µg/l)
Tm (µg/l)
Yb (µg/l)
Lu (µg/l)
Incubation time [h]
Incubation time [h]
Incubation time [h]
Incubation time [h]

Figure 4.6. Histograms representing Rare Earth Elements concentrations in liquid fraction at the sampling points. The individual values are shown in the table 4.11

Table 4.11 Concentrations of Cr, Cu, Ni, Pb, and Zn in the liquid fraction of soil at different sampling points

Soil	*E_H windows*	*E_H (6 hour)*	*pH (6 hour)*		*Y*	*La*	*Ce*	*Pr*	*Nd*	*Sm*	*Eu*	*Gd*	*Tb*	*Dy*	*Ho*	*Er*	*Tm*	*Yb*	*Lu*
					µg/l	µg/l	µg/l	µg/l	µg/l	µg/l	µg/l	µg/l	µg/l	µg/l	µg/l	µg/l	µg/l	µg/l	µg/l
Valentino	initial point	357	7.3		0.3	0.2	0.3	0.1	0.2	0.1	<LOD	0.1	<LOD	0.1	<LOD	<LOD	<LOD	<LOD	<LOD
				±SD	0.04	0.05	0.1	0.00002	0.04	0.01		0.01		0.005		<LOD		<LOD	
	-200	-213	5.7		0.8	0.3	0.6	0.1	0.4	0.1	<LOD	0.1	<LOD	0.1	<LOD	0.1	<LOD	0.1	<LOD
				±SD	0.2	0.04	0.1	0.01	0.05	0.01		0.02		0.023		0.02		0.01	
	-100	-109	6.1		0.4	0.2	0.4	0.1	0.3	0.1	<LOD	0.1	<LOD	0.1	<LOD	0.1	<LOD	0.1	<LOD
				±SD	0.2	0.1	0.1	0.02	0.1	0.02		0.02		0.030		<LOD		<LOD	
	0	-7	5.7		0.4	0.3	0.5	0.1	0.3	0.1	<LOD	0.1	<LOD	0.1	<LOD	<LOD	<LOD	<LOD	<LOD
				±SD	0.1	0.04	0.1	0.01	0.1	0.01		0.01		0.01		<LOD		<LOD	
	100	86	5.4		0.4	0.3	0.6	0.1	0.4	0.1	<LOD	0.1	<LOD	0.1	<LOD	<LOD	<LOD	<LOD	<LOD
				±SD	0.1	0.1	0.1	0.02	0.1	0.02		0.02		0.01		<LOD		<LOD	
	200	212	6.9		0.3	0.1	0.3	0.04	0.2	0.04	0.0	0.04	<LOD	0.04	<LOD	0.02	<LOD	0.02	<LOD
				±SD	0.1	0.1	0.2	0.04	0.2	0.04		0.04		0.02		0.01		0.01	
	300	307	7.1		0.2	0.1	0.1	0.02	0.1	0.02	<LOD	0.02	<LOD	0.02	<LOD	0.01	<LOD	0.01	<LOD
				±SD	0.1	0.02	0.05	0.01	0.03	0.01		0.01		0.01		0.01		<LOD	
	400	411	7.3		0.2	0.1	0.1	0.02	0.1	0.01	0.01	0.02	<LOD	0.03		0.02	<LOD	0.02	<LOD
				±SD	0.03	0.004	0.01	0.003	0.01	0.002	0.0001	0.002		0.004	<LOD	0.003		0.002	
	500	494	6.8		0.1	0.1	0.1	0.02	0.1	0.02	0.01	0.02	<LOD	0.03		0.02	<LOD	0.02	<LOD
				±SD	0.02	0.02	0.04	0.01	0.02	0.004	0.002	0.003		0.004		0.002		0.004	
Pellerina	initial point	298	7.3		0.4	0.1	0.2	<LOD	0.2	<LOD	<LOD	0.1	<LOD	0.1	<LOD	<LOD	<LOD	0.1	<LOD
				±SD	0.03	0.01	0.011		0.009			0.004		0.01		<LOD		<LOD	
	-200	-210	5.8		0.9	0.3	0.7	0.1	0.4	0.1	<LOD	0.1	<LOD	0.1	<LOD	0.1	<LOD	0.1	<LOD
				±SD	0.2	0.04	0.1	0.01	0.1	0.02		0.03		0.04		0.03		0.02	
	-100	-63	6.4		0.3	0.1	0.3	<LOD	0.2	0.1	<LOD	0.1	<LOD	0.1	<LOD	<LOD	<LOD	<LOD	<LOD
				±SD	0.04	0.02	0.04		0.03	<LOD		0.004		<LOD		<LOD		<LOD	
	0	-14	6.1		0.3	0.2	0.3	0.1	0.2	0.1	<LOD	0.1	<LOD	0.1	<LOD	<LOD	<LOD	<LOD	<LOD
				±SD	0.02	0.03	0.04		0.02	<LOD		0.01		<LOD		<LOD		<LOD	
	100	57	6.9		0.2	0.1	0.2	<LOD	0.1	<LOD	<LOD	<LOD	<LOD	<LOD	<LOD	<LOD	<LOD	<LOD	<LOD
				±SD	0.01	0.01	0.02		0.01	<LOD				<LOD		<LOD		<LOD	
	200	204	7.4		0.1	0.03	0.1	0.01	0.04	0.01	<LOD	0.02	<LOD	0.01	<LOD	<LOD	<LOD	<LOD	<LOD

			±SD	0.02	0.01	0.03	0.004	0.02	0.003		0.0002		0.0001		<LOD		<LOD	
	300	329	7.8	0.1	0.1	0.1	0.02	0.1	0.02	<LOD	0.02	<LOD	0.02	<LOD	<LOD	<LOD	<LOD	<LOD
			±SD	0.01	0.01	0.01	0.001	0.01	0.002		0.002		0.002		<LOD		<LOD	
	400	418	7.8	0.1	0.04	0.1	0.01	0.1	0.01	0.01	0.02	<LOD	0.02	<LOD	0.01	<LOD	0.02	<LOD
			±SD	0.02	0.02	0.03	0.004	0.02	0.003	0.0003	0.01		0.004		0.001		0.003	
	500	533	7.3	0.1	0.03	0.1	0.01	0.04	<LOD	0.01	0.02	<LOD	0.02	<LOD	0.01	<LOD	0.02	<LOD
			±SD	0.00	0.002	0.004	0.0005	0.001		0.0003	0.003		0.001		0.0003		0.01	
	initial point	402	7.3	0.3	0.2	0.4	0.1	0.2	0.1	<LOD	0.1	<LOD	0.1			<LOD		<LOD
			±SD	0.1	0.1	0.1	0.01	0.1	0.01		0.01		0.01	<LOD				
	-200	-205	5.7	1.2	0.4	0.8	0.1	0.5	0.1	<LOD	0.2	<LOD	0.2		0.1	<LOD	0.1	
			±SD	0.1	0.03	0.05	0.01	0.03	0.01		0.005		0.01	<LOD	0.01		0.02	
	-100	-142	6.5	0.3	0.2	0.3	<LOD	0.2	<LOD	<LOD	0.1	<LOD			<LOD	<LOD	<LOD	<LOD
			±SD	0.0	0.02	0.04		0.03			0.002			<LOD				
	0	-1	5.8	0.4	0.3	0.5	0.1	0.3	0.1	<LOD	0.1	<LOD	0.1		<LOD	<LOD	<LOD	<LOD
			±SD	0.1	0.1	0.1	0.01	0.1	0.01		0.01			<LOD				
	100	72	5.8	0.4	0.3	0.6	0.1	0.4	0.1	<LOD	0.1	<LOD	0.1		<LOD	<LOD	<LOD	<LOD
			±SD	0.1	0.1	0.2	0.03	0.1	0.03		0.04							
	200	262	7.2	0.1	0.1	0.1	0.02	0.1	0.02	0.01	0.03	0.003	0.02	0.003	0.01	0.002	0.01	0.0004
			±SD	0.1	0.1	0.1	0.01	0.1	0.02	0.01	0.02	0.000	0.01	0.000	0.0002	0.000	0.005	0.000
	300	335	7.5	0.1	0.04	0.1	0.01	0.05	0.02	0.01	0.01	0.002	0.01	0.003	0.01	0.002	0.002	0.00003
			±SD	0.0	0.02	0.05	0.005	0.02	0.002	0.000	0.001	0.000	0.001	0.000		0.000	0.000	0.000
	400	401	7.7	0.1	0.1	0.2	0.02	0.1	0.03	0.01	0.02	<LOD	0.02	<LOD	0.01	<LOD	0.02	<LOD
			±SD	0.04	0.1	0.1	0.02	0.1	0.00001	0.003	0.01		0.01		0.0002		0.004	
	500	509	7.0	0.2	0.1	0.2	0.03	0.1	0.04	0.02	0.03	<LOD	0.03	<LOD	0.02	<LOD	0.02	<LOD
			±SD	0.1	0.1	0.2	0.02	0.1	0.01	0.003	0.02		0.01		0.002		0.01	
	initial point	386	7.3	<LOD	<LOD	<LOD	<LOD	<LOD	<LOD	<LOD	<LOD	<LOD	<LOD	<LOD	<LOD	<LOD	<LOD	<LOD
			±SD															
	-200	-192	6.0	0.2	<LOD	0.1	<LOD	0.1	<LOD	<LOD	<LOD	<LOD	<LOD	<LOD	<LOD	<LOD	<LOD	<LOD
			±SD	0.02		0.01		0.0										
	-100	-125	6.4	0.1	<LOD	0.1	<LOD	<LOD	<LOD	<LOD	<LOD	<LOD	<LOD	<LOD	<LOD	<LOD	<LOD	<LOD
			±SD	0.1														
	0	-1	6.4	0.1	<LOD	<LOD	<LOD	<LOD	<LOD	<LOD	<LOD	<LOD	<LOD	<LOD	<LOD	<LOD	<LOD	<LOD
			±SD															
	100	97	5.9	0.066	0.051	0.077	<LOD	<LOD	<LOD	<LOD	<LOD	<LOD	<LOD	<LOD	<LOD	<LOD	<LOD	<LOD
			±SD	0.005		0.014												
	200	206	7.4		0.0003	<LOD	<LOD	<LOD	<LOD	<LOD	<LOD	<LOD	<LOD	<LOD	<LOD	<LOD	<LOD	<LOD
			±SD	0.001	0.001													

Sangone

Shanty Town

300	324	7.6		0.004	0.006	0.009	0.001	0.012	<LOD	<LOD	<LOD	<LOD	<LOD	<LOD	<LOD	<LOD	<LOD	<LOD
			±SD	0.012	0.006	0.014	0.002											
400	408	7.1		0.026	0.025	0.043	<LOD	0.027	<LOD	<LOD	<LOD	<LOD	0.01	<LOD	<LOD	<LOD	<LOD	<LOD
			±SD	0.016	0.0003													
500	499	6.6		0.019	0.012	0.014	<LOD	0.012	<LOD	<LOD	<LOD	<LOD	<LOD	<LOD	<LOD	<LOD	<LOD	<LOD
			±SD	0.002	0.00001	0.004		0.001										

For Valentino and Sangone, Nd, Sm, Eu, and Gd show higher concentrations in the redox windows of -200 mV and +100 mV, where both soils recorded a pH of approximately 5.5. In fact, the solubility of metals that can occur as free hydrated cations generally increases with decreasing pH.

Valentino shows that Nd to Lu correlate negatively with both E_H and pH, while Y, La, Ce, and Pr show no correlation. This suggests a possible influence of anthropogenic or geochemical factors on the distribution of REE in this soil. In Pellerina, all REE correlate negatively with E_H, while with pH there is a more evident negative correlation for Y and the elements from Nd to Lu, and a weaker correlation for La, Ce, and Pr. Sangone shows the same correlations with pH as Pellerina, while with E_H not. In ShantyTown, a negative correlation between many REE and E_H is confirmed; Eu, Ce, and Pr show a moderate negative correlation. pH shows a negative correlation with Y and the elements between Nd and Lu, confirming the results observed in the other soils. The negative correlations between REE with pH and E_H suggest a possible influence of redox processes and pH variations on the mobility of these elements in the soil.

In all soils, there is a strong positive correlation between DOC and many REE, suggesting a significant link with the presence of OM in the soil (Marsac et al., 2011, 2010). Specifically, the correlations are stronger for Valentino with the elements from Nd to Lu, for Pellerina with Y and the elements from Nd to Lu (weaker with La, Ce, Pr), for Sangone strong with the elements from Nd to Lu (weaker with Y), and finally Shanty Town strong correlation with Nd, Sm, and the elements from Gd to Lu (weaker with Y).

On the contrary, negative correlations with DIC are observed, indicating a complex interaction between REE and carbonates. In detail, a negative correlation with the elements from Nd to Lu is evident in Valentino and Sangone, in Pellerina with all REE (weaker for La, Ce, Pr); in ShantyTown, the correlation with DIC is not significant for any of the REE, differing slightly from the results observed in the other soils.

An important factor could be the influence of OM, which determines the temporal dynamics of soluble REE. Due to the presence of many negatively charged sites, OM has a high capacity to complex and adsorb cations, and therefore act as ligands for REE, influencing their distribution and mobility in the soil. Conversely, the negative correlation with carbonates (DIC) suggests a possible competition for adsorption

sites in the soil, perhaps linked to the ability of carbonates to bind and immobilize some elements.

Table 4.12 Spermann correlation coefficients. ***significant at 0.01 level*

V	E_H	pH	DOC	DIC	SO_4^{2-}	Fe(II)	P	Fe	Mn	Y	La	Ce	Pr	Nd	Sm	Eu	Gd	Tb	Dy	Ho	Er	Tm	Yb	Lu
E_H	1	0.61**	-0.95**	0.61**	n.c.	-0.65**	-0.50**	-0.63**	-0.68**	n.c.	n.c.	n.c.	n.c.	-0.78**	-0.81**	-0.76**	-0.82**	-0.85**	-0.86**	-0.87**	-0.89**	-0.89**	-0.90**	-0.88**
pH		1	-0.66**	0.76**	n.c.	-0.89**	n.c.	-0.84**	-0.83**	n.c.	n.c.	n.c.	n.c.	-0.85**	-0.83**	-0.85**	-0.82**	-0.81**	-0.80**	-0.79**	-0.77**	-0.74**	-0.74**	-0.77**
DOC			1	-0.61**	n.c.	0.68**	0.55**	0.68**	0.68**	n.c.	n.c.	n.c.	n.c.	0.83**	0.84**	0.78**	0.85**	0.88**	0.88**	0.88**	0.89**	0.89**	0.89**	0.86**
DIC				1	n.c.	-0.89**	n.c.	-0.89**	-0.76**	n.c.	n.c.	n.c.	n.c.	-0.71**	-0.69**	-0.63**	-0.68**	-0.66**	-0.65**	-0.64**	-0.62**	-0.61**	-0.64**	-0.63**
SO_4^{2-}					1	-0.55**	n.c.	-0.51**	-0.56**	n.c.	n.c.	n.c.	n.c.	n.c.	n.c.	n.c.	n.c.	n.c.	n.c.	n.c.	n.c.	n.c.	n.c.	n.c.
Fe(II)						1	0.55**	0.95**	0.93**	n.c.	n.c.	n.c.	n.c.	0.83**	0.80**	0.82**	0.78**	0.76**	0.76**	0.75**	0.75**	0.72**	0.72**	0.75**
P							1	0.59**	0.60**	n.c.	n.c.	n.c.	n.c.	0.68**	0.68**	0.61**	0.65**	0.66**	0.68**	0.67**	0.68**	0.62**	0.65**	0.64**
Fe								1	0.86**	-0.50**	n.c.	n.c.	n.c.	0.84**	0.81**	0.72**	0.79**	0.75**	0.75**	0.74**	0.72**	0.69**	0.70**	0.71**
Mn									1	n.c.	n.c.	n.c.	n.c.	0.82**	0.80**	0.85**	0.77**	0.76**	0.77**	0.77**	0.77**	0.75**	0.76**	0.78**
Y										1	0.72**	0.78**	0.80**	n.c.	n.c.	n.c.	n.c.	n.c.	n.c.	n.c.	n.c.	n.c.	n.c.	n.c.
La											1	0.93**	0.98**	n.c.	n.c.	n.c.	n.c.	n.c.	n.c.	n.c.	n.c.	n.c.	n.c.	n.c.
Ce												1	0.93**	n.c.	n.c.	n.c.	n.c.	n.c.	n.c.	n.c.	n.c.	n.c.	n.c.	n.c.
Pr													1	n.c.	n.c.	n.c.	n.c.	n.c.	n.c.	n.c.	n.c.	n.c.	n.c.	n.c.
Nd														1	0.99**	0.93**	0.98**	0.96**	0.96**	0.96**	0.94**	0.91**	0.93**	0.93**
Sm															1	0.92**	0.99**	0.98**	0.98**	0.98**	0.96**	0.94**	0.94**	0.95**
Eu																1	0.92**	0.91**	0.92**	0.92**	0.93**	0.90**	0.89**	0.92**
Gd																	1	0.98**	0.98**	0.98**	0.97**	0.94**	0.94**	0.96**
Tb																		1	0.99**	0.99**	0.98**	0.97**	0.96**	0.98**
Dy																			1	0.99**	0.99**	0.96**	0.97**	0.98**
Ho																				1	0.99**	0.97**	0.96**	0.98**
Er																					1	0.98**	0.96**	0.98**
Tm																						1	0.96**	0.98**
Yb																							1	0.97**
Lu																								1

E	E_H	pH	DOC	DIC	SO_4^{2-}	Fe(II)	P	Fe	Mn	Y	La	Ce	Pr	Nd	Sm	Eu	Gd	Tb	Dy	Ho	Er	Tm	Yb	Lu
E_H	1	0.81**	-0.96**	0.62**	n.c.	-0.83**	n.c.	-0.84**	-0.87**	-0.84**	-0.65**	-0.70**	-0.65**	-0.91**	-0.90**	-0.79**	-0.93**	-0.94**	-0.93**	-0.95**	-0.94**	-0.93**	-0.92**	-0.97**
pH		1	-0.82**	0.64**	n.c.	-0.89**	n.c.	-0.77**	-0.85**	-0.71**	-0.52**	-0.56**	-0.50**	-0.79**	-0.79**	-0.89**	-0.79**	-0.80**	-0.81**	-0.80**	-0.80**	-0.82**	-0.82**	-0.84**
DOC			1	-0.67**	-0.52**	0.87**	n.c.	0.87**	0.90**	0.81**	0.63**	0.66**	0.62**	0.92**	0.90**	0.81**	0.93**	0.93**	0.92**	0.93**	0.94**	0.92**	0.91**	0.95**
DIC				1	0.75**	-0.76**	n.c.	-0.76**	-0.71**	-0.66**	-0.54**	-0.53**	-0.52**	-0.76**	-0.75**	-0.66**	-0.73**	-0.71**	-0.70**	-0.70**	-0.69**	-0.71**	-0.68**	-0.66**
SO_4^{2-}					1	n.c.	n.c.	-0.60**	-0.55**	-0.55**	-0.55**	-0.52**	-0.53**	-0.60**	-0.59**	n.c.	-0.58**	-0.58**	-0.55**	-0.54**	-0.56**	-0.55**	-0.53**	-0.53**
Fe(II)						1	n.c.	0.90**	0.88**	0.74**	0.57**	0.61**	0.55**	0.87**	0.86**	0.79**	0.86**	0.86**	0.86**	0.86**	0.85**	0.86**	0.85**	0.86**
P							1	n.c.	n.c.	0.52**	0.57**	0.58**	0.59**	n.c.	n.c.	n.c.	n.c.	n.c.	n.c.	n.c.	n.c.	n.c.	n.c.	n.c.
Fe								1	0.83**	0.87**	0.78**	0.82**	0.77**	0.96**	0.95**	0.71**	0.95**	0.93**	0.94**	0.93**	0.93**	0.93**	0.92**	0.90**
Mn									1	0.70**	0.49**	0.54**	n.c.	0.84**	0.83**	0.85**	0.84**	0.86**	0.86**	0.86**	0.87**	0.84**	0.85**	0.88**
Y										1	0.92**	0.94**	0.92**	0.91**	0.88**	0.72**	0.91**	0.90**	0.92**	0.90**	0.90**	0.94**	0.88**	0.89**
La											1	0.98**	0.99**	0.79**	0.76**	0.57**	0.78**	0.77**	0.77**	0.76**	0.76**	0.79**	0.74**	0.73**
Ce												1	0.99**	0.83**	0.80**	0.58**	0.82**	0.81**	0.83**	0.81**	0.81**	0.84**	0.78**	0.78**
Pr													1	0.80**	0.77**	0.55**	0.78**	0.78**	0.78**	0.78**	0.77**	0.80**	0.75**	0.74**
Nd														1	0.98**	0.78**	0.99**	0.98**	0.98**	0.98**	0.98**	0.98**	0.96**	0.95**
Sm															1	0.78**	0.98**	0.98**	0.97**	0.97**	0.97**	0.96**	0.95**	0.94**
Eu																1	0.76**	0.79**	0.79**	0.79**	0.78**	0.78**	0.80**	0.82**
Gd																	1	0.98**	0.99**	0.98**	0.99**	0.98**	0.96**	0.96**
Tb																		1	0.98**	0.99**	0.98**	0.98**	0.96**	0.97**
Dy																			1	0.99**	0.99**	0.99**	0.97**	0.97**
Ho																				1	0.98**	0.98**	0.96**	0.98**
Er																					1	0.98**	0.96**	0.97**
Tm																						1	0.95**	0.97**
Yb																							1	0.97**
Lu																								1

S	E_H	pH	DOC	DIC	SO_4^{2-}	Fe(II)	P	Fe	Mn	Y	La	Ce	Pr	Nd	Sm	Eu	Gd	Tb	Dy	Ho	Er	Tm	Yb	Lu
E_H	1	0.75**	-0.94**	0.62**	n.c.	-0.72**	n.c.	-0.65**	-0.72**	-0.63**	n.c.	n.c.	n.c.	-0.72**	-0.74**	-0.69**	-0.78**	-0.78**	-0.77**	-0.79**	-0.80**	-0.80**	-0.76**	-0.83**
pH		1	-0.80**	0.71**	n.c.	-0.85**	n.c.	-0.79**	-0.78**	-0.67**	-0.58**	-0.51**	-0.53**	-0.88**	-0.89**	-0.85**	-0.89**	-0.89**	-0.89**	-0.90**	-0.89**	-0.88**	-0.89**	-0.89**
DOC			1	-0.68**	-0.56**	0.77**	0.50**	0.74**	0.74**	0.57**	n.c.	n.c.	n.c.	0.81**	0.81**	0.70**	0.83**	0.84**	0.82**	0.83**	0.85**	0.84**	0.81**	0.88**
DIC				1	0.73**	-0.87**	n.c.	-0.86**	-0.81**	n.c.	n.c.	n.c.	n.c.	-0.65**	-0.64**	-0.62**	-0.66**	-0.64**	-0.66**	-0.66**	-0.67**	-0.66**	-0.61**	-0.66**
SO_4^{2-}					1	-0.68**	n.c.	-0.67**	-0.74**	n.c.	n.c.	n.c.	n.c.	-0.49**	n.c.	n.c.	n.c.	n.c.	n.c.	n.c.	n.c.	n.c.	n.c.	n.c.
Fe(II)						1	n.c.	0.92**	0.85**	n.c.	n.c.	n.c.	n.c.	0.83**	0.83**	0.74**	0.84**	0.84**	0.83**	0.84**	0.84**	0.82**	0.82**	0.83**
P							1	n.c.	n.c.	n.c.	n.c.	n.c.	n.c.	n.c.	n.c.	n.c.	n.c.	n.c.	n.c.	n.c.	n.c.	n.c.	n.c.	n.c.
Fe								1	0.78**	0.57**	0.64**	0.60**	0.60**	0.92**	0.89**	0.70**	0.88**	0.90**	0.89**	0.90**	0.89**	0.88**	0.89**	0.87**
Mn									1	n.c.	n.c.	n.c.	n.c.	0.74**	0.72**	0.86**	0.75**	0.73**	0.73**	0.74**	0.75**	0.73**	0.69**	0.76**
Y										1	0.90**	0.88**	0.90**	0.79**	0.81**	0.73**	0.81**	0.79**	0.81**	0.81**	0.81**	0.82**	0.78**	0.78**
La											1	0.98**	0.98**	0.81**	0.80**	0.64**	0.78**	0.77**	0.79**	0.78**	0.77**	0.78**	0.77**	0.73**
Ce												1	0.99**	0.77**	0.77**	0.53**	0.74**	0.74**	0.76**	0.74**	0.73**	0.74**	0.74**	0.69**
Pr													1	0.78**	0.78**	0.57**	0.76**	0.75**	0.77**	0.75**	0.74**	0.75**	0.74**	0.70**
Nd														1	0.99**	0.82**	0.98**	0.98**	0.99**	0.98**	0.98**	0.97**	0.97**	0.96**
Sm															1	0.81**	0.99**	0.99**	1.00**	0.99**	0.99**	0.98**	0.98**	0.97**
Eu																1	0.83**	0.81**	0.81**	0.82**	0.82**	0.82**	0.79**	0.82**
Gd																	1	1.00**	0.99**	1.00**	0.99**	0.99**	0.97**	0.98**
Tb																		1	0.99**	0.99**	0.99**	0.98**	0.97**	0.97**
Dy																			1	1.00**	1.00**	0.98**	0.98**	0.98**
Ho																				1	1.00**	0.99**	0.98**	0.98**
Er																					1	0.99**	0.97**	0.98**
Tm																						1	0.98**	0.98**
Yb																							1	0.97**
Lu																								1

T	E_H	pH	DOC	DIC	SO_4^{2-}	Fe(II)	P	Fe	Mn	Y	La	Ce	Pr	Nd	Sm	Eu	Gd	Tb	Dy	Ho	Er	Tm	Yb	Lu
E_H	1	0.56**	-0.97**	0.63**	n.c.	-0.75**	-0.77**	-0.78**	-0.63**	-0.67**	n.c.	-0.51**	-0.51**	-0.86**	-0.87**	-0.50**	-0.88**	-0.89**	-0.88**	-0.90**	-0.82**	-0.90**	-0.80**	-0.88**
pH		1	-0.53**	0.60**	n.c.	-0.79**	-0.66**	-0.63**	-0.77**	-0.60**	n.c.	n.c.	n.c.	-0.69**	-0.73**	-0.87**	-0.72**	-0.71**	-0.68**	-0.68**	-0.73**	-0.72**	-0.60**	-0.73**
DOC			1	-0.64**	n.c.	0.77**	0.75**	0.83**	0.67**	0.58**	n.c.	n.c.	n.c.	0.82**	0.82**	n.c.	0.83**	0.83**	0.82**	0.85**	0.76**	0.82**	0.69**	0.82**
DIC				1	n.c.	-0.85**	-0.49**	-0.76**	-0.71**	n.c.	n.c.	n.c.	n.c.	-0.49**	-0.50**	n.c.	n.c.	n.c.	n.c.	n.c.	n.c.	n.c.	n.c.	n.c.
SO_4^{2-}					1	n.c.	n.c.	n.c.	n.c.	n.c.	n.c.	n.c.	n.c.	n.c.	n.c.	n.c.	n.c.	n.c.	n.c.	n.c.	n.c.	n.c.	n.c.	n.c.
Fe(II)						1	0.76**	0.93**	0.90**	0.63**	0.57**	0.55**	0.51**	0.82**	0.83**	0.61**	0.82**	0.83**	0.81**	0.82**	0.81**	0.83**	0.68**	0.84**
P							1	0.77**	0.68**	0.71**	0.66**	0.69**	0.67**	0.81**	0.82**	0.62**	0.87**	0.84**	0.83**	0.81**	0.81**	0.84**	0.75**	0.85**
Fe								1	0.85**	0.63**	0.63**	0.64**	0.60**	0.86**	0.86**	n.c.	0.83**	0.83**	0.85**	0.85**	0.80**	0.80**	0.69**	0.81**
Mn									1	0.55**	0.52**	n.c.	n.c.	0.71**	0.73**	0.55**	0.72**	0.73**	0.72**	0.71**	0.73**	0.72**	0.51**	0.73**
Y										1	0.83**	0.86**	0.88**	0.84**	0.85**	0.69**	0.86**	0.83**	0.87**	0.86**	0.88**	0.89**	0.84**	0.88**
La											1	0.97**	0.96**	0.76**	0.73**	0.51**	0.72**	0.67**	0.73**	0.71**	0.74**	0.68**	0.71**	0.70**
Ce												1	0.98**	0.81**	0.79**	0.54**	0.75**	0.70**	0.78**	0.77**	0.78**	0.73**	0.78**	0.74**
Pr													1	0.79**	0.77**	0.51**	0.77**	0.70**	0.77**	0.76**	0.76**	0.73**	0.79**	0.73**
Nd														1	0.98**	0.68**	0.94**	0.96**	0.97**	0.97**	0.96**	0.94**	0.89**	0.95**
Sm															1	0.74**	0.94**	0.95**	0.98**	0.99**	0.97**	0.95**	0.88**	0.96**
Eu																1	0.68**	0.69**	0.70**	0.70**	0.75**	0.70**	0.62**	0.72**
Gd																	1	0.96**	0.95**	0.95**	0.92**	0.95**	0.88**	0.96**
Tb																		1	0.97**	0.96**	0.96**	0.96**	0.86**	0.96**
Dy																			1	0.99**	0.97**	0.96**	0.84**	0.96**
Ho																				1	0.95**	0.96**	0.88**	0.96**
Er																					1	0.96**	0.85**	0.96**
Tm																						1	0.89**	0.99**
Yb																							1	0.89**
Lu																								1

In the Valentino soil, a positive correlation is observed between the elements from Nd to Lu with Fe(II), Fe, Mn, and P, suggesting an association with the availability of these elements in the soil. However, Y correlates negatively with Fe, indicating a different behavior compared to other REE.

In the Pellerina soil, a strong positive correlation is confirmed between Y and the elements from Nd to Lu with Fe(II) and Mn, while La, Ce, Pr correlate moderately; all REE correlate with Fe; correlations with P are present only for La, Ce, and Pr.

In the Sangone soil, a positive correlation is observed between all REE and Fe, again stronger between Y and the elements from Nd to Lu, and more moderate for La, Ce, Pr; the elements from Nd to Lu correlate significantly with Fe(II) and Mn, while Y, La, Ce, and Pr show no correlation. No REE show correlations with P.

In the ShantyTown soil, a positive correlation is highlighted between Fe(II) and Fe with Nd, Sm, and the elements from Gd to Lu, while Y, La, Ce, Pr, and Eu correlate moderately. P correlates with all REE, with only Eu showing lower values. Correlations with Mn are higher with Nd, Sm, Gd, Tm, Lu, while they are lower for Y, La, Eu, Yb, and finally not significant for Ce and Pr.

All REE except Eu correlate negatively with SO_4^{2-} only in Pellerina, while the other soils do not correlate with this compound.

Processes of adsorption/desorption and precipitation of Fe and Mn oxide compounds could affect the distribution and mobility of REE. Strong positive associations were also identified with Fe and Mn in solutions. REE may be liberated when Fe-Mn (oxyhydr)oxides dissolve under reducing circumstances. In this instance, a correlation is evident among the varying degrees of release in solution among the distinct soils. Indeed, we observe a reduced release of REE in Pellerina and Shanty Town, mirroring the discrepancies in Fe release within the same soils. Under oxidized and alkaline conditions, Fe and Mn oxides precipitate, potentially immobilizing REE through adsorption or co-precipitation. Specifically, REE present in solution as free ions REE^{3+} or $REE(OH)^{2+}$ or $REE(CO_3)^{+}$ could bind with -OH- on the surface of Fe-Mn oxides. Since the surface charge is pH-dependent: as pH rises, negative sites proliferate, potentially enhancing adsorption on minerals (Bau, 1999; Ohta and Kawabe, 2001; Ratié et al., 2023). The presence of phosphorus might promote the creation of stable complexes with REE, thereby increasing their mobility in the soil.

In all soils, a certain co-variation among different REE is observed, indicating a relative uniformity in the mechanisms influencing the distribution and mobilization of these elements. However, some REE, such as Eu, exhibit less pronounced correlations with other REE, suggesting potential differences in their behavior or sources of origin.

The observed correlations could be attributed to the specific chemical properties of REE, such as their affinity for certain organic or inorganic ligands in the soil. Additionally, anthropogenic activities, such as heavy metal pollution or the use of phosphate fertilizers, may have influenced the distribution and mobility of REE in urban soils. Soil submergence may create anaerobic conditions favoring the solubilization and mobility of certain REE, while the presence of Fe and Mn compounds could influence their speciation and sorption in the soil.

CHAPTER 5

Conclusions

Chapter 2:

Our research revealed several key findings on pollution dynamics, with a specific focus on the role of fine soil particles contributing to air pollution. The results confirm that PTE concentrate in fine soil particles and road dust. Although this phenomenon is not new, our research provides additional empirical data, further supporting the idea that fine particles play a central role in an exposure risk scenario. This concentration of PTE has significant implications for the dispersion of pollutants in the environment, particularly in urban areas. Indeed, due to the use of Pb isotopes as effective tracers to identify pollution sources, the clear presence of the anthropogenic isotope signature in the fine fraction below 10 µm (Res-BS and Res-RD) is evident. The overlap of the isotopic ratio in the different environmental media demonstrates the intimate interaction between these environmental compartments and emphasizes the active contribution of fine soil fraction to pollution in urban areas. The complexity of pollution sources in our study area is manifested through a considerable coefficient of variation of isotopic signatures, indicating the impact of both diffuse and point source contamination due to atmospheric deposition of current and past emissions. However, in the resuspended samples, the Pb isotopic signature remains relatively unchanged from samples belonging to neighboring sites, while showing the same isotopic signature of leaded gasoline in the historical samples from the early 2000s. These results not only affirm the applicability of Pb isotopes as tracers but underline the complexity of contemporary pollution sources. These findings have implications for policy makers, as they highlight the significant and underestimated role of soil in the overall contribution to air pollution. Recognizing the importance of soil contamination in the context of air quality management is crucial for designing policies that aim to mitigate air pollution, improve public health, and reduce associated economic and environmental costs. Indeed, air pollution has significant economic and financial implications, impacting not only public health but also productivity and health budgets. Improving air quality can lead to substantial benefits; stricter regulation is therefore necessary.

Chapter 3:

The study aimed to optimize mineralization procedures, assess REE contamination in urban and electronics-waste landfill soils, and investigate REE association with anthropogenic contaminants in urban

areas. These objectives were pursued to understand the sources and implications of REE contamination and provide insights for future source apportionment and regulatory efforts. The optimized method, Method D, showed superior efficiency in extracting REE from soil samples, ensuring accurate quantification and reliable analysis. With high extraction efficiencies and reproducibility, this method lays the groundwork for precise assessment of REE contamination. Our investigation into REE contamination in urban soils revealed significant spatial variations and contamination hotspots: in park soils were accumulated especially near industrial areas. The complex interplay between land use, industrialization, and waste disposal practices shapes the heterogeneous REE distribution in urban environments. The non-unique REE normalization pattern among the samples suggests anthropogenic input. Moreover, exploring REE association with anthropogenic contaminants identified distinct contamination factors, offering a framework to understand contamination sources and pathways. Continued research and collaboration are crucial for addressing challenges posed by emerging contaminants like REE and safeguarding environmental and human health in urban areas.

Chapter 4:

The study try to assess risk conditions induced by natural events in urbanized areas, focusing on the city of Turin as a case study. The interaction between local geomorphology and extensive anthropization significantly complicates this assessment, particularly regarding flooding phenomena in lowland urbanized areas. The study delves into the use of innovative microcosm systems to highlight the effects of changing redox conditions caused by flooding on the release of PTE and REE from contaminated soils. These microcosm systems offer precise control over redox conditions, enabling investigation into the processes governing contaminant release mechanisms, including the influence of E_H, pH, iron, manganese, organic carbon, dissolved inorganic carbon, and sulfate.

The solubility and mobility of trace elements (zinc (Zn), chromium (Cr), nickel (Ni), copper (Cu), and lead (Pb)) are intricately linked to various soil parameters. pH emerges as a key regulator, influencing the speciation and solubility, with higher concentrations observed under reducing conditions and lower pH levels. The presence of organic matter significantly affects the mobility, with correlations suggesting its role as a carrier, particularly for Ni and Cu. Iron and manganese oxides play crucial roles in sorption mechanisms, affecting the bioavailability and mobility, especially under oxidizing conditions. Carbonates appear to result in release of PTE at acidic pH and reducing conditions, and their

immobilization under oxidizing conditions at basic pH. In comparison to other PTE, copper exhibits inverse dynamics, characterized by higher mobility under basic pH and oxidizing conditions. This phenomenon is likely attributed to the pronounced influence of sulfates on copper behavior.

The release of REE in the liquid fraction of soil exhibits notable differences compared to PTE. Specifically, REE such as Yttrium (Y), Cerium (Ce), Neodymium (Nd), Samarium (Sm), Gadolinium (Gd), Europium (Eu), Dysprosium (Dy), and Ytterbium (Yb) demonstrate increased mobility under reducing conditions with acidic pH, contrasting with PTE. Discrepancies observed among different soils analyzed suggest potential anthropogenic influences altering REE presence and speciation, possibly stemming from industrial activities and phosphate fertilizer usage. Lanthanum (La), Cerium (Ce), and Praseodymium (Pr) exhibit distinct mobility and behavior relative to other REE, possibly due to their disparate origins (anthropogenic and/or natural) or inherent chemical-physical properties such as steric bulk and ionic radius, affecting sorption capacity. pH and redox potential (E_H) notably impact REE mobility, with organic matter content correlating with REE concentrations akin to PTE. Interactions with carbonates and sulfates further modulate REE distribution, while specific associations with Fe, Mn, and phosphorus suggest intricate relationships with soil chemistry. Co-variation patterns among REE suggest common influencing mechanisms, yet deviations imply variations in behavior or differing sources of origin.

REFERENCES

Abel, S., Nehls, T., Mekiffer, B., Mathes, M., Thieme, J., Wessolek, G., 2015. Pools of sulfur in urban rubble soils. J Soils Sediments 15, 532–540. https://doi.org/10.1007/s11368-014-1014-1

Aeppli, M., Vranic, S., Kaegi, R., Kretzschmar, R., Brown, A.R., Voegelin, A., Hofstetter, T.B., Sander, M., 2019. Decreases in Iron Oxide Reducibility during Microbial Reductive Dissolution and Transformation of Ferrihydrite. Environ. Sci. Technol. 53, 8736–8746. https://doi.org/10.1021/acs.est.9b01299

Ajmone-Marsan, F., Biasioli, M., 2010. Trace elements in soils of urban areas. Water Air Soil Pollut. 213, 121–143. https://doi.org/10.1007/s11270-010-0372-6

Ajmone-Marsan, F., Biasioli, M., Kralj, T., Grčman, H., Davidson, C.M., Hursthouse, A.S., Madrid, L., Rodrigues, S., 2008. Metals in particle-size fractions of the soils of five European cities. Environmental Pollution 152, 73–81. https://doi.org/10.1016/j.envpol.2007.05.020

Ajmone-Marsan, F., Padoan, E., Madrid, F., Vrščaj, B., Biasioli, M., Davidson, C.M., 2019. Metal Release under Anaerobic Conditions of Urban Soils of Four European Cities. Water Air Soil Pollut 230, 53. https://doi.org/10.1007/s11270-019-4101-5

Alves, C.A., Gomes, J., Nunes, T., Duarte, M., Calvo, A., Custódio, D., Pio, C., Karanasiou, A., Querol, X., 2015. Size-segregated particulate matter and gaseous emissions from motor vehicles in a road tunnel. Atmospheric Research 153, 134–144. https://doi.org/10.1016/j.atmosres.2014.08.002

Alves, C.A., Vicente, A.M.P., Calvo, A.I., Baumgardner, D., Amato, F., Querol, X., Pio, C., Gustafsson, M., 2020. Physical and chemical properties of non-exhaust particles generated from wear between pavements and tyres. Atmospheric Environment 224, 117252. https://doi.org/10.1016/j.atmosenv.2019.117252

Amato, F., Alastuey, A., Karanasiou, A., Lucarelli, F., Nava, S., Calzolai, G., Severi, M., Becagli, S., Gianelle, V.L., Colombi, C., Alves, C., Custódio, D., Nunes, T., Cerqueira, M., Pio, C., Eleftheriadis, K., Diapouli, E., Reche, C., Minguillón, M.C., Manousakas, M.-I., Maggos, T., Vratolis, S., Harrison, R.M., Querol, X., 2016. AIRUSE-LIFE+: a harmonized PM speciation and source apportionment in five southern European cities. Atmos. Chem. Phys. 16, 3289–3309. https://doi.org/10.5194/acp-16-3289-2016

Amato, F., Pandolfi, M., Escrig, A., Querol, X., Alastuey, A., Pey, J., Perez, N., and Hopke, P. K., 2009. Quantifying road dust resuspension in urban environment by Multilinear Engine: A comparison with PMF2, Atmos. Environ., 43, 2770–2780

Amato, F., Schaap, M., Denier Van der Gon, H.A.C., Pandolfi, M., Alastuey, A.,Keuken, M., Querol, X., 2012. Effect of rain events on the mobility of road dust load in two Dutch and Spanish roads. Atmos. Environ. 62, 352e358. http://doi.org/10.1016/j.atmosenv.2012.08.042

Antoniadis, V., Levizou, E., Shaheen, S.M., Ok, Y.S., Sebastian, A., Baum, C., Prasad, M.N.V., Wenzel, W.W., Rinklebe, J., 2017. Trace elements in the soil-plant interface: Phytoavailability, translocation, and phytoremediation–A review. Earth-Science Reviews 171, 621–645. https://doi.org/10.1016/j.earscirev.2017.06.005

Antoniadis, V., Shaheen, S.M., Tsadilas, C.D., Selim, M.H., Rinklebe, J., 2018. Zinc sorption by different soils as affected by selective removal of carbonates and hydrous oxides. Applied Geochemistry 88, 49–58. https://doi.org/10.1016/j.apgeochem.2017.04.007

Ardini, F., Soggia, F., Rugi, F., Udisti, R., Grotti, M., 2010. Comparison of inductively coupled plasma spectrometry techniques for the direct determination of rare earth elements in digests from geological samples. Analytica Chimica Acta 678, 18–25. https://doi.org/10.1016/j.aca.2010.07.036

ARPA Piemonte, 2020. Spazializzazione e valori di fondo naturale delle concentrazioni di Cromo, Nichel e Cobalto nei suoli del comune di Torino e cintura. Deliberazione della Giunta Regionale 2 luglio 2021, n. 8-3474

Bao, Z., Zhao, Z., 2008. Geochemistry of mineralization with exchangeable REY in the weathering crusts of granitic rocks in South China. Ore Geology Reviews 33, 519–535. https://doi.org/10.1016/j.oregeorev.2007.03.005

Bau, M., 1991. Rare-earth element mobility during hydrothermal and metamorphic fluid-rock interaction and the significance of the oxidation state of europium. Chemical Geology 93, 219–230. https://doi.org/10.1016/0009-2541(91)90115-8

Bau, M., 1999. Scavenging of dissolved yttrium and rare earths by precipitating iron oxyhydroxide: experimental evidence for Ce oxidation, Y-Ho fractionation, and lanthanide tetrad effect. Geochimica et Cosmochimica Acta 63, 67–77. https://doi.org/10.1016/S0016-7037(99)00014-9

Becker, F., Marcantonio, F., Datta, S., Wichterich, C., Cizmas, L., Surber, J., Kennedy, K., Bowles, E., 2022. Tracking the source of contaminant lead in children's blood. Environmental Research 212, 113307. https://doi.org/10.1016/j.envres.2022.113307

Bern, C.R., Walton-Day, K., Naftz, D.L., 2019. Improved enrichment factor calculations through principal component analysis: Examples from soils near breccia pipe uranium mines, Arizona,

USA. Environmental Pollution 248, 90–100. https://doi.org/10.1016/j.envpol.2019.01.122
Berrone, G., Sala, A., Gagliardi, G., Gasparini, C., Tommasi, D., Marinetto, F., 2019. MOBILITÀ VEICOLARE IN PIEMONTE, available at www.regione.piemonte.it and at www.5t.torino.it
Bi, C., Zhou, Y., Chen, Z., Jia, J., Bao, X., 2018. Heavy metals and lead isotopes in soils, road dust and leafy vegetables and health risks via vegetable consumption in the industrial areas of Shanghai, China. Science of The Total Environment 619–620, 1349–1357. https://doi.org/10.1016/j.scitotenv.2017.11.177
Bi, X., Zhang, M., Wu, Y., Fu, Z., Sun, G., Shang, L., Li, Z., Wang, P., 2020. Distribution patterns and sources of heavy metals in soils from an industry undeveloped city in Southern China. Ecotoxicology and Environmental Safety 205, 111115. https://doi.org/10.1016/j.ecoenv.2020.111115
Biasioli, M., Barberis, R., Ajmone Marsan, F., 2006. The influence of a large city on some soil properties and metals content. Science of The Total Environment 356, 154–164. https://doi.org/10.1016/j.scitotenv.2005.04.033
Biasioli, M., Grčman, H., Kralj, T., Madrid, F., Díaz-Barrientos, E., Ajmone-Marsan, F., 2007. Potentially Toxic Elements Contamination in Urban Soils: A Comparison of Three European Cities. J. Environ. Qual. 36, 70–79. https://doi.org/10.2134/jeq2006.0254
Bini, C., 2013. Geology and Geomorphology, in: Costantini, E.A.C., Dazzi, C. (Eds.), The Soils of Italy, World Soils Book Series. Springer Netherlands, Dordrecht, pp. 39–56. https://doi.org/10.1007/978-94-007-5642-7_3
Bispo, F.H.A., de Menezes, M.D., Fontana, A., Sarkis, J.E. de S., Gonçalves, C.M., de Carvalho, T.S., Curi, N., Guilherme, L.R.G., 2021. Rare earth elements (REEs): geochemical patterns and contamination aspects in Brazilian benchmark soils. Environmental Pollution 289, 117972. https://doi.org/10.1016/j.envpol.2021.117972
Bispo, F.H.A., de Menezes, M.D., Fontana, A., Sarkis, J.E. de S., Gonçalves, C.M., de Carvalho, T.S., Curi, N., Guilherme, L.R.G., 2021. Rare earth elements (REEs): geochemical patterns and contamination aspects in Brazilian benchmark soils. Environmental Pollution 289, 117972. https://doi.org/10.1016/j.envpol.2021.117972
Blodau, C., 2006. A review of acidity generation and consumption in acidic coal mine lakes and their watersheds. Science of The Total Environment 369, 307–332. https://doi.org/10.1016/j.scitotenv.2006.05.004
Borghi, A., d'Atri, A., Martire, L., Castelli, D., Costa, E., Dino, G., Favero Longo, S.E., Ferrando, S., Gallo, L.M., Giardino, M., Groppo, C.,

Piervittori, R., Rolfo, F., Rossetti, P., Vaggelli, G., 2014. Fragments of the Western Alpine Chain as Historic Ornamental Stones in Turin (Italy): Enhancement of Urban Geological Heritage through Geotourism. Geoheritage 6, 41–55. https://doi.org/10.1007/s12371-013-0091-7

Borowiak, K., Lisiak, M., Kanclerz, J., Budka, A., Mleczek, M., Niedzielski, P., Adamska, A., Janicka, E., 2018. Relations between rare earth elements accumulation in Taraxacum officinale L. and land use in an urban area – A preliminary study. Ecological Indicators 94, 22–27. https://doi.org/10.1016/j.ecolind.2018.06.046

Broom-Fendley, S., Siegfried, P.R., Wall, F., O'Neill, M., Brooker, R.A., Fallon, E.K., Pickles, J.R., Banks, D.A., 2021. The origin and composition of carbonatite-derived carbonate-bearing fluorapatite deposits. Miner Deposita 56, 863–884. https://doi.org/10.1007/s00126-020-01010-7

Bullock, P., Gregory, P.J. (Eds.), 1991. Soils in the Urban Environment, 1st ed. Wiley. https://doi.org/10.1002/9781444310603

Burghardt, W., 1994. Soils in urban and industrial environments. J Plant Nutrition & Soil 157, 205–214. https://doi.org/10.1002/jpln.19941570308

Cao, X., Chen, Y., Gu, Z., Wang, X., 2000. Determination of Trace Rare Earth Elements in Plant and Soil Samples by Inductively Coupled Plasma-Mass Spectrometry. International Journal of Environmental Analytical Chemistry 76, 295–309. https://doi.org/10.1080/03067310008034137

Cao, X., Chen, Y., Wang, X., Deng, X., 2001. Effects of redox potential and pH value on the release of rare earth elements from soil. Chemosphere 44, 655–661. https://doi.org/10.1016/S0045-6535(00)00492-6

Censi, P., Cibella, F., Falcone, E.E., Cuttitta, G., Saiano, F., Inguaggiato, C., Latteo, V., 2017. Rare earths and trace elements contents in leaves: A new indicator of the composition of atmospheric dust. Chemosphere 169, 342–350. https://doi.org/10.1016/j.chemosphere.2016.11.085

Chang, X., Yu, Y., Li, Y.-X., 2021. Response of antimony distribution in street dust to urban road traffic conditions. Journal of Environmental Management 296, 113219. https://doi.org/10.1016/j.jenvman.2021.113219

Cheisson, T., Schelter, E.J., 2019. Rare earth elements: Mendeleev's bane, modern marvels. Science 363, 489–493. https://doi.org/10.1126/science.aau7628

Chen, L.-M., Zhang, G.-L., Jin, Z.-D., 2014. Rare earth elements of a 1000-year paddy soil chronosequence: Implications for sediment provenances, parent material uniformity and pedological

changes. Geoderma 230–231, 274–279. https://doi.org/10.1016/j.geoderma.2014.03.023
Cicchella, D., Hoogewerff, J., Albanese, S., Adamo, P., Lima, A., Taiani, M.V.E., De Vivo, B., 2016. Distribution of toxic elements and transfer from the environment to humans traced by using lead isotopes. A case of study in the Sarno River basin, south Italy. Environ Geochem Health 38, 619–637. https://doi.org/10.1007/s10653-015-9748-2
Colombo, C., Miano, T., 2015. Metodi di Analisi chimica del suolo. 3rd ed. Società Italiana della Scienza del Suolo. Pubblicità & Stampa, Modugno (BA) (in Italian)
Contiero, P., Boffi, R., Tagliabue, G., Scaburri, A., Tittarelli, A., Bertoldi, M., Borgini, A., Favia, I., Ruprecht, A.A., Maiorino, A., Voza, A., Ripoll Pons, M., Cau, A., DeMarco, C., Allegri, F., Tresoldi, C., Ciccarelli, M., 2019. A Case-Crossover Study to Investigate the Effects of Atmospheric Particulate Matter Concentrations, Season, and Air Temperature on Accident and Emergency Presentations for Cardiovascular Events in Northern Italy. IJERPH 16, 4627. https://doi.org/10.3390/ijerph16234627
D. Lgs 117/2008Decreto Legislativo 30 maggio 2008, n. 117 pubblicato nella Gazzetta Ufficiale n. 157 del 7 luglio 2008 - Gestione dei rifiuti delle industrie estrattive
D.Lgs. 152/2006. Gazzetta Ufficiale della Repubblica Italiana, Decreto legislativo 3 aprile 2006, n. 152 - Norme in materia ambientale.
Davranche, M., Grau, G., Dia, A., Le Coz-Bouhnik, M., Marsac, R., Pédrot, M., Pourret, O., 2016. Rare Earth Elements in Wetlands, in: Trace Elements in Waterlogged Soils and Sediments. CRC Press, Boca Raton, pp. 135–162. https://doi.org/10.1201/9781315372952-8
De La Paix, M.J., Lanhai, L., Xi, C., Ahmed, S., Varenyam, A., 2013. SOIL DEGRADATION AND ALTERED FLOOD RISK AS A CONSEQUENCE OF DEFORESTATION. Land Degrad Dev 24, 478–485. https://doi.org/10.1002/ldr.1147
De Luca, D.A., Lasagna, M., Debernardi, L., 2020. Hydrogeology of the western Po plain (Piedmont, NW Italy). Journal of Maps 16, 265–273. https://doi.org/10.1080/17445647.2020.1738280
De Silva, S., Ball, A.S., Indrapala, D.V., Reichman, S.M., 2021. Review of the interactions between vehicular emitted potentially toxic elements, roadside soils, and associated biota. Chemosphere 263, 128135. https://doi.org/10.1016/j.chemosphere.2020.128135
Dehghani, S., Moore, F., Vasiluk, L., Hale, B.A., 2018. The geochemical fingerprinting of geogenic particles in road deposited dust from Tehran metropolis, Iran: Implications for provenance tracking. Journal of Geochemical Exploration 190, 411–423. https://doi.org/10.1016/j.gexplo.2018.04.011

Dino, G.A., Clemente, P., Lasagna, M., Passarella, I., Ajmone Marsan, F., De Luca, D.A., 2015. Industrial Chance to Recover Residual Sludge from Dimension Stones in Civil and Environmental Applications, in: Lollino, G., Manconi, A., Guzzetti, F., Culshaw, M., Bobrowsky, P., Luino, F. (Eds.), Engineering Geology for Society and Territory - Volume 5. Springer International Publishing, Cham, pp. 1309–1313. https://doi.org/10.1007/978-3-319-09048-1_250

Doe, B.R., 1970. Lead Isotopes. Springer Berlin Heidelberg, Berlin, Heidelberg. https://doi.org/10.1007/978-3-642-87280-8

Dogan, E., Cuomo, F., Battisti, L., 2023. Reviving Urban Greening in Post-Industrial Landscapes: The Case of Turin. Sustainability 15, 12760. https://doi.org/10.3390/su151712760

Du Laing, G., Rinklebe, J., Vandecasteele, B., Meers, E., Tack, F.M.G., 2009. Trace metal behaviour in estuarine and riverine floodplain soils and sediments: A review. Science of The Total Environment 407, 3972–3985. https://doi.org/10.1016/j.scitotenv.2008.07.025

El-Naggar, A., Shaheen, S.M., Hseu, Z.-Y., Wang, S.-L., Ok, Y.S., Rinklebe, J., 2019. Release dynamics of As, Co, and Mo in a biochar treated soil under pre-definite redox conditions. Science of The Total Environment 657, 686–695. https://doi.org/10.1016/j.scitotenv.2018.12.026

Environmental Inorganic Chemistry, 1988. . Elsevier. https://doi.org/10.1016/C2009-0-07927-6

Facchetti, S., 1989. Lead in petrol. The isotopic lead experiment. Acc. Chem. Res. 22, 370–374. https://doi.org/10.1021/ar00166a005

Fan, P., Ouyang, Z., Basnou, C., Pino, J., Park, H., Chen, J., 2017. Nature-based solutions for urban landscapes under post-industrialization and globalization: Barcelona versus Shanghai. Environmental Research 156, 272–283. https://doi.org/10.1016/j.envres.2017.03.043

Fendorf, S., 1996. Sorption Mechanisms of Lanthanum on Oxide Minerals. Clays and Clay Minerals 44, 220–227. https://doi.org/10.1346/CCMN.1996.0440207

Fernández-Caliani, J.C., Grantcharova, M.M., 2021. Enrichment and Fractionation of Rare Earth Elements in an Estuarine Marsh Soil Receiving Acid Discharges from Legacy Sulfide Mine Wastes. Soil Systems 5, 66. https://doi.org/10.3390/soilsystems5040066

Ferrat, M., Weiss, D.J., Strekopytov, S., 2012. A single procedure for the accurate and precise quantification of the rare earth elements, Sc, Y, Th and Pb in dust and peat for provenance tracing in climate and environmental studies. Talanta 93, 415–423. https://doi.org/10.1016/j.talanta.2012.01.052

Ferreira, A.J.D., Soares, D., Serrano, L.M.V., Walsh, R.P.D., Dias-Ferreira, C., Ferreira, C.S.S., 2016. Roads as sources of heavy metals in urban areas. The Covões catchment experiment,

Coimbra, Portugal. J Soils Sediments 16, 2622–2639. https://doi.org/10.1007/s11368-016-1492-4
Ferreira, M. da S., Fontes, M.P.F., Bellato, C.R., Marques Neto, J. de O., Lima, H.N., Fendorf, S., 2021. Geochemical signatures and natural background values of rare earth elements in soils of Brazilian Amazon. Environmental Pollution 277, 116743. https://doi.org/10.1016/j.envpol.2021.116743
Florido, M.C., Madrid, F., Ajmone-Marsan, F., 2011. Variations of Metal Availability and Bio-accessibility in Water-Logged Soils with Various Metal Contents: In Vitro Experiments. Water Air Soil Pollut 217, 149–156. https://doi.org/10.1007/s11270-010-0575-x
Frohne, T., Rinklebe, J., Diaz-Bone, R.A., 2014. Contamination of Floodplain Soils along the Wupper River, Germany, with As, Co, Cu, Ni, Sb, and Zn and the Impact of Pre-definite Redox Variations on the Mobility of These Elements. Soil and Sediment Contamination: An International Journal 23, 779–799. https://doi.org/10.1080/15320383.2014.872597
Funari, V., Bokhari, S.N.H., Vigliotti, L., Meisel, T., Braga, R., 2016. The rare earth elements in municipal solid waste incinerators ash and promising tools for their prospecting. Journal of Hazardous Materials 301, 471–479. https://doi.org/10.1016/j.jhazmat.2015.09.015
Gelly, R., Fekiacova, Z., Guihou, A., Doelsch, E., Deschamps, P., Keller, C., 2019. Lead, zinc, and copper redistributions in soils along a deposition gradient from emissions of a Pb-Ag smelter decommissioned 100 years ago. Science of The Total Environment 665, 502–512. https://doi.org/10.1016/j.scitotenv.2019.02.092
Gioia, S.M.C.L., Babinski, M., Weiss, D.J., Spiro, B., Kerr, A.A.F.S., Veríssimo, T.G., Ruiz, I., Prates, J.C.M., 2017. An isotopic study of atmospheric lead in a megacity after phasing out of leaded gasoline. Atmospheric Environment 149, 70–83. https://doi.org/10.1016/j.atmosenv.2016.10.049
Giordano, A., Malandrino, M., Ajmone Marsan, F., Padoan, E., 2024. Potentially toxic elements and lead isotopic signatures in the 10 μm fraction of urban dust: Environmental risk enhanced by resuspension of contaminated soils. Environmental Research 242, 117664. https://doi.org/10.1016/j.envres.2023.117664
Gonzalez, R.O., Strekopytov, S., Amato, F., Querol, X., Reche, C., Weiss, D., 2016. New Insights from Zinc and Copper Isotopic Compositions into the Sources of Atmospheric Particulate Matter from Two Major European Cities. Environ. Sci. Technol. 50, 9816–9824. https://doi.org/10.1021/acs.est.6b00863
Graf, D.L., 1980. Chemical Equilibria in Soils. Clays and Clay Minerals 28, 319–319. https://doi.org/10.1346/CCMN.1980.0280411

Grawunder, A., Merten, D., Büchel, G., 2014. Origin of middle rare earth element enrichment in acid mine drainage-impacted areas. Environ Sci Pollut Res 21, 6812–6823. https://doi.org/10.1007/s11356-013-2107-x

Grigoratos, T., Martini, G., 2015. Brake wear particle emissions: a review. Environ Sci Pollut Res 22, 2491–2504. https://doi.org/10.1007/s11356-014-3696-8

Grybos, M., Davranche, M., Gruau, G., Petitjean, P., 2007. Is trace metal release in wetland soils controlled by organic matter mobility or Fe-oxyhydroxides reduction? Journal of Colloid and Interface Science 314, 490–501. https://doi.org/10.1016/j.jcis.2007.04.062

Gupta, S.K., Goyal, M.R., Singh, A. (Eds.), 2018. Engineering practices for management of soil salinity: agricultural, physiological, and adaptive approaches. Apple Academic Press, Waretown, NJ.

Gwenzi, W., Mangori, L., Danha, C., Chaukura, N., Dunjana, N., Sanganyado, E., 2018. Sources, behaviour, and environmental and human health risks of high-technology rare earth elements as emerging contaminants. Science of The Total Environment 636, 299–313. https://doi.org/10.1016/j.scitotenv.2018.04.235

Hagmann, D.F., Kruge, M.A., Cheung, M., Mastalerz, M., Gallego, J.L.R., Singh, J.P., Krumins, J.A., Li, X.N., Goodey, N.M., 2019. Environmental forensic characterization of former rail yard soils located adjacent to the Statue of Liberty in the New York/New Jersey harbor. Science of The Total Environment 690, 1019–1034. https://doi.org/10.1016/j.scitotenv.2019.06.495

Hanke, A., Cerli, C., Muhr, J., Borken, W., Kalbitz, K., 2013. Redox control on carbon mineralization and dissolved organic matter along a chronosequence of paddy soils. European J Soil Science 64, 476–487. https://doi.org/10.1111/ejss.12042

Hans Wedepohl, K., 1995. The composition of the continental crust. Geochimica et Cosmochimica Acta 59, 1217–1232. https://doi.org/10.1016/0016-7037(95)00038-2

Hansson, S.V., Grusson, Y., Chimienti, M., Claustres, A., Jean, S., Le Roux, G., 2019. Legacy Pb pollution in the contemporary environment and its potential bioavailability in three mountain catchments. Science of The Total Environment 671, 1227–1236. https://doi.org/10.1016/j.scitotenv.2019.03.403

Harkins, W.D., 1917. THE EVOLUTION OF THE ELEMENTS AND THE STABILITY OF COMPLEX ATOMS. I. A NEW PERIODIC SYSTEM WHICH SHOWS A RELATION BETWEEN THE ABUNDANCE OF THE ELEMENTS AND THE STRUCTURE OF THE NUCLEI OF ATOMS. J. Am. Chem. Soc. 39, 856–879. https://doi.org/10.1021/ja02250a002

Hatje, V., Bruland, K.W., Flegal, A.R., 2016. Increases in Anthropogenic Gadolinium Anomalies and Rare Earth Element Concentrations

in San Francisco Bay over a 20 Year Record. Environ. Sci. Technol. 50, 4159–4168. https://doi.org/10.1021/acs.est.5b04322
Hirabayashi, Y., Kanae, S., 2009. First estimate of the future global population at risk of flooding. Hydrological Research Letters 3, 6–9. https://doi.org/10.3178/hrl.3.6
Howard, J.L., Orlicki, K.M., 2015. Effects of Anthropogenic Particles on the Chemical and Geophysical Properties of Urban Soils, Detroit, Michigan: Soil Science 180, 154–166. https://doi.org/10.1097/SS.0000000000000122
Hu, X., Sun, Y., Ding, Z., Zhang, Y., Wu, J., Lian, H., Wang, T., 2014. Lead contamination and transfer in urban environmental compartments analyzed by lead levels and isotopic compositions. Environmental Pollution 187, 42–48. https://doi.org/10.1016/j.envpol.2013.12.025
Hu, Z., Haneklaus, S., Sparovek, G., Schnug, E., 2006. Rare Earth Elements in Soils. Communications in Soil Science and Plant Analysis 37, 1381–1420. https://doi.org/10.1080/00103620600628680
IARC Scientific Publication No. 161: Air Pollution and Cancer. [(accessed on 13 September 2019)]; Available online: http://www.iarc.fr/en/publications/books/sp161/AirPollutionandCancer161.pdf
Implementation of the Directive 2008/50/EC of the European Parliament and of the Council of 21 May 2008 on ambient air quality and cleaner air for Europe, adopted in Italy in 2010, 2008.
Jalali, J., Gaudin, P., Ammar, E., Lebeau, T., 2020. Bioaugmentation coupled with phytoextraction for the treatment of Cd and Sr, and reuse opportunities for phosphogypsum rare earth elements. Journal of Hazardous Materials 399, 122821. https://doi.org/10.1016/j.jhazmat.2020.122821
Janots, E., Bernier, F., Brunet, F., Muñoz, M., Trcera, N., Berger, A., Lanson, M., 2015. Ce(III) and Ce(IV) (re)distribution and fractionation in a laterite profile from Madagascar: Insights from in situ XANES spectroscopy at the Ce LIII-edge. Geochimica et Cosmochimica Acta 153, 134–148. https://doi.org/10.1016/j.gca.2015.01.009
Jim, C.Y., 1998. Impacts of intensive urbanization on trees in Hong Kong. Envir. Conserv. 25, 146–159. https://doi.org/10.1017/S0376892998000198
Johnson, C.C., 2011. Mapping the chemical environment of urban areas. Wiley-Blackwell, Chichester, West Sussex, UK Hoboken, NJ.
Kelepertzis, E., Argyraki, A., 2015. Geochemical associations for evaluating the availability of potentially harmful elements in urban soils: Lessons learnt from Athens, Greece. Applied Geochemistry 59, 63–73. https://doi.org/10.1016/j.apgeochem.2015.03.019

Kelepertzis, E., Argyraki, A., Chrastný, V., Botsou, F., Skordas, K., Komárek, M., Fouskas, A., 2020. Metal(loid) and isotopic tracing of Pb in soils, road and house dusts from the industrial area of Volos (central Greece). Science of The Total Environment 725, 138300. https://doi.org/10.1016/j.scitotenv.2020.138300

Kelepertzis, E., Galanos, E., Mitsis, I., 2013. Origin, mineral speciation and geochemical baseline mapping of Ni and Cr in agricultural topsoils of Thiva Valley (central Greece). Journal of Geochemical Exploration 125, 56–68. https://doi.org/10.1016/j.gexplo.2012.11.007

Kelepertzis, E., Komárek, M., Argyraki, A., Šillerová, H., 2016. Metal(loid) distribution and Pb isotopic signatures in the urban environment of Athens, Greece. Environmental Pollution 213, 420–431. https://doi.org/10.1016/j.envpol.2016.02.049

Khademi, H., Gabarrón, M., Abbaspour, A., Martínez-Martínez, S., Faz, A., Acosta, J.A., 2019. Environmental impact assessment of industrial activities on heavy metals distribution in street dust and soil. Chemosphere 217, 695–705. https://doi.org/10.1016/j.chemosphere.2018.11.045

Khodadadi, N., Amini, A., Dehbandi, R., 2022. Contamination, probabilistic health risk assessment and quantitative source apportionment of potentially toxic metals (PTMs) in street dust of a highly developed city in north of Iran. Environmental Research 210, 112962. https://doi.org/10.1016/j.envres.2022.112962

Khondoker, R., Weiss, D., van de Flierdt, T., Rehkämper, M., Kreissig, K., Coles, B.J., Strekopytov, S., Humphreys-Williams, E., Dong, S., Bory, A., Bout-Roumazeilles, V., Smichowski, P., Cid-Agüero, P., Babinski, M., Losno, R., Monna, F., 2018. New constraints on elemental and Pb and Nd isotope compositions of South American and Southern African aerosol sources to the South Atlantic Ocean. Geochemistry 78, 372–384. https://doi.org/10.1016/j.chemer.2018.05.001

Kirk, G.J.D., Ahmad, A.R., Nye, P.H., 1990. Coupled diffusion and oxidation of ferrous iron in soils. II. A model of the diffusion and reaction of O 2 , Fe 2+ , H + and HCO 3 − in soils and a sensitivity analysis of the model. Journal of Soil Science 41, 411–431. https://doi.org/10.1111/j.1365-2389.1990.tb00076.x

Kudas, D., Wnęk, A., Zając, E., 2024. Soil sealing changes in selected functional urban areas in Poland in 2012–2018. Journal of Water and Land Development 219–227. https://doi.org/10.24425/jwld.2024.149123

Lahd Geagea, M., Stille, P., Gauthier-Lafaye, F., Millet, M., 2008. Tracing of Industrial Aerosol Sources in an Urban Environment Using Pb, Sr, and Nd Isotopes. Environ. Sci. Technol. 42, 692–698. https://doi.org/10.1021/es071704c

Laidlaw, M.A.S., Filippelli, G.M., 2008. Resuspension of urban soils as a persistent source of lead poisoning in children: A review and new directions. Applied Geochemistry 23, 2021–2039.

Laveuf, C., Cornu, S., 2009. A review on the potentiality of Rare Earth Elements to trace pedogenetic processes. Geoderma 154, 1–12. https://doi.org/10.1016/j.geoderma.2009.10.002

Li, F., Jinxu, Y., Shao, L., Zhang, G., Wang, J., Jin, Z., 2018. Delineating the origin of Pb and Cd in the urban dust through elemental and stable isotopic ratio: A study from Hangzhou City, China. Chemosphere 211, 674–683. https://doi.org/10.1016/j.chemosphere.2018.07.199

Li, X., Chen, Zhibiao, Chen, Zhiqiang, Zhang, Y., 2013. A human health risk assessment of rare earth elements in soil and vegetables from a mining area in Fujian Province, Southeast China. Chemosphere 93, 1240–1246. https://doi.org/10.1016/j.chemosphere.2013.06.085

Li, Y., Ajmone-Marsan F., Padoan E., 2021. Health risk assessment via ingestion and inhalation of soil PTE of an urban area. Chemosphere 281, 130964. https://doi.org/10.1016/j.chemosphere.2021.130964

Li, Y., Gao, B., Xu, D., Lu, J., Zhou, H., Gao, L., 2022. Heavy metals in the water-level-fluctuation zone soil of the three Gorges Reservoir, China: Remobilization and catchment-wide transportation. Journal of Hydrology 612, 128108. https://doi.org/10.1016/j.jhydrol.2022.128108

Li, Y., Padoan, E., Ajmone-Marsan, F., 2021. Soil particle size fraction and potentially toxic elements bioaccessibility: A review. Ecotoxicology and Environmental Safety 209, 111806. https://doi.org/10.1016/j.ecoenv.2020.111806

Li, Z., Liang, T., Li, K., Wang, P., 2020. Exposure of children to light rare earth elements through ingestion of various size fractions of road dust in REEs mining areas. Science of The Total Environment 743, 140432. https://doi.org/10.1016/j.scitotenv.2020.140432

Liang, S.-Y., Cui, J.-L., Bi, X.-Y., Luo, X.-S., Li, X.-D., 2019. Deciphering source contributions of trace metal contamination in urban soil, road dust, and foliar dust of Guangzhou, southern China. Science of The Total Environment 695, 133596. https://doi.org/10.1016/j.scitotenv.2019.133596

Liang, T., Ding, S., Song, W., Chong, Z., Zhang, C., Li, H., 2008. A review of fractionations of rare earth elements in plants. Journal of Rare Earths 26, 7–15. https://doi.org/10.1016/S1002-0721(08)60027-7

Lima, A.T., Ottosen, L., 2021. Recovering rare earth elements from contaminated soils: Critical overview of current remediation technologies. Chemosphere 265, 129163. https://doi.org/10.1016/j.chemosphere.2020.129163

Lindsay, W.L., 1979. Chemical equilibria in soils. Wiley, New York.
Liu, Q., Shi, H., An, Y., Ma, J., Zhao, W., Qu, Y., Chen, H., Liu, L., Wu, F., 2023. Source, environmental behavior and potential health risk of rare earth elements in Beijing urban park soils. Journal of Hazardous Materials 445, 130451. https://doi.org/10.1016/j.jhazmat.2022.130451
Long, Z., Zhu, H., Bing, H., Tian, X., Wang, Z., Wang, X., Wu, Y., 2021. Contamination, sources and health risk of heavy metals in soil and dust from different functional areas in an industrial city of Panzhihua City, Southwest China. Journal of Hazardous Materials 420, 126638. https://doi.org/10.1016/j.jhazmat.2021.126638
Lozano, A., Ayora, C., Fernández-Martínez, A., 2020. Sorption of rare earth elements on schwertmannite and their mobility in acid mine drainage treatments. Applied Geochemistry 113, 104499. https://doi.org/10.1016/j.apgeochem.2019.104499
Luo, X., Bing, H., Luo, Z., Wang, Y., Jin, L., 2019. Impacts of atmospheric particulate matter pollution on environmental biogeochemistry of trace metals in soil-plant system: A review. Environmental Pollution 255, 113138. https://doi.org/10.1016/j.envpol.2019.113138
Luo, Y., Yuan, H., Zhao, J., Qi, Y., Cao, W.-W., Liu, J.-M., Guo, W., Bao, Z.-H., 2021. Multiple factors influence bacterial community diversity and composition in soils with rare earth element and heavy metal co-contamination. Ecotoxicology and Environmental Safety 225, 112749. https://doi.org/10.1016/j.ecoenv.2021.112749
Marsac, R., Davranche, M., Gruau, G., Dia, A., 2010. Metal loading effect on rare earth element binding to humic acid: Experimental and modelling evidence. Geochimica et Cosmochimica Acta 74, 1749–1761. https://doi.org/10.1016/j.gca.2009.12.006
Mendez, M.J., Panebianco, J.E., Buschiazzo, D.E., 2013. A new dust generator for laboratory dust emission studies. Aeolian Research 8, 59–64. https://doi.org/10.1016/j.aeolia.2012.10.007
Migaszewski, Z.M., Gałuszka, A., Dołęgowska, S., 2016. Rare earth and trace element signatures for assessing an impact of rock mining and processing on the environment: Wiśniówka case study, south-central Poland. Environ Sci Pollut Res 23, 24943–24959. https://doi.org/10.1007/s11356-016-7713-y
Mihajlovic, J., Bauriegel, A., Stärk, H.-J., Roßkopf, N., Zeitz, J., Milbert, G., Rinklebe, J., 2019. Rare earth elements in soil profiles of various ecosystems across Germany. Applied Geochemistry 102, 197–217. https://doi.org/10.1016/j.apgeochem.2019.02.002
Mihajlovic, J., Stärk, H.-J., Rinklebe, J., 2014. Geochemical fractions of rare earth elements in two floodplain soil profiles at the Wupper

River, Germany. Geoderma 228–229, 160–172. https://doi.org/10.1016/j.geoderma.2013.12.009
Miranda, L.S., Ayoko, G.A., Egodawatta, P., Goonetilleke, A., 2022. Adsorption-desorption behavior of heavy metals in aquatic environments: Influence of sediment, water and metal ionic properties. Journal of Hazardous Materials 421, 126743. https://doi.org/10.1016/j.jhazmat.2021.126743
Mleczek, P., Borowiak, K., Budka, A., Niedzielski, P., 2018. Relationship between concentration of rare earth elements in soil and their distribution in plants growing near a frequented road. Environ Sci Pollut Res 25, 23695–23711. https://doi.org/10.1007/s11356-018-2428-x
Morton-Bermea, O., Rodríguez-Salazar, M.T., Hernández-Alvarez, E., García-Arreola, M.E., Lozano-Santacruz, R., 2011. Lead isotopes as tracers of anthropogenic pollution in urban topsoils of Mexico City. Geochemistry 71, 189–195. https://doi.org/10.1016/j.chemer.2011.03.003
Naccarato, A., Tassone, A., Cavaliere, F., Elliani, R., Pirrone, N., Sprovieri, F., Tagarelli, A., Giglio, A., 2020. Agrochemical treatments as a source of heavy metals and rare earth elements in agricultural soils and bioaccumulation in ground beetles. Science of The Total Environment 749, 141438. https://doi.org/10.1016/j.scitotenv.2020.141438
Nazzal, Y., Rosen, M.A., Al-Rawabdeh, A.M., 2013. Assessment of metal pollution in urban road dusts from selected highways of the Greater Toronto Area in Canada. Environ Monit Assess 185, 1847–1858. https://doi.org/10.1007/s10661-012-2672-3
Oddo, G., 1914. Die Molekularstruktur der radioaktiven Atome. Z. Anorg. Chem. 87, 253–268. https://doi.org/10.1002/zaac.19140870118
Ohta, A., Kawabe, I., 2001. REE(III) adsorption onto Mn dioxide (δ-MnO2) and Fe oxyhydroxide: Ce(III) oxidation by δ-MnO2. Geochimica et Cosmochimica Acta 65, 695–703. https://doi.org/10.1016/S0016-7037(00)00578-0
Orani, A.M., Vassileva, E., Azemard, S., Alonso-Hernandez, C., 2020. Trace elements contamination assessment in marine sediments from different regions of the Caribbean Sea. Journal of Hazardous Materials 399, 122934. https://doi.org/10.1016/j.jhazmat.2020.122934
Ortega, J.A., Razola, L., Garzón, G., 2014. Recent human impacts and change in dynamics and morphology of ephemeral rivers. Nat. Hazards Earth Syst. Sci. 14, 713–730. https://doi.org/10.5194/nhess-14-713-2014
Paatero P., Tapper U., 1994. Positive matrix factorization: A non-negative factor model with optimal utilization of error estimates of data values. Environmetrics 5(2), 111-126.

Pachon, J.E., Vanegas, S., Saavedra, C., Amato, F., Silva, L.F.O., Blanco, K., Chaparro, R., Casas, O.M., 2021. Evaluation of factors influencing road dust loadings in a Latin American urban center. Journal of the Air & Waste Management Association 71, 268–280. https://doi.org/10.1080/10962247.2020.1806946

Padoan, E., Amato, F., 2018. Vehicle Non-Exhaust Emissions, in: Non-Exhaust Emissions. Elsevier, pp. 21–65. https://doi.org/10.1016/B978-0-12-811770-5.00002-9

Padoan, E., Maffia, J., Balsari, P., Ajmone-Marsan, F., Dinuccio, E., 2021. Soil PM10 emission potential under specific mechanical stress and particles characteristics. Science of The Total Environment 779, 146468. https://doi.org/10.1016/j.scitotenv.2021.146468

Padoan, E., Malandrino, M., Giacomino, A., Grosa, M.M., Lollobrigida, F., Martini, S., Abollino, O., 2016. Spatial distribution and potential sources of trace elements in PM10 monitored in urban and rural sites of Piedmont Region. Chemosphere 145, 495–507. https://doi.org/10.1016/j.chemosphere.2015.11.094

Padoan, E., Romè, C., Ajmone-Marsan, F., 2017. Bioaccessibility and size distribution of metals in road dust and roadside soils along a peri-urban transect. Science of The Total Environment 601–602, 89–98. https://doi.org/10.1016/j.scitotenv.2017.05.180

Pant, P., Harrison, R.M., 2013. Estimation of the contribution of road traffic emissions to particulate matter concentrations from field measurements: A review. Atmospheric Environment 77, 78–97. https://doi.org/10.1016/j.atmosenv.2013.04.028

Pinto, J., Quiroz, D., Delvasto, P., Blanco, S., 2018. Characterization of a zinc-nickel alloy coating obtained from an electrolytic bath produced with spent batteries as raw materials. J. Phys.: Conf. Ser. 1119, 012005. https://doi.org/10.1088/1742-6596/1119/1/012005

Poggio, L., Vrščaj, B., Schulin, R., Hepperle, E., Ajmone Marsan, F., 2009. Metals pollution and human bioaccessibility of topsoils in Grugliasco (Italy). Environmental Pollution 157, 680–689. https://doi.org/10.1016/j.envpol.2008.08.009

Ponting, J., Kelly, T.J., Verhoef, A., Watts, M.J., Sizmur, T., 2021. The impact of increased flooding occurrence on the mobility of potentially toxic elements in floodplain soil – A review. Science of The Total Environment 754, 142040. https://doi.org/10.1016/j.scitotenv.2020.142040

Pouyat, R.V., Day, S.D., Brown, S., Schwarz, K., Shaw, R.E., Szlavecz, K., Trammell, T.L.E., Yesilonis, I.D., 2020. Urban Soils, in: Pouyat, R.V., Page-Dumroese, D.S., Patel-Weynand, T., Geiser, L.H. (Eds.), Forest and Rangeland Soils of the United States Under Changing Conditions. Springer International Publishing,

Cham, pp. 127–144. https://doi.org/10.1007/978-3-030-45216-2_7

Pourret, O., Davranche, M., Gruau, G., Dia, A., 2007. Organic complexation of rare earth elements in natural waters: Evaluating model calculations from ultrafiltration data. Geochimica et Cosmochimica Acta 71, 2718–2735. https://doi.org/10.1016/j.gca.2007.04.001

Raaschou-Nielsen, O., Andersen, Z.J., Beelen, R., Samoli, E., Stafoggia, M., Weinmayr, G., Hoffmann, B., Fischer, P., Nieuwenhuijsen, M.J., Brunekreef, B., Xun, W.W., Katsouyanni, K., Dimakopoulou, K., Sommar, J., Forsberg, B., Modig, L., Oudin, A., Oftedal, B., Schwarze, P.E., Nafstad, P., De Faire, U., Pedersen, N.L., Östenson, C.-G., Fratiglioni, L., Penell, J., Korek, M., Pershagen, G., Eriksen, K.T., Sørensen, M., Tjønneland, A., Ellermann, T., Eeftens, M., Peeters, P.H., Meliefste, K., Wang, M., Bueno-de-Mesquita, B., Key, T.J., De Hoogh, K., Concin, H., Nagel, G., Vilier, A., Grioni, S., Krogh, V., Tsai, M.-Y., Ricceri, F., Sacerdote, C., Galassi, C., Migliore, E., Ranzi, A., Cesaroni, G., Badaloni, C., Forastiere, F., Tamayo, I., Amiano, P., Dorronsoro, M., Trichopoulou, A., Bamia, C., Vineis, P., Hoek, G., 2013. Air pollution and lung cancer incidence in 17 European cohorts: prospective analyses from the European Study of Cohorts for Air Pollution Effects (ESCAPE). The Lancet Oncology 14, 813–822. https://doi.org/10.1016/S1470-2045(13)70279-1

Ramírez, O., Sánchez de la Campa, A.M., Amato, F., Moreno, T., Silva, L.F., de la Rosa, J.D., 2019. Physicochemical characterization and sources of the thoracic fraction of road dust in a Latin American megacity. Science of The Total Environment 652, 434–446. https://doi.org/10.1016/j.scitotenv.2018.10.214

Ramírez-Guinart, O., Salaberria, A., Vidal, M., Rigol, A., 2018. Dependence of samarium-soil interaction on samarium concentration: Implications for environmental risk assessment. Environmental Pollution 234, 439–447. https://doi.org/10.1016/j.envpol.2017.11.072

Ramos, S.J., Dinali, G.S., Oliveira, C., Martins, G.C., Moreira, C.G., Siqueira, J.O., Guilherme, L.R.G., 2016. Rare Earth Elements in the Soil Environment. Curr Pollution Rep 2, 28–50. https://doi.org/10.1007/s40726-016-0026-4

Ratié, G., Zhang, K., Iqbal, M., Vantelon, D., Mahé, F., Rivard, C., Komárek, M., Bouhnik-Le Coz, M., Dia, A., Hanna, K., Davranche, M., Marsac, R., 2023. Driving forces of Ce(III) oxidation to Ce(IV) onto goethite. Chemical Geology 633, 121547. https://doi.org/10.1016/j.chemgeo.2023.121547

Reddy, K.R., DeLaune, R.D., 2008. Biogeochemistry of Wetlands, 0 ed. CRC Press. https://doi.org/10.1201/9780203491454

Rinklebe, J., Shaheen, S.M., Yu, K., 2016. Release of As, Ba, Cd, Cu, Pb, and Sr under pre-definite redox conditions in different rice paddy soils originating from the U.S.A. and Asia. Geoderma 270, 21–32. https://doi.org/10.1016/j.geoderma.2015.10.011

Roth, G.A., Johnson, C., Abajobir, A., Abd-Allah, F., Abera, S.F., Abyu, G., Ahmed, M., Aksut, B., Alam, T., Alam, K., Alla, F., Alvis-Guzman, N., Amrock, S., Ansari, H., Ärnlöv, J., Asayesh, H., Atey, T.M., Avila-Burgos, L., Awasthi, A., Banerjee, A., Barac, A., Bärnighausen, T., Barregard, L., Bedi, N., Belay Ketema, E., Bennett, D., Berhe, G., Bhutta, Z., Bitew, S., Carapetis, J., Carrero, J.J., Malta, D.C., Castañeda-Orjuela, C.A., Castillo-Rivas, J., Catalá-López, F., Choi, J.-Y., Christensen, H., Cirillo, M., Cooper, L., Criqui, M., Cundiff, D., Damasceno, A., Dandona, L., Dandona, R., Davletov, K., Dharmaratne, S., Dorairaj, P., Dubey, M., Ehrenkranz, R., El Sayed Zaki, M., Faraon, E.J.A., Esteghamati, A., Farid, T., Farvid, M., Feigin, V., Ding, E.L., Fowkes, G., Gebrehiwot, T., Gillum, R., Gold, A., Gona, P., Gupta, R., Habtewold, T.D., Hafezi-Nejad, N., Hailu, T., Hailu, G.B., Hankey, G., Hassen, H.Y., Abate, K.H., Havmoeller, R., Hay, S.I., Horino, M., Hotez, P.J., Jacobsen, K., James, S., Javanbakht, M., Jeemon, P., John, D., Jonas, J., Kalkonde, Y., Karimkhani, C., Kasaeian, A., Khader, Y., Khan, A., Khang, Y.-H., Khera, S., Khoja, A.T., Khubchandani, J., Kim, D., Kolte, D., Kosen, S., Krohn, K.J., Kumar, G.A., Kwan, G.F., Lal, D.K., Larsson, A., Linn, S., Lopez, A., Lotufo, P.A., El Razek, H.M.A., Malekzadeh, R., Mazidi, M., Meier, T., Meles, K.G., Mensah, G., Meretoja, A., Mezgebe, H., Miller, T., Mirrakhimov, E., Mohammed, S., Moran, A.E., Musa, K.I., Narula, J., Neal, B., Ngalesoni, F., Nguyen, G., Obermeyer, C.M., Owolabi, M., Patton, G., Pedro, J., Qato, D., Qorbani, M., Rahimi, K., Rai, R.K., Rawaf, S., Ribeiro, A., Safiri, S., Salomon, J.A., Santos, I., Santric Milicevic, M., Sartorius, B., Schutte, A., Sepanlou, S., Shaikh, M.A., Shin, M.-J., Shishehbor, M., Shore, H., Silva, D.A.S., Sobngwi, E., Stranges, S., Swaminathan, S., Tabarés-Seisdedos, R., Tadele Atnafu, N., Tesfay, F., Thakur, J.S., Thrift, A., Topor-Madry, R., Truelsen, T., Tyrovolas, S., Ukwaja, K.N., Uthman, O., Vasankari, T., Vlassov, V., Vollset, S.E., Wakayo, T., Watkins, D., Weintraub, R., Werdecker, A., Westerman, R., Wiysonge, C.S., Wolfe, C., Workicho, A., Xu, G., Yano, Y., Yip, P., Yonemoto, N., Younis, M., Yu, C., Vos, T., Naghavi, M., Murray, C., 2017. Global, Regional, and National Burden of Cardiovascular Diseases for 10 Causes, 1990 to 2015. Journal of the American College of Cardiology 70, 1–25. https://doi.org/10.1016/j.jacc.2017.04.052

Rupp, H., Rinklebe, J., Bolze, S., Meissner, R., 2010. A scale-dependent approach to study pollution control processes in wetland soils

using three different techniques. Ecological Engineering 36, 1439–1447. https://doi.org/10.1016/j.ecoleng.2010.06.024
Sager, M., Wiche, O., 2024. Rare Earth Elements (REE): Origins, Dispersion, and Environmental Implications—A Comprehensive Review. Environments 11, 24. https://doi.org/10.3390/environments11020024
Salem, M., Souissi, R., Souissi, F., Abbes, N., Moutte, J., 2019. Phosphoric acid purification sludge: Potential in heavy metals and rare earth elements. Waste Management 83, 46–56. https://doi.org/10.1016/j.wasman.2018.10.040
Scalenghe, R., Marsan, F.A., 2009. The anthropogenic sealing of soils in urban areas. Landscape and Urban Planning 90, 1–10. https://doi.org/10.1016/j.landurbplan.2008.10.011
Shaheen, S.M., Ali, R.A., Abowaly, M.E., Rabie, A.E.-M.A., El Abbasy, N.E., Rinklebe, J., 2018. Assessing the mobilization of As, Cr, Mo, and Se in Egyptian lacustrine and calcareous soils using sequential extraction and biogeochemical microcosm techniques. Journal of Geochemical Exploration 191, 28–42. https://doi.org/10.1016/j.gexplo.2018.05.003
Shaheen, S.M., Frohne, T., White, J.R., DeLaune, R.D., Rinklebe, J., 2017. Redox-induced mobilization of copper, selenium, and zinc in deltaic soils originating from Mississippi (U.S.A.) and Nile (Egypt) River Deltas: A better understanding of biogeochemical processes for safe environmental management. Journal of Environmental Management 186, 131–140. https://doi.org/10.1016/j.jenvman.2016.05.032
Shaheen, S.M., Rinklebe, J., Frohne, T., White, J.R., DeLaune, R.D., 2016. Redox effects on release kinetics of arsenic, cadmium, cobalt, and vanadium in Wax Lake Deltaic freshwater marsh soils. Chemosphere 150, 740–748. https://doi.org/10.1016/j.chemosphere.2015.12.043
Shaheen, S.M., Rinklebe, J., Rupp, H., Meissner, R., 2014. Lysimeter trials to assess the impact of different flood–dry-cycles on the dynamics of pore water concentrations of As, Cr, Mo and V in a contaminated floodplain soil. Geoderma 228–229, 5–13. https://doi.org/10.1016/j.geoderma.2013.12.030
Shajib, M.T.I., Hansen, H.C.B., Liang, T., Holm, P.E., 2020. Rare earth elements in surface specific urban runoff in Northern Beijing. Science of The Total Environment 717, 136969. https://doi.org/10.1016/j.scitotenv.2020.136969
Shi, G., Chen, Z., Xu, S., Zhang, J., Wang, L., Bi, C., Teng, J., 2008. Potentially toxic metal contamination of urban soils and roadside dust in Shanghai, China. Environmental Pollution 156, 251–260. https://doi.org/10.1016/j.envpol.2008.02.027
Skougaard Kaspersen, P., Høegh Ravn, N., Arnbjerg-Nielsen, K., Madsen, H., Drews, M., 2017. Comparison of the impacts of

urban development and climate change on exposing European cities to pluvial flooding. Hydrol. Earth Syst. Sci. 21, 4131–4147. https://doi.org/10.5194/hess-21-4131-2017

Šmuc, N.R., Dolenec, T., Serafimovski, T., Dolenec, M., Vrhovnik, P., 2012. Geochemical characteristics of rare earth elements (REEs) in the paddy soil and rice (Oryza sativa L.) system of Kočani Field, Republic of Macedonia. Geoderma 183–184, 1–11. https://doi.org/10.1016/j.geoderma.2012.03.009

Stotzky, G., 2016. Microbial Respiration, in: Norman, A.G. (Ed.), Agronomy Monographs. American Society of Agronomy, Soil Science Society of America, Madison, WI, USA, pp. 1550–1572. https://doi.org/10.2134/agronmonogr9.2.c62

Sun, G., Li, Z., Liu, T., Chen, J., Wu, T., Feng, X., 2017. Rare earth elements in street dust and associated health risk in a municipal industrial base of central China. Environ Geochem Health 39, 1469–1486. https://doi.org/10.1007/s10653-017-9982-x

Suzuki, Y., Hikida, S., Furuta, N., 2011. Cycling of rare earth elements in the atmosphere in central Tokyo. J. Environ. Monit. 13, 3420. https://doi.org/10.1039/c1em10590f

Tan, Q., Li, J., Zeng, X., 2015. Rare Earth Elements Recovery from Waste Fluorescent Lamps: A Review. Critical Reviews in Environmental Science and Technology 45, 749–776. https://doi.org/10.1080/10643389.2014.900240

Tepe, N., Romero, M., Bau, M., 2014. High-technology metals as emerging contaminants: Strong increase of anthropogenic gadolinium levels in tap water of Berlin, Germany, from 2009 to 2012. Applied Geochemistry 45, 191–197. https://doi.org/10.1016/j.apgeochem.2014.04.006

TGM, 2018. Average annual daily traffic on road element BDTRE, https://www.regione.piemonte.it.

Tyler, G., 2004. Rare earth elements in soil and plant systems - A review. Plant Soil 267, 191–206. https://doi.org/10.1007/s11104-005-4888-2

Tranvik, L.J., 1998. Degradation of Dissolved Organic Matter in Humic Waters by Bacteria, in: Hessen, D.O., Tranvik, L.J. (Eds.), Aquatic Humic Substances, Ecological Studies. Springer Berlin Heidelberg, Berlin, Heidelberg, pp. 259–283. https://doi.org/10.1007/978-3-662-03736-2_11

Trommetter, G., Dumoulin, D., Billon, G., 2020. Direct determination of rare earth elements in natural water and digested sediment samples by inductively coupled plasma quadrupole mass spectrometry using collision cell. Spectrochimica Acta Part B: Atomic Spectroscopy 171, 105922. https://doi.org/10.1016/j.sab.2020.105922

Van Donkelaar, A., Martin, R.V., Brauer, M., Boys, B.L., 2015. Use of Satellite Observations for Long-Term Exposure Assessment of

Global Concentrations of Fine Particulate Matter. Environ Health Perspect 123, 135–143. https://doi.org/10.1289/ehp.1408646

Verma, A., Kumar, R., Yadav, S., 2020. Distribution, pollution levels, toxicity, and health risk assessment of metals in surface dust from Bhiwadi industrial area in North India. Human and Ecological Risk Assessment: An International Journal 26, 2091–2111. https://doi.org/10.1080/10807039.2019.1650328

VIIAS Project, Metodi per la Valutazione Integrata dell'Impatto Ambientale e Sanitario dell'inquinamento atmosferico, https://www.viias.it/pagine/impatto-sulla-salute.

Vlasov, D., Kosheleva, N., Kasimov, N., 2021. Spatial distribution and sources of potentially toxic elements in road dust and its PM10 fraction of Moscow megacity. Science of The Total Environment 761, 143267. https://doi.org/10.1016/j.scitotenv.2020.143267

Wang, L., Liao, C., Yang, Y., Xu, H., Xiao, Y., Yan, C., 2017. Effects of organic acids on the leaching process of ion-adsorption type rare earth ore. Journal of Rare Earths 35, 1233–1238. https://doi.org/10.1016/j.jre.2017.07.001

Wang, S., Xiong, Z., Wang, L., Yang, X., Yan, X., Li, Y., Zhang, C., Liang, T., 2022. Potential hot spots contaminated with exogenous, rare earth elements originating from e-waste dismantling and recycling. Environmental Pollution 309, 119717. https://doi.org/10.1016/j.envpol.2022.119717

Wang, X., Zhang, Q., Mao, S., Cheng, W., 2019. A Theoretical Study on the Electronic Structure and Floatability of Rare Earth Elements (La, Ce, Nd and Y) Bearing Fluorapatite. Minerals 9, 500. https://doi.org/10.3390/min9080500

Wei, J., Wang, C., Yin, S., Pi, X., Jin, L., Li, Z., Liu, J., Wang, L., Yin, C., Ren, A., 2020. Concentrations of rare earth elements in maternal serum during pregnancy and risk for fetal neural tube defects. Environment International 137, 105542. https://doi.org/10.1016/j.envint.2020.105542

Weishaar, J.L., Aiken, G.R., Bergamaschi, B.A., Fram, M.S., Fujii, R., Mopper, K., 2003. Evaluation of Specific Ultraviolet Absorbance as an Indicator of the Chemical Composition and Reactivity of Dissolved Organic Carbon. Environ. Sci. Technol. 37, 4702–4708. https://doi.org/10.1021/es030360x

Wilson, M.J., 2004. Weathering of the primary rock-forming minerals: processes, products and rates. Clay miner. 39, 233–266. https://doi.org/10.1180/0009855043930133

Wind, T., Stubner, S., Conrad, R., 1999. Sulfate-reducing Bacteria in Rice Field Soil and on Rice Roots. Systematic and Applied Microbiology 22, 269–279. https://doi.org/10.1016/S0723-2020(99)80074-5

World Health Organization Mortality Database. [(accessed on 18 November 2019)]; Available online: http://apps.who.int/healthinfo/statistics/mortality/whodpms/

World Health Organization. Regional Office for Europe. (2015). Economic cost of the health impact of air pollution in Europe: clean air, health and wealth. World Health Organization. Regional Office for Europe. https://iris.who.int/handle/10665/350716

Wu, L., Taylor, M.P., Handley, H.K., 2017. Remobilisation of industrial lead depositions in ash during Australian wildfires. Science of The Total Environment 599–600, 1233–1240. https://doi.org/10.1016/j.scitotenv.2017.05.044

Xiao, W., Jones, A.M., Li, X., Collins, R.N., Waite, T.D., 2018. Effect of Shewanella oneidensis on the Kinetics of Fe(II)-Catalyzed Transformation of Ferrihydrite to Crystalline Iron Oxides. Environ. Sci. Technol. 52, 114–123. https://doi.org/10.1021/acs.est.7b05098

Yadav, I.C., Devi, N.L., Singh, V.K., Li, J., Zhang, G., 2019. Spatial distribution, source analysis, and health risk assessment of heavy metals contamination in house dust and surface soil from four major cities of Nepal. Chemosphere 218, 1100–1113. https://doi.org/10.1016/j.chemosphere.2018.11.202

Yan, L., Franco, A.-M., Elio, P., 2021. Health risk assessment via ingestion and inhalation of soil PTE of an urban area. Chemosphere 281, 130964. https://doi.org/10.1016/j.chemosphere.2021.130964

Yang, J.-L., Zhang, G.-L., 2015. Formation, characteristics and eco-environmental implications of urban soils – A review. Soil Science and Plant Nutrition 61, 30–46. https://doi.org/10.1080/00380768.2015.1035622

Yang, Z., Wullschleger, S.D., Liang, L., Graham, D.E., Gu, B., 2016. Effects of warming on the degradation and production of low-molecular-weight labile organic carbon in an Arctic tundra soil. Soil Biology and Biochemistry 95, 202–211. https://doi.org/10.1016/j.soilbio.2015.12.022

Yu, C., Drake, H., Mathurin, F.A., Åström, M.E., 2017. Cerium sequestration and accumulation in fractured crystalline bedrock: The role of Mn-Fe (hydr-)oxides and clay minerals. Geochimica et Cosmochimica Acta 199, 370–389. https://doi.org/10.1016/j.gca.2016.11.044-

Yu, K., Böhme, F., Rinklebe, J., Neue, H.-U., DeLaune, R.D., 2007. Major Biogeochemical Processes in Soils-A Microcosm Incubation from Reducing to Oxidizing Conditions. Soil Science Soc of Amer J 71, 1406–1417. https://doi.org/10.2136/sssaj2006.0155

Yu, K., Rinklebe, J., 2011. Advancement in soil microcosm apparatus for biogeochemical research. Ecological Engineering 37, 2071–2075. https://doi.org/10.1016/j.ecoleng.2011.08.017

Yuan, Y., Cave, M., Zhang, C., 2018. Using Local Moran's I to identify contamination hotspots of rare earth elements in urban soils of London. Applied Geochemistry 88, 167–178. https://doi.org/10.1016/j.apgeochem.2017.07.011

Zahran, S., Mielke, H.W., McElmurry, S.P., Filippelli, G.M., Laidlaw, M.A.S., Taylor, M.P., 2013. Determining the relative importance of soil sample locations to predict risk of child lead exposure. Environment International 60, 7–14. https://doi.org/10.1016/j.envint.2013.07.004

Zhang, B., Zhang, H., He, J., Zhou, S., Dong, H., Rinklebe, J., Ok, Y.S., 2023. Vanadium in the Environment: Biogeochemistry and Bioremediation. Environ. Sci. Technol. 57, 14770–14786. https://doi.org/10.1021/acs.est.3c04508

Zhang, Y., Hu, C., Luo, W., 2014. Influences of Electron Donor, Bicarbonate, and Sulfate on Bioreduction Processes and Manganese/Copper Redistributions among Minerals in a Water-Saturated Sediment. Soil and Sediment Contamination: An International Journal 23, 94–106. https://doi.org/10.1080/15320383.2013.779631

Zhu, C., Tian, H., Hao, J., 2020. Global anthropogenic atmospheric emission inventory of twelve typical hazardous trace elements, 1995–2012. Atmospheric Environment 220, 117061.

Ziegler, D., Malandrino, M., Barolo, C., Adami, G., Sacco, M., Pitasi, F., Abollino, O., Giacomino, A., 2021. Influence of start-up phase of an incinerator on inorganic composition and lead isotope ratios of the atmospheric PM10. Chemosphere 266, 129091. https://doi.org/10.1016/j.chemosphere.2020.129091